Relativistic eikonal formalism applied to inclusive quasielastic proton-induced nuclear reactions

Nortin Titus

Dissertation presented for the Degree of Doctor of Philosophy at Stellenbosch University

Promoter: Dr. B. I. S. van der Ventel

Co-promoter: Prof. G. C. Hillhouse

December 2010

Declaration

By submitting this dissertation electronically, I declare that the entirety of the work contained therein is my own, original work, that I am the owner of the copyright thereof (unless to the extent explicitly otherwise stated) and that I have not previously in its entirety or in part submitted it for obtaining any qualification.

....

Signature Date

Abstract

In this dissertation we present, for the first time, a relativistic distorted wave impulse approximation formalism to describe quasielastic proton-nucleus scattering. We start from a full many-body description of the transition matrix element and show systematically how to derive the equivalent two-body form. This procedure allows for a clear and unambiguous method to introduce relativistic distorted waves. It is shown that the polarized double differential cross section may be written as the contraction of two tensors namely, the hadronic tensor (describing the projectile and ejectile), and the polarization tensor describing the target nucleus. The basic nucleon-nucleon (NN) interaction is described by the SPVAT or IA1 representation of the NN scattering matrix. Analytical expressions are derived for the polarization tensor using a Fermi gas model for the target nucleus. The nuclear distortion effects on the projectile and ejectile are described using the relativistic eikonal formalism. The expression for the double differential cross section is a nine dimensional oscillatory integral and an efficient procedure is developed to calculate this quantity. Comparison of Gaussian, Monte Carlo and quasi-Monte Carlo numerical integration schemes reveal that for this work, Gaussian quadrature is best suited for this problem. Traditional Gaussian quadrature is used to generate single variable functions whereby these functions are used in combination with modern software such as MATLAB to complete the computation of the full multidimensional integral in a reasonable amount of time. Even though the calculation of the cross section for a single value of the energy transfer is still time consuming, the computational time can be decreased by spreading the calculational burden across a number of nodes in a cluster computing system. A test calculation is performed whereby a proton with incident laboratory energy of 400 MeV is scattered off a ^{40}Ca target nucleus at $\theta_{cm} = 40^{\circ}$. For this reaction we calculate the unpolarized double differential cross section, as well as a complete set of spin observables namely A_y, $D_{\ell',\ell}$, $D_{s's}$, D_{nn},$D_{s'\ell}$ and $D_{\ell's}$. We find that the distortions lead to a reduction of the unpolarized double differential cross section. On the other hand the spin observables are complex entities which show no uniformity in behaviour. However, the differences between the distorted wave spin observables and that of the plane wave observables are minor and we conclude that distortions have little effect on spin observables.

Samevatting

Hierdie proefskrif bevat, vir die eerste keer, 'n relatiwistiese vervormdegolf impuls benadering formalisme vir die beskrywing van kwasielastiese proton-kern verstrooiing. Daar word aangetoon hoe om stapsgewys te gaan vanaf 'n veel-deeltjie beskrywing van die oorgangsmatriks element na die ekwivalente twee-deeltjie vorm. Hierdie metode laat toe dat die vervormde golwe op 'n duidelike en ondubbelsinnige manier ingevoer kan word. Daar word aangetoon dat die gepolariseerde dubbele differensiële kansvlak geskryf kan word as die kontraksie van twee tensore naamlik, die hadroniese tensor (wat die projektiel en uitgaande nukleon beskryf), sowel as die polarisasie tensor wat die kern beskryf. Die basiese kern-kern (NN) wisselwerking word beskryf deur gebruik te maak van die SPVAT of IA1 daarstelling van die NN verstrooiingsmatriks. Analitiese uitdrukkings word ook afgelei vir die polarisasie tensor binne die Fermi gas model. Die vervormdegolf beskrywing van die projektiel en uitgaande deeltjie word gedoen deur gebruik te maak van die eikonal vervormdegolf benadering. Die uitdrukking vir die ongepolariseerde dubbele differsieële kansvlak bevat 'n nege dimensioneële ossilatoriese integraal en 'n prakties-effektiewe prosedure is ontwikkel om hierdie waarneembare te bereken. Vegelyking van Gauss, Monte Carlo en kwasi-Monte Carlo numeriese integrasie tegnieke het uitgewys dat die Gauss integrasie tegniek die beste geskik is om die probleem op te los. Die gebruik van Gauss integrasie om funksies te bereken wat afhanklik is van net een veranderlike en dit te kombineer met moderne sagteware programme soos MATLAB laat ons toe om die gepolariseerde dubbele differensieële kansvlak te bekeren in 'n redelike tyd. Alhoewel die berekening van die kansvlak vir een waarde van die energie-oordrag nogsteeds tydrowend is, word dit bespoedig deur die berekeningslas te versprei oor 'n aantal nodusse in 'n rekenaarbondel sisteem. 'n Toets berekening word gedoen waarby 'n proton met inkomende laboratoriese energie van 400 MeV vanaf 'n ^{40}Ca kern verstrooi word teen 'n hoek van $\theta_{cm} = 40^0$. Vir hierdie reaksie word die ongepolariseerde dubbele differensieële kansvlak bereken sowel as 'n volledige stel spin waarneembares naamlik A_y, $D_{\ell',\ell}$, $D_{s's}$, D_{nn}, $D_{s'\ell}$ en $D_{\ell's}$. Daar word gevind dat die versteurings lei tot 'n afname in die differensieële kansvlak. Die spin waarneembares egter, is komplekse hoeveelhede wat geen univorme gedrag toon nie. Die verskil tussen die vervormde golf spin waarneembares en die van vlak golf waarneembares is minimaal en ons lei daarvan af dat spin waarneembares onsensitief is teen oor versteurings.

Acknowledgments

I want to express my sincere gratitude to the following people and institutions for their help and support and who contributed to the successfull completion of the dissertation:

- Dr. B.I.S. van der Ventel and Prof. G.C. Hillhouse for taking me on as a PhD student. Thank you Brandon and Greg for your intense support, devotion and dedication to me as your student. Thank you for the fruitful and character building discussions around Physics and life in general.
- Harriet Louis for your unwaivering support and devotion. Thank you for being in the trenches with me and inspiring me.
- The Namibian Government Scholarship & Training Program for their generous financial support from 2005 to 2009.
- The Department of Physics at the University of Stellenbosch, its staff and post-graduate students with whom I have built an invaluable relationship.
- My friend, colleague and team mate, Dawie van Niekerk for wonderful discussions on quasielastic scattering and the beauty of the response of the nucleus in nuclear scattering reactions.
- To Heleen Randall, Christine Ruperti and Avdil Lackey who took care of all the necessary administration. I value your contribution very highly and thank you for your impeccable professionalism. Also thank you for the regular lunch dates and chats.
- A thank you to 'Uncle Davie' (Pool) and 'Uncle-Stan' (February).
- My family and friends. There are too many to mention and each one of you played a special part.
- My parents 'Mummie en Deddie' who have supported and encouraged me. You have been my rock and a blessing that I cannot thank my Lord enough for.

Finally, I want to say thank you to my Heavenly Father, without whom this would have been impossible.

...in memory of my brother and friend Byron Lyle Rousseau

(04/07/1977 - 19/01/2007)

Contents

List of Figures

List of Tables

Chapter 1

Introduction

Quasielastic scattering (QES) reactions for incident nucleon energies ranging between 100 MeV and 500 MeV are the dominant reaction mechanisms in proton-nucleus scattering [1]. At these energies the wavelength of the projectile is of the same order as the size of the nucleon and is therefore assumed to directly probe nucleons inside the nuclear medium [2]. For a fixed scattering angle, a typical spectrum is shown in FIG. 1.1 and is characterized by a broad hump or peak in the differential cross section versus energy transferred, ω, spectrum. The hump is located at higher excitation energies in the spectrum and is clearly separated from the discrete states, which show up as narrow spikes at the lower end of the spectrum. Using non-relativistic kinematics one can show that the width of the quasielastic peak is related to the initial Fermi momentum of the struck nucleon in the target nucleus. With increasing incident energies the height of the hump increases and the centroid moves to higher energies, whereas its magnitude decreases and the width of the peak widens with increasing scattering angle. FIG. 1.1 also shows that a large percentage of the area under the spectrum spans the quasielastic region. This large percentage indicates its frequent occurrence as a reaction channel, making it a very important reaction to study and understand. The energy associated with the centroid of the quasielastic peak, characterized by a broad hump in the inclusive excitation spectrum, closely follows free nucleon-nucleon (NN) scattering kinematics.

Quasielastic proton-nucleus scattering is an attractive process to study since it behaves qualitatively like free NN scattering but in the nuclear medium. It therefore provides a way to study medium-modifications of the NN interaction. The first relativistic model for quasielastic scattering was developed by Horowitz, Iqbal and Murdock [3, 4, 5] and was named the Relativistic Plane Wave Impulse Approximation (RPWIA). The basic assumptions of the model were mostly motivated by experimental evidence and included:

(i) The reaction is considered to be a single-step process whereby the incident proton interacts with only one target nucleon.

(ii) The nucleons are described by plane wave Dirac spinors. The assumption was that spin observ-

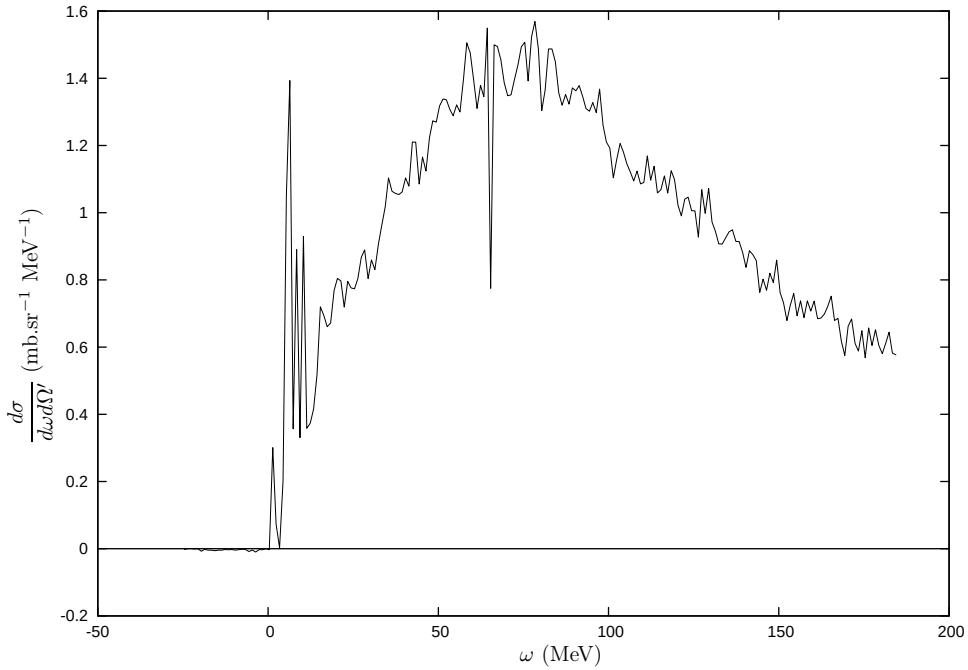

FIG. 1.1: *Unpolarized double differential cross sections for the inclusive* $^{40}Ca(p,p')$ *reaction for incident proton energy with* $T_{lab} = 400$ *MeV and scattering angle* $\theta_{lab} = 20°$.

ables (being ratios of polarized cross sections) are mostly insensitive to distortions.

The NN interaction was described by the SPVAT form which is a five-term representation in terms of a set of linearly independent Dirac matrices. This is commonly called the IA1 representation in the literature. Since the spin observables are practically identical for a large range of closed shell nuclei [6], the target was described as a Fermi gas model. One of the key features of the model was the use of an effective nucleon mass in the context of the Walecka model. The use of effective nucleon masses for the projectile, target and ejectile nucleons lead to a significant result known as the 'quenching effect' in the analysing power for the reaction $^{40}Ca(\vec{p},\vec{p}')$ for incident proton energy of 500 MeV and laboratory scattering angle of 18.5°. This was an important result since it showed that an effective mass calculation could give a better description of the data when compared to a free mass calculation. However, the effective mass concept did not work for the *complete set* of spin observables.

The study of quasielastic proton-nucleus scattering has been investigated in a series of papers by the Nuclear Theory group of the Department of Physics at Stellenbosch University [7, 8, 9, 10, 11, 12]. This was motivated not only by the many improvements which could be made to the original RPWIA model, but also by the close proximity of the 200 MeV proton accelerator facility, iThemba LABS (formerly known as the National Accelerator Center) and the subsequent possibility of measuring spin observables such as A_y and D_{nn}. One of the most important findings was that if one replaces the ambiguous SPVAT form of the NN scattering matrix with a general Lorentz invariant representation,

then the quenching effect is not as pronounced [11]. The IA2 model is a general Lorentz invariant representation of the scattering matrix $\hat{F}$ and contains 44 independent scattering amplitudes consistent with parity and time invariance and charge symmetry [13]. In addition, both effective masses and free mass calculations represented the spin observable scattering data at 500 MeV equally well. Also no effective mass combination could be found such that the IA2 representation consistently predicts *both* (p, p') and (p, n) spin observable data for energies below 500 MeV [12]. Although the model was more sophisticated than the IA1 representation, it still failed to yield consistent predictions of spin observables.

Another suggestion to address some of the RPWIA inconsistencies is to include distortions in the incoming and outgoing wave functions rather than the concept of effective masses [10, 14]. As mentioned above in the context of the RPWIA, all calculations for the inclusive quasielastic scattering (p, p') reaction that were done used plane waves to describe the projectile and target nucleons. The effect of distortions were mainly incorporated in the concept of effective masses. The use of plane waves is a massive simplification to what these particles actually experience. In reality the projectile and ejectile experience strong scalar and vector optical potentials in the presence of the nuclear medium. Similarly, the target nucleon also experiences strong scalar and vector boundstate potentials.

Thesis Motivation

The goals of this thesis are the following:

(i) Develop a consistent and fully relativistic formalism in order to calculate the double differential cross section for quasielastic proton-nucleus scattering.

(ii) Include, for the first time, the use of relativistic distorted waves to describe the projectile and ejectile.

(iii) Investigate the use of quadrature schemes to efficiently handle multi-dimensional integrals where the integrand has a strong oscillatory character.

(iv) Calculate, for the first time, the unpolarized double differential cross section and a complete set of spin observables namely A_y, $D_{\ell',\ell}$, $D_{s's}$, D_{nn}, $D_{s'\ell}$ and $D_{\ell's}$, using relativistic distorted waves.

The fundamental quantity which must be calculated is the invariant matrix element defined as

$$\mathcal{M} \;=\; \langle\, f \mid \hat{F} \mid i \,\rangle \tag{1.1}$$

where $\mid i \,\rangle$ and $\mid f \,\rangle$ denote initial and final nuclear states, respectively and $\hat{F}$ is the scattering operator which connects the final and initial states. In general these quantities are extremely complicated since the nucleus is a complicated many-body system. In the original model of Horowitz *et al.* they exploited the experimental features of quasielastic scattering to directly model the initial states as

simple two-body states and (in addition) using Dirac plane waves. One of the goals of this thesis is to start from a fully many-body formulation and systematically derive the two-body form. This leads to a representation where the inclusion of distortions can be done very naturally. We will also show that the cross section can be written as a contraction between two tensors, namely a projectile tensor describing the projectile/ejectile and a target tensor describing the nuclear target. This is analogous to what we find in for example two-body electron-proton scattering. However, here the complexity is greatly increased due to many factors discussed later. However, the "modular" form of the expression allows one to systematically investigate effects such as distortions and different models for the nuclear target. Our model still uses the IA1 representation, however. This is due to the following reasons. Even though one should in principle use the more complete IA2 representation this may not be the best place to start. As this thesis will show, the inclusion of distortions leads to many numerical complications, and if one was to combine this with the IA2 form, it could be very difficult to disentangle different effects. From a pedagogical point of view it is therefore best to first use the IA1 representation. A numerical implementation of the IA2 representation is a very complicated matter as shown in the work of Tjon and Wallace and Van der Ventel *et al.* Besides, the IA1 calculation should always serve as a baseline for the full IA2 calculation since the latter contains the SPVAT form as a special case.

As mentioned above, one of the main goals of this thesis is to provide the first calculation of quasielastic spin observables using relativistic distorted waves. Here one has to make a choice between using a full partial wave expansion or some other approximation which captures the main features of distortion effects whilst still allowing numerical results in a reasonable time. In this work we employ the eikonal formalism for a number of reasons: (i) it has been successfully used in numerous studies of nuclear scattering reactions [3, 15, 16, 17, 18], (ii) it allows one a measure of analytical tractability which is very difficult if one was to employ a full partial wave expansion and (iii) as will be shown in this thesis it offers a speed advantage compared to a full partial wave expansion.

The problem of partial waves is circumvented in this work and the Dirac eikonal distorted wave function is used in a Relativistic Distorted Wave Impulse Approximation (RDWIA) formalism. The derived expression for the double differential cross section is however a nine dimensional integral and even though the Dirac eikonal distorted wave functions eases the numerical challenge to a degree, it was still not clear if traditional quadrature techniques will perform appropriately in computing the multidimensional integrals. We test three popular quadrature methods namely Gaussian quadrature, Monte Carlo integration and quasi-Monte Carlo integration schemes and establish that traditional Gaussian integration *suited our application better* than a Monte Carlo type integration scheme. Although Gaussian integration proves to be the most effective for the integrations, the full nine dimensional integral still carries an enormous computational time penalty. We therefore resort to computing a five dimensional integral, which results in a function dependent on a single variable. A Fourier series is then used to fit this resultant function. Using the fitting function we are then able to perform the full integration and calculate the polarized double differential cross section in a reasonable amount of time. Furthermore, it is possible to calculate spin observables.

Even though we show by means of a sample calculation that it is in principle possible to attempt a full calculation of the inclusive differential cross section for proton-nucleus scattering, the numerical difficulty and complexity of this calculation remains an enormous challenge.

The thesis is organized as follows: In chapter two we introduce the invariant matrix element and show that we can write the differential cross section as a contraction between a projectile tensor and a target tensor. We show how we include the eikonal distorted waves into the projectile tensor and we derive an analytical expression for the target polarization. In chapter three we explore fully the numerical analysis that accompanied the calculation of the distorted wave double differential cross section. Finally, in chapter four we present our results, discuss the main features and end with a summary of this work.

Chapter 2

Theoretical Formalism

In this chapter we present a complete derivation of the polarized double differential cross section for quasielastic proton-nucleus scattering. We start with the general form of the differential cross section and connect that to the invariant matrix element. We then analyze the matrix element and build distortions into this quantity. We will then derive the polarization tensor for the scalar-scalar case.

2.1 Differential cross section

An inclusive nuclear reaction is A + B → C + anything, where either A, B or C is a nucleus. For the inclusive reaction given in Eq. (2.1)

$$\text{proton} + X \longrightarrow \text{nucleon} + X', \tag{2.1}$$

the differential cross section is given by [19]

$$d\sigma = \frac{1}{|\mathbf{v}_1 - \mathbf{v}_2|}\left(\frac{M^2}{E(\mathbf{k})E(\mathbf{k}')}\right)(2\pi)^4\delta(k + K - k' - K')\frac{d^3k'}{(2\pi)^3}\frac{d^3K'}{(2\pi)^3}|\mathcal{M}|^2. \tag{2.2}$$

In Eq. (2.2), $\mathbf{v}_1$ and $\mathbf{v}_2$ are the velocities of the projectile and the target nucleus, $\mathcal{M}$ the transition matrix element for this particular reaction, M the free nucleon mass and k, k', K and K' the asymtotic four-momenta of the projectile, ejectile nucleons, target and residual nucleus respectively.

2.1.1 Kinematics

We begin by considering Eq. (2.2) in which we factor the four momentum delta function into the energy and three dimensional momentum delta function

$$(2\pi)^4\delta(k + K - k' - K') = 2\pi\delta(E(\mathbf{k}) + E(\mathbf{K}) - E(\mathbf{k}') - E(\mathbf{K}'))(2\pi)^3\delta(\mathbf{k} + \mathbf{K} - \mathbf{k}' - \mathbf{K}'). \tag{2.3}$$

The recoil nucleus is undetected in the inclusive reaction and we can then perform the integration over $\mathbf{K}'$ in the three dimensional delta function above. This results in[1]

$$(2\pi)^4\delta(E_{\mathbf{k}} + E_{\mathbf{K}} - E_{\mathbf{k}'} - E_{\mathbf{K}'}). \tag{2.4}$$

Next, from $E^2 = \mathbf{k}^2 + M^2$ it follows that $EdE = kdk$ and we can then write the ejectile's volume element d^3k' in spherical coordinates as

$$d^3k' = \mathbf{k}'^{\,2}dk'(\sin\theta' d\theta' d\phi') = k' E_{\mathbf{k}'} dE' d\Omega', \tag{2.5}$$

where $dE' = d(E_{\mathbf{k}'})$ and $k' = |\mathbf{k}'|$. The energy transfer ω is defined as

$$\omega = E_{\mathbf{k}} - E_{\mathbf{k}'}. \tag{2.6}$$

Substituting the above equations into Eq. (2.2) the differential cross section becomes

$$d\sigma = \frac{1}{(2\pi)^2|\mathbf{v}_1 - \mathbf{v}_2|}\left(\frac{M^2 k' E_{\mathbf{k}'} dE' d\Omega'}{E_{\mathbf{k}} E_{\mathbf{k}'}}\right)\delta\left[\omega - E_{\mathbf{K}'} + E_{\mathbf{K}}\right]|\mathcal{M}|^2. \tag{2.7}$$

Rearranging terms, results in

$$d\sigma = \frac{M^2}{(2\pi)^2}\left(\frac{k' E_{\mathbf{k}'} dE' d\Omega'}{|\mathbf{v}_1 - \mathbf{v}_2| E_{\mathbf{k}} E_{\mathbf{k}'}}\right)|\mathcal{M}|^2\delta\left[\omega - (E_{\mathbf{K}'} - E_{\mathbf{K}})\right]. \tag{2.8}$$

Eq. (2.8) is valid in any Lorentz system. At this point we need to choose a specific reference frame in order to calculate spin observables. The relativistic distorted waves are traditionally calculated in the proton-nucleus center-of-mass (c.m.) frame and we choose this reference frame which is defined as

$$\mathbf{k} + \mathbf{K} = \mathbf{k}' + \mathbf{K}', \tag{2.9}$$

which implies that the scattering four momenta are then

$$k = (E_{\mathbf{k}}, \mathbf{k}), \tag{2.10}$$

$$K = (E_{\mathbf{k}}, -\mathbf{k}), \tag{2.11}$$

$$k' = \left(E_{\mathbf{k}'}, \mathbf{k}'\right), \tag{2.12}$$

$$K' = \left(E_{\mathbf{k}'}, -\mathbf{k}'\right). \tag{2.13}$$

[1] In the derivation we denote the energy of the nucleon with momentum $\mathbf{k}$ by means of a subscript of the particle's momentum $E(\mathbf{k}') \rightarrow E_{\mathbf{k}'}$.

From the conservation of energy

$$\left(\mathbf{k}^2+M^2\right)^{\frac{1}{2}}+\left(\mathbf{k}^2+M_t^2\right)^{\frac{1}{2}}=\left(\mathbf{k}'^2+M^2\right)^{\frac{1}{2}}+\left(\mathbf{k}'^2+M_t^2\right)^{\frac{1}{2}}, \tag{2.14}$$

from which it is clear that

$$k=k'. \tag{2.15}$$

Eq. (2.8) now reads

$$d\sigma=\frac{M^2}{(2\pi)^2}\left(\frac{kdE'd\Omega'}{|\mathbf{v}_1-\mathbf{v}_2|E_{\mathbf{k}}}\right)|\mathcal{M}|^2\delta\left[\omega-(E_{\mathbf{K}'}-E_{\mathbf{K}})\right]. \tag{2.16}$$

The velocity dependent term in the differential cross section is elimated by making the following algebraic replacement [20]

$$\begin{aligned}
|\mathbf{v}_1-\mathbf{v}_2|\left[E_{\mathbf{k}}\right]_{\text{proj}}\left[E_{\mathbf{k}}\right]_t &= \left[(\mathbf{k}\cdot\mathbf{K})^2-M^2M_t^2\right]^{\frac{1}{2}} \\
|\mathbf{v}_1-\mathbf{v}_2|\left[E_{\mathbf{k}}\right]_{\text{proj}} &= \frac{\left[(\mathbf{k}\cdot\mathbf{K})^2-M^2M_t^2\right]^{\frac{1}{2}}}{\left[E_{\mathbf{k}}\right]_t} \\
|\mathbf{v}_1-\mathbf{v}_2|\left[E_{\mathbf{k}}\right]_{\text{proj}} &= \frac{\left[(\mathbf{k}\cdot\mathbf{K})^2-M^2M_t^2\right]^{\frac{1}{2}}}{\left(\mathbf{k}^2+M_t^2\right)^{\frac{1}{2}}}.
\end{aligned} \tag{2.17}$$

The numerator on the R.H.S of Eq. (2.17) becomes

$$\begin{aligned}
\left[(\mathbf{k}\cdot\mathbf{K})^2-M^2M_t^2\right]^{\frac{1}{2}} &= \left[(E_kE_K-(\mathbf{k}\cdot-\mathbf{k}))^2-M^2M_t^2\right]^{\frac{1}{2}} \\
&= k\left(E_k+E_K\right) \\
&= k\left[\left(\mathbf{k}^2+M^2\right)^{\frac{1}{2}}+\left(\mathbf{k}^2+M_t^2\right)^{\frac{1}{2}}\right].
\end{aligned}$$

We now have that

$$\left[(\mathbf{k}\cdot\mathbf{K}-M^2M_t^2\right]^{\frac{1}{2}}=k\left[\left(\mathbf{k}^2+M^2\right)^{\frac{1}{2}}+\left(\mathbf{k}^2+M_t^2\right)^{\frac{1}{2}}\right] \tag{2.18}$$

and

$$|\mathbf{v}_1-\mathbf{v}_2|\cdot\left[E_{\mathbf{k}}\right]_{\text{proj}}=\frac{k\left[\left(\mathbf{k}^2+M^2\right)^{\frac{1}{2}}+\left(\mathbf{k}^2+M_t^2\right)^{\frac{1}{2}}\right]}{\left(\mathbf{k}^2+M_t^2\right)^{\frac{1}{2}}}. \tag{2.19}$$

We replace and cancel terms in Eq. (2.16) which results in

$$d\sigma=\frac{M^2}{(2\pi)^2}\left(\frac{\left(\mathbf{k}^2+M_t^2\right)^{\frac{1}{2}}dE'd\Omega'}{\left[\left(\mathbf{k}^2+M^2\right)^{\frac{1}{2}}+\left(\mathbf{k}^2+M_t^2\right)^{\frac{1}{2}}\right]}\right)|\mathcal{M}|^2\delta\left[\omega-(E_{\mathbf{K}'}-E_{\mathbf{K}})\right]. \tag{2.20}$$

Finally grouping kinematic terms together and for the inclusive reaction we have to sum over all possible final nuclear states (here we replace $E_{\mathbf{K}}$ with E_0 and $E_{\mathbf{K}'}$ with E_n)

$$\frac{d\sigma}{dE'd\Omega'} = \left(\frac{M^2 \left(\mathbf{k}^2 + M_t^2\right)^{\frac{1}{2}}}{4\pi^2 \left[\left(\mathbf{k}^2 + M^2\right)^{\frac{1}{2}} + \left(\mathbf{k}^2 + M_t^2\right)^{\frac{1}{2}} \right]} \right) \sum_n |\mathcal{M}|^2 \delta \left[\omega - (E_n - E_0) \right]. \tag{2.21}$$

We now rewrite Eq. (2.2) in terms of the double differential cross section as

$$\frac{d\sigma}{dE'd\Omega'} = K \sum_n |\mathcal{M}|^2 \ \delta(\omega - (E_n - E_0)), \tag{2.22}$$

where

$$K = \frac{M^2 \left(\mathbf{k}^2 + M_t^2\right)^{\frac{1}{2}}}{4\pi^2 \left[\left(\mathbf{k}^2 + M^2\right)^{\frac{1}{2}} + \left(\mathbf{k}^2 + M_t^2\right)^{\frac{1}{2}} \right]} \tag{2.23}$$

is a pure kinematic factor. By using the identity

$$\mathrm{Im} \left\{ \frac{1}{\omega - (E_n - E_0) + i\epsilon} \right\} = -\pi \delta(\omega - (E_n - E_0)), \tag{2.24}$$

Eq. (2.22) is now written as

$$\frac{d\sigma}{dE'd\Omega'} = -\frac{1}{\pi} K \ \mathrm{Im} \left\{ \sum_n |\mathcal{M}|^2 \ \frac{1}{\omega - (E_n - E_0) + i\epsilon} \right\}. \tag{2.25}$$

Eq. (2.25) is the main result for this section. $\mathcal{M}^2$ is a purely real quantity, but in Eq. (2.25), we have related the polarized double differential cross section to the matrix element. As we will show in a subsequent section, the advantage of writing it in this form is that one can then relate the nuclear response to the imaginary part of the target tensor. The target tensor or polarization tensor is a many-body entity which can then be calculated using well-known many-body techniques.

To end this section we indicate how we calculate the kinematic quantities mentioned in the preceding text. We have chosen the center-of-mass reference frame for our calculation. We choose the incident momentum $\mathbf{k}$ to correspond to the $\hat{z}$-direction shown in FIG. 2.1 and from which we can calculate the associated energy by

$$k = \sqrt{E_{\mathbf{k}}^2 - M^2}. \tag{2.26}$$

The total energy of the projectile in the proton-nucleus center-of-mass frame is given by [21, 22]

$$E_{\mathbf{k}} = \frac{M^2 + M_t(M + T_{lab})}{\sqrt{(M + M_t)^2 + 2M_t T_{lab}}}, \tag{2.27}$$

where T_{lab} is the incident energy in the laboratory frame and M_t is the mass of the target. For a fixed

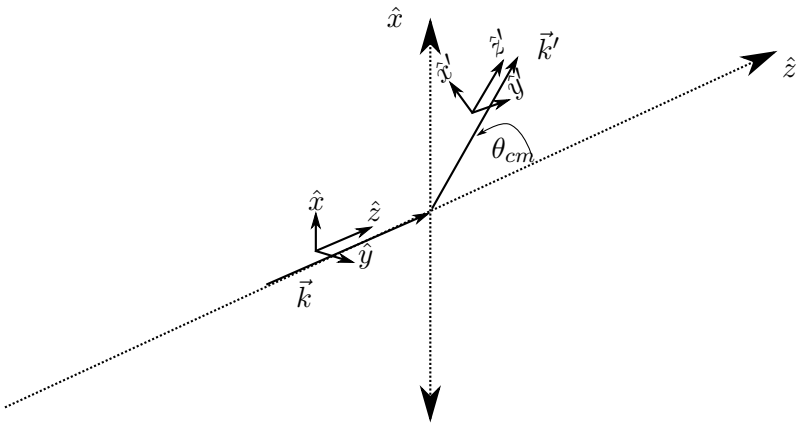

FIG. 2.1: *Initial and final proton-nucleus center-of-mass reference frames.*

energy transfer ω to the target nucleus and fixed center-of-mass scattering angle θ_{cm} the ejectile energy is given by

$$E_{\mathbf{k}'} = E_{\mathbf{k}} - \omega \tag{2.28}$$

from which its magnitude can be computed using Eq. (2.26) with $E_{\mathbf{k}}$ replaced with $E_{\mathbf{k}'}$. In Cartesian components then the momentum of the ejectile is given by

$$k'_x = k' \sin\theta_{cm}, \tag{2.29}$$
$$k'_y = 0, \tag{2.30}$$
$$k'_z = k' \cos\theta_{cm}. \tag{2.31}$$

2.1.2 Spin observables

The NN force is dependent on the spin orientations of the interacting particles. Using polarized beams polarization observables can be measured in the laboratory. The unit vectors $\hat{\mathbf{l}}$, $\hat{\mathbf{s}}$ and $\hat{\mathbf{n}}$ are defined in terms of the initial and final momenta where the longitudinal direction is given by

$$\hat{\mathbf{l}} = \frac{\mathbf{k}}{|\mathbf{k}|} \tag{2.32}$$

and

$$\hat{\mathbf{l}}' = \frac{\mathbf{k}'}{|\mathbf{k}'|}. \tag{2.33}$$

The $\hat{\mathbf{n}}$ direction is the direction 'normal' to the scattering plane

$$\hat{\mathbf{n}} = \frac{\mathbf{k} \times \mathbf{k}'}{|\mathbf{k} \times \mathbf{k}'|}. \tag{2.34}$$

The sideways direction $\hat{\mathbf{s}}$ is then

$$\hat{\mathbf{s}} = \hat{\mathbf{n}} \times \hat{\mathbf{l}}. \tag{2.35}$$

The polarization observables are defined as linear combinations of polarized double differential cross sections. For simplicity we let

$$d\sigma_{s_z s'_z} = \frac{d\sigma}{d\Omega' dE'}(s_i, s_f), \tag{2.36}$$

where $s_i = (j, s_z)$ and $s_f = (i', s'_z)$ refer to the initial and final spin polarizations respectively and $j \in \left\{\hat{\mathbf{l}}; \hat{\mathbf{s}}; \hat{\mathbf{n}}\right\}$ and $i' \in \left\{\hat{\mathbf{l}}'; \hat{\mathbf{s}}'; \hat{\mathbf{n}}'\right\}$. We introduce the shorthand notation u to designate the spin projection direction $s_z = \frac{1}{2}$ or 'spin-up' and d to designate the spin projection direction $s_z = -\frac{1}{2}$ or 'spin down'. Polarization observables are then calculated as follows

$$D_{i'j} = \frac{d\sigma_{uu} - d\sigma_{du} - d\sigma_{ud} + d\sigma_{dd}}{d\sigma_{uu} + d\sigma_{du} + d\sigma_{ud} + d\sigma_{dd}}. \tag{2.37}$$

The analyzing power A_y is the ratio of initially polarized nucleons left unpolarized after interacting with the target nucleus and is calculated using

$$A_y = \frac{(d\sigma_{uu} + d\sigma_{du}) - (d\sigma_{ud} + d\sigma_{dd})}{d\sigma_{uu} + d\sigma_{du} + d\sigma_{ud} + d\sigma_{dd}}. \tag{2.38}$$

2.1.3 The transition amplitude

Next we will turn our attention to the invariant matrix element that contains all the dynamics of the scattering process. We work in natural units where we have set $\hbar = c = 1$. For the inclusive quasielastic scattering reaction the transition matrix element $\mathcal{M}$ is given by [15]

$$\begin{aligned} \mathcal{M} \quad = \quad & \int d^4x\, d^4x' \prod_{i=1}^{A} d^4y_i \prod_{j=1}^{A} d^4y'_j \left[\bar{\psi}^{(-)}(x', \mathbf{k}', \hat{\mathbf{i}}', s') \otimes \bar{\Phi}_f(y'_1, ..., y'_j, ..., y'_A)\right] \\ & \times \hat{F}_{many}(x, x', \{y\}, \{y'\}) \left[\psi^{(+)}(x, \mathbf{k}, \hat{\mathbf{i}}, s) \otimes \Phi_i(y_1, ..., y_i, ..., y_A)\right]. \end{aligned} \tag{2.39}$$

In Eq. (2.39)

- x, x', y and y' are four-vectors;
- The Kronecker product is denoted by $\otimes$;
- $\psi^{(+)}(x, \mathbf{k}, \hat{\mathbf{i}}, s)$ is the relativistic distorted wave function of the projectile with outgoing boundary conditions indicated by the subscript $(+)$ and with asymptotic three-momentum $\mathbf{k}$ in the proton-nucleus center-of-mass system and spin projection s along an arbitrary quantization axis $\hat{\mathbf{i}}$ in the rest frame of the projectile;
- $\bar{\psi}^{(-)}(x', \mathbf{k}', \hat{\mathbf{i}}', s') = \psi^{\dagger(-)}(x', \mathbf{k}', \hat{\mathbf{i}}', s')\gamma^0$, where $\psi^{(-)}(x', \mathbf{k}', \hat{\mathbf{i}}', s')$ is the relativistic distorted wave function of the ejectile nucleon, with incoming boundary conditions denoted by the superscript

(-) with asymptotic three-momentum $\mathbf{k}'$ in the nucleon-nucleus center-of-mass system and spin projection s' along an arbitrary quantization axis $\hat{\mathbf{i}}'$ in the rest frame of the ejectile;

- $\Phi_i(y_1, ..., y_i, ..., y_A)$ is the initial many-body ground state of the nucleus; a function of all A constituent target nucleons;
- $\bar{\Phi}_f(y'_1, ..., y'_j, ..., y'_A)$ is the final many-body ground state of the nucleus; a function of all A constituent target nucleons;
- $\hat{F}_{many}(x, x', \{y\}, \{y'\})$ which is the many-body operator that connects the initial and final states.

We now give our conventions for the Fourier transforms used in the analysis to follow. The Fourier transform of $f(k)$ where k is a four-vector is defined as

$$f(x) = \int \frac{d^4k}{(2\pi)^4} e^{-ik\cdot x} f(k) \tag{2.40}$$

and the inverse transform is

$$f(k) = \int d^4x \; e^{-ik\cdot x} f(x). \tag{2.41}$$

It follows that

$$\delta(x - x') = \int \frac{d^4k}{(2\pi)^4} e^{-ik\cdot(x-x')} \tag{2.42}$$

and

$$(2\pi)^4 \delta(k - k') = \int d^4x \; e^{-ix\cdot(k-k')}. \tag{2.43}$$

The completeness relation is

$$1 = \int \frac{d^4p}{(2\pi)^4} |p\rangle\langle p| \tag{2.44}$$

from which we obtain

$$\langle x|x'\rangle = \int \frac{d^4p}{(2\pi)^4} \langle x|p\rangle\langle p|x'\rangle = \delta(x - x') \tag{2.45}$$

as well as

$$\langle x|p\rangle = e^{-ip\cdot x}, \tag{2.46}$$

$$\langle p|x'\rangle = e^{ip\cdot x'}. \tag{2.47}$$

Quasielastic scattering is modeled as a single step reaction, where the projectile is assumed to interact with only **one bound** target nucleon in the target nucleus. Based on this, our many body operator $\hat{F}_{many}$ can be approximated by a two-body operator

$$\hat{F}_{many}(x, x', \{y\}, \{y'\}) = \sum_{i=1}^{A} \langle x' \, y'_i \,|\, \hat{F} \,|\, x \, y_i \,\rangle \prod_{j=1, j\neq i}^{A} \delta(y'_j - y_j), \tag{2.48}$$

where $\hat{F}$ is now a **two-body** operator connecting the initial state with the final states and $\delta(y'_j - y_j)$ refer to the spectator nucleons of the target nucleus. Inserting this two-body operator in Eq. (2.39) results in

$$\begin{aligned}\mathcal{M} &= \sum_{i=1}^{A}\int d^4x d^4x' d^4y_i d^4y'_i \left(\prod_{j=1,j\neq i}^{A} d^4y'_j\ \delta(y'_j - y_j)\right)\left[\bar{\psi}^{(-)}(x',\mathbf{k}',\hat{\mathbf{i}}',s')\otimes\bar{\Phi}_f(y'_1,...,y'_i,...,y'_A)\right] \\ &\times\langle x'\,y'_i\mid\hat{F}\mid x\,y_i\rangle\left[\psi^{(+)}(x,\mathbf{k},\hat{\mathbf{i}},s)\otimes\Phi_i(y_1,...,y_i,...,y_A)\right], \qquad (2.49)\end{aligned}$$

where we have used

$$\sum_{i=1}^{A} d^4y'_j = \sum_{i=1}^{A} d^4y'_i\left(\prod_{j=1,j\neq i}^{A} d^4y'_j\right).$$

Next we change basis, from position space to momentum space by inserting a complete set of momentum eigenstates. The right hand side of Eq. (2.48) becomes

$$\sum_{i=1}^{A}\langle x'\,y'_i\mid\hat{F}\mid x\,y_i\rangle = \sum_{i=1}^{A}\int\frac{d^4p}{(2\pi)^4}\frac{d^4p'}{(2\pi)^4}\frac{d^4p_i}{(2\pi)^4}\frac{d^4p'_i}{(2\pi)^4}e^{ip\cdot x}e^{-ip'\cdot x'}e^{ip\cdot y_i}e^{-ip'_i\cdot y'_i}\langle p'\,p'_i\mid\hat{F}\mid p\,p_i\rangle. \qquad (2.50)$$

Eq. (2.49) becomes

$$\begin{aligned}\mathcal{M} &= \sum_{i=1}^{A}\int d^4x d^4x' d^4y_i d^4y'_i\left(\prod_{j=1,j\neq i}^{A} d^4y'_j\ \delta(y'_j - y_j)\right)\int\frac{d^4p}{(2\pi)^4}\frac{d^4p'}{(2\pi)^4}\frac{d^4p_i}{(2\pi)^4}\frac{d^4p'_i}{(2\pi)^4} \\ &\times e^{ip\cdot x}e^{-ip'\cdot x'}e^{ip\cdot y_i}e^{-ip'_i\cdot y'_i}\left[\bar{\psi}^{(-)}(x',\mathbf{k}',\hat{\mathbf{i}}',s')\otimes\bar{\Phi}_f(y'_1,...,y'_i,...,y'_A)\right] \\ &\times\langle p'\,p'_i\mid\hat{F}\mid p\,p_i\rangle\left[\psi^{(+)}(x,\mathbf{k},\hat{\mathbf{i}},s)\otimes\Phi_i(y_1,...,y_i,...,y_A)\right]. \qquad (2.51)\end{aligned}$$

Now assume that the time-dependence is given by

$$\psi^{(+)}(x,\mathbf{k},\hat{\mathbf{i}},s) = e^{-iE_{\mathbf{k}}x_0}\psi^{(+)}(\mathbf{x},\mathbf{k},\hat{\mathbf{i}},s), \qquad (2.52)$$

$$\bar{\psi}^{(-)}(x',\mathbf{k}',\hat{\mathbf{i}}',s') = e^{iE_{\mathbf{k}'}x'_0}\bar{\psi}^{(-)}(\mathbf{x}',\mathbf{k}',\hat{\mathbf{i}}',s'), \qquad (2.53)$$

$$\Phi_i(y_1,...,y_i,...,y_A) = \left[\prod_{j=1,j\neq i}^{A} e^{-iK_{j,0}y_{j,0}}\right]e^{-iK_{i,0}y_{i,0}}\Phi_i(\mathbf{y}_1,...,\mathbf{y}_i,...,\mathbf{y}_A), \qquad (2.54)$$

$$\bar{\Phi}_f(y'_1,...,y'_i,...,y'_A) = \left[\prod_{j=1,j\neq i}^{A} e^{iK'_{j,0}y'_{j,0}}\right]e^{iK'_{i,0}y'_{i,0}}\bar{\Phi}_f(\mathbf{y}'_1,...,\mathbf{y}'_i,...,\mathbf{y}'_A). \qquad (2.55)$$

Inserting Eqs. (2.52-2.55) into Eq. (2.51) and separating the temporal components from the space components results in

$$\begin{aligned}
\mathcal{M} &= \sum_{i=1}^{A}\int\left(\prod_{j=1,j\neq i}^{A} d^4y'_j\ \delta(y'_j-y_j)\right)\int dx_0dx'_0dy_{i,0}dy'_{i,0}\frac{dp_0}{2\pi}\frac{dp'_0}{2\pi}\frac{dp_{i,0}}{2\pi}\frac{dp'_{i,0}}{2\pi}\\
&\times e^{-iE_{\mathbf{k}}x_0}e^{iE_{\mathbf{k}'}x'_0}e^{-iK_{i,0}y_{i,0}}e^{iK'_{i,0}y'_{i,0}}\left[\prod_{m=1,m\neq i}^{A} e^{-iK_{m,0}y_{m,0}}\right]\left[\prod_{n=1,n\neq i}^{A} e^{iK'_{n,0}y'_{n,0}}\right]\\
&\times e^{ip_ox_0}e^{-ip'_ox'_0}e^{ip_{i,o}y_{i,0}}e^{-ip'_{i,o}y'_{i,0}}\int d^3x\ d^3x\ 'd^3y_id^3y'_i\frac{d^3p}{(2\pi)^3}\frac{d^3p'}{(2\pi)^3}\frac{d^3p_i}{(2\pi)^3}\frac{d^3p'_i}{(2\pi)^3}\\
&\times e^{-i\mathbf{p}\cdot\mathbf{x}}e^{i\mathbf{p}'\cdot\mathbf{x}'}e^{-i\mathbf{p}_i\cdot\mathbf{y}_i}e^{i\mathbf{p}'_i\cdot\mathbf{y}'_i}\left[\bar{\psi}^{(-)}(\mathbf{x}',\mathbf{k}',\hat{\mathbf{i}}',s')\otimes\bar{\Phi}_f(\mathbf{y}'_1,...,\mathbf{y}'_i,...,\mathbf{y}'_A)\right]\\
&\times\langle\mathbf{p}'\,\mathbf{p}'_i\mid\hat{F}\mid\mathbf{p}\,\mathbf{p}_i\rangle\left[\psi^{(+)}(\mathbf{x},\mathbf{k},\hat{\mathbf{i}},s)\otimes\Phi_i(\mathbf{y}_1,...,\mathbf{y}_i,...,\mathbf{y}_A)\right] \qquad (2.56)
\end{aligned}$$

and after some simplifying

$$\begin{aligned}
\mathcal{M} &= \sum_{i=1}^{A}\Delta_i\int d^3x\ d^3x'\ d^3y_id^3y'_i\frac{d^3p}{(2\pi)^3}\frac{d^3p'}{(2\pi)^3}\frac{d^3p_i}{(2\pi)^3}\frac{d^3p'_i}{(2\pi)^3}e^{-i\mathbf{p}\cdot\mathbf{x}}e^{i\mathbf{p}'\cdot\mathbf{x}'}e^{-i\mathbf{p}_i\cdot\mathbf{y}_i}e^{i\mathbf{p}'_i\cdot\mathbf{y}'_i}\\
&\times\left[\bar{\psi}^{(-)}(\mathbf{x}',\mathbf{k}',\hat{\mathbf{i}}',s')\otimes\bar{\Phi}_f(\mathbf{y}'_1,...,\mathbf{y}'_i,...,\mathbf{y}'_A)\right]\langle\mathbf{p}'\,\mathbf{p}'_i\mid\hat{F}\mid\mathbf{p}\,\mathbf{p}_i\rangle\\
&\times\left[\psi^{(+)}(\mathbf{x},\mathbf{k},\hat{\mathbf{i}},s)\otimes\Phi_i(\mathbf{y}_1,...,\mathbf{y}_i,...,\mathbf{y}_A)\right], \qquad (2.57)
\end{aligned}$$

where

$$\begin{aligned}
\Delta_i &= \int\left(\prod_{j=1,j\neq i}^{A} d^4y'_j\ \delta(y'_j-y_j)\right)\int dx_0dx'_0dy_{i,0}dy'_{i,0}\frac{dp_0}{2\pi}\frac{dp'_0}{2\pi}\frac{dp_{i,0}}{2\pi}\frac{dp'_{i,0}}{2\pi}\\
&\times e^{-iE_{\mathbf{k}}x_0}e^{iE_{\mathbf{k}'}x'_0}e^{-iK_{i,0}y_{i,0}}e^{iK'_{i,0}y'_{i,0}}\left[\prod_{m=1,m\neq i}^{A} e^{-iK_{m,0}y_{m,0}}\right]\left[\prod_{n=1,n\neq i}^{A} e^{iK'_{n,0}y'_{n,0}}\right]\\
&\times e^{ip_o\cdot x_0}e^{-ip'_o\cdot x'_0}e^{ip_{i,o}\cdot y_{i,0}}e^{-ip'_{i,o}\cdot y'_{i,0}}. \qquad (2.58)
\end{aligned}$$

To progress further we must choose a representation of our two-body operator $\hat{F}$. We choose the IA1 representation

$$\langle\mathbf{p}'\,\mathbf{p}'_i\mid\hat{F}\mid\mathbf{p}\,\mathbf{p}_i\rangle=(2\pi)^3\delta(\mathbf{p}+\mathbf{p}_i-\mathbf{p}'-\mathbf{p}'_i)\sum_{L=S}^{T}F_L(\mathbf{p},\mathbf{p}_i,\mathbf{p}',\mathbf{p}'_i)(\lambda^L\otimes\lambda_L). \qquad (2.59)$$

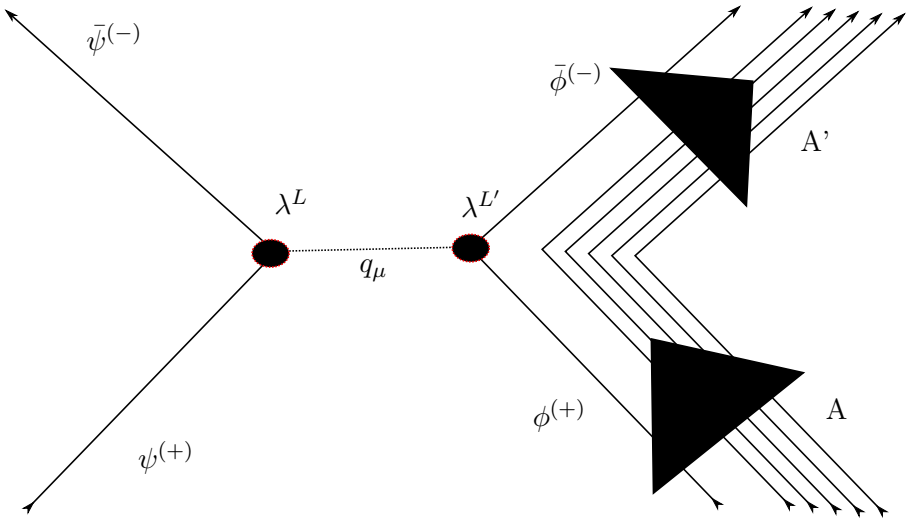

FIG. 2.2: *Schematic diagram of the Relativistic Plane Wave Impulse Approximation for inclusive quasielastic proton-nucleus scattering.*

In Eq. (2.59):

1. Three-momentum conservation is explicitly enforced: $\mathbf{p} + \mathbf{p}_i = \mathbf{p}' + \mathbf{p}'_i$.

2. $\lambda^L \in \{I_4, \gamma^5, \gamma^\mu, \gamma^5\gamma^\mu, \sigma^{\mu\nu}\}$ where $L = S, P, V, A, T$. This is the well-known SPVAT or IA1 form of the scattering operator. Ambiguities associated with this form of $\hat{F}$ were first pointed out in Ref.[23, 24], however this representation was successfully employed in elastic [25, 26], quasielastic [5, 10] and inelastic proton nucleus scattering [15, 17, 27].

3. F_L is the complex NN amplitude.

Inserting Eq. (2.59) into Eq. (2.57) and performing the integration over the momentum, $\mathbf{p}'_i$, of the undetected recoil nucleus as follows:

$$\int \frac{d^3p}{(2\pi)^3}\frac{d^3p'}{(2\pi)^3}\frac{d^3p_i}{(2\pi)^3} e^{-i\mathbf{p}\cdot\mathbf{x}} e^{i\mathbf{p}'\cdot\mathbf{x}'} e^{-i\mathbf{p}_i\cdot\mathbf{y}_i} e^{i\mathbf{p}'_i\cdot\mathbf{y}'_i}\, d^3p'_i\, \delta(\mathbf{p}+\mathbf{p}_i-\mathbf{p}'-\mathbf{p}'_i) \sum_{L=S}^{T} F_L(\mathbf{p},\mathbf{p}_i,\mathbf{p}',\mathbf{p}'_i)(\lambda^L \otimes \lambda_L)$$

$$= \int \frac{d^3p}{(2\pi)^3}\frac{d^3p'}{(2\pi)^3}\frac{d^3p_i}{(2\pi)^3} e^{-i\mathbf{p}\cdot\mathbf{x}} e^{i\mathbf{p}'\cdot\mathbf{x}'} e^{-i\mathbf{p}_i\cdot\mathbf{y}_i} e^{i(\mathbf{p}+\mathbf{p}_i-\mathbf{p}')\cdot\mathbf{y}'_i} \sum_{L=S}^{T} F_L(\mathbf{p},\mathbf{p}_i,\mathbf{p}')(\lambda^L \otimes \lambda_L)$$

.

$$= \int \frac{d^3p}{(2\pi)^3}\frac{d^3p'}{(2\pi)^3}\frac{d^3p_i}{(2\pi)^3} e^{-i\mathbf{p}\cdot(\mathbf{y}_i-\mathbf{x})} e^{i\mathbf{p}'\cdot(\mathbf{x}'-\mathbf{y}'_i)} e^{-i\mathbf{p}_i\cdot(\mathbf{y}'_i-\mathbf{y}_i)} \sum_{L=S}^{T} F_L(\mathbf{p},\mathbf{p}_i,\mathbf{p}')(\lambda^L \otimes \lambda_L). \tag{2.60}$$

Substituting Eq. (2.60) into Eq. (2.57) results in

$$\begin{aligned}\mathcal{M} &= \sum_{i=1}^{A}\Delta_i\sum_{L=S}^{T}\int d^3x\, d^3x' d^3y_i d^3y_i' \frac{d^3p}{(2\pi)^3}\frac{d^3p'}{(2\pi)^3}\frac{d^3p_i}{(2\pi)^3} e^{-i\mathbf{p}\cdot(\mathbf{y}_i-\mathbf{x})} e^{i\mathbf{p}'\cdot(\mathbf{x}'-\mathbf{y}_i')} e^{-i\mathbf{p}_i\cdot(\mathbf{y}_i'-\mathbf{y}_i)} \\ &\times\left[\bar{\psi}^{(-)}(\mathbf{x}',\mathbf{k}',\hat{\mathbf{i}}',s')\otimes\bar{\Phi}_f(\mathbf{y}_1',...,\mathbf{y}_i',...,\mathbf{y}_A')\right] F_L(\mathbf{p},\mathbf{p}_i,\mathbf{p}')(\lambda^L\otimes\lambda_L) \\ &\times\left[\psi^{(+)}(\mathbf{x},\mathbf{k},\hat{\mathbf{i}},s)\otimes\Phi_i(\mathbf{y}_1,...,\mathbf{y}_i,...,\mathbf{y}_A)\right]. \end{aligned} \tag{2.61}$$

The relativistic free NN scattering amplitudes are normally extracted from free NN scattering experiments via a suitable phase shift analysis, such as the well known Arndt phases [28]. The explicit dependence of $\hat{F}$ on the 'local' momenta $\mathbf{p},\mathbf{p}_i$ and $\mathbf{p}'$ in Eq. (2.61) is thereby replaced by the corresponding asymptotic values $\mathbf{k},\mathbf{K}_i$ and $\mathbf{k}'$. Hence we make the replacement

$$F_L(\mathbf{p},\mathbf{p}_i,\mathbf{p}') \longrightarrow F_L(\mathbf{k},\mathbf{K}_i,\mathbf{k}'). \tag{2.62}$$

The only dependence on the momenta $\mathbf{p},\mathbf{p}_i$ and $\mathbf{p}'$ are now buried in the exponentials and we can systematically perform the integrals over these variables, i.e.

$$\int d^3p\; e^{-i\mathbf{p}\cdot(\mathbf{y}_i-\mathbf{x})} = (2\pi)^3\delta(\mathbf{y}_i-\mathbf{x}). \tag{2.63}$$

The result is a product of delta functions, i.e.

$$\delta(\mathbf{x}'-\mathbf{y}_i')\delta(\mathbf{y}_i-\mathbf{x})\delta(\mathbf{y}_i'-\mathbf{y}_i). \tag{2.64}$$

Eq. (2.61) becomes

$$\begin{aligned}\mathcal{M} &= \sum_{i=1}^{A}\Delta_i\sum_{L=S}^{T}\int d^3x\, d^3x' d^3y_i d^3y_i' \delta(\mathbf{x}'-\mathbf{y}_i')\delta(\mathbf{y}_i-\mathbf{x})\delta(\mathbf{y}_i'-\mathbf{y}_i) \\ &\times\left[\bar{\psi}^{(-)}(\mathbf{x}',\mathbf{k}',\hat{\mathbf{i}}',s')\otimes\bar{\Phi}_f(\mathbf{y}_1',...,\mathbf{y}_i',...,\mathbf{y}_A')\right] \\ &\times F_L(\mathbf{k},\mathbf{K}_i,\mathbf{k}')(\lambda^L\otimes\lambda_L)\left[\psi^{(+)}(\mathbf{x},\mathbf{k},\hat{\mathbf{i}},s)\otimes\Phi_i(\mathbf{y}_1,...,\mathbf{y}_i,...,\mathbf{y}_A)\right]. \end{aligned} \tag{2.65}$$

Performing the integration over $\mathbf{y}_i'$ in the three-dimensional delta function, Eq. (2.65) becomes

$$\begin{aligned}\mathcal{M} &= \sum_{i=1}^{A}\Delta_i\sum_{L=S}^{T}\int d^3x\, d^3x' d^3y_i \delta(\mathbf{x}'-\mathbf{y}_i)\delta(\mathbf{y}_i-\mathbf{x})\left[\bar{\psi}^{(-)}(\mathbf{x}',\mathbf{k}',\hat{\mathbf{i}}',s')\otimes\bar{\Phi}_f(\mathbf{y}_1',...,\mathbf{y}_i,...,\mathbf{y}_A')\right] \\ &\times F_L(\mathbf{k},\mathbf{K}_i,\mathbf{k}')(\lambda^L\otimes\lambda_L)\left[\psi^{(+)}(\mathbf{x},\mathbf{k},\hat{\mathbf{i}},s)\otimes\Phi_i(\mathbf{y}_1,...,\mathbf{y}_i,...,\mathbf{y}_A)\right]. \end{aligned} \tag{2.66}$$

Doing systematically the same for $\mathbf{y}_i$ and for $\mathbf{x}'$, Eq. (2.65) becomes

$$\mathcal{M} = \sum_{i=1}^{A} \Delta_i \sum_{L=S}^{T} \int d^3x \left[\bar{\psi}^{(-)}(\mathbf{x}, \mathbf{k}', \hat{\mathbf{i}}', s') \otimes \bar{\Phi}_f(\mathbf{y}'_1, ..., \mathbf{x}, ..., \mathbf{y}'_A) \right] F_L(\mathbf{k}, \mathbf{K}_i, \mathbf{k}')(\lambda^L \otimes \lambda_L)$$
$$\times \left[\psi^{(+)}(\mathbf{x}, \mathbf{k}, \hat{\mathbf{i}}, s) \otimes \Phi_i(\mathbf{y}_1, ..., \mathbf{x}, ..., \mathbf{y}_A) \right]. \tag{2.67}$$

By making use of the identity

$$(A \otimes B)(C \otimes D) = AC \otimes BD \tag{2.68}$$

repeatedly, Eq. (2.67) becomes

$$\mathcal{M} = \sum_{i=1}^{A} \Delta_i \sum_{L=S}^{T} F_L(\mathbf{k}, \mathbf{K}_i, \mathbf{k}') \int d^3x \left[\bar{\psi}^{(-)}(\mathbf{x}, \mathbf{k}', \hat{\mathbf{i}}', s') \lambda^L \psi^{(+)}(\mathbf{x}, \mathbf{k}, \hat{\mathbf{i}}, s) \right]$$
$$\left[\bar{\Phi}_f(\mathbf{y}'_1, ..., \mathbf{x}, ..., \mathbf{y}'_A) \lambda_L \Phi_i(\mathbf{y}_1, ..., \mathbf{x}, ..., \mathbf{y}_A) \right]. \tag{2.69}$$

The target space contains initial and final many-body wave functions and is still extremely complicated. We now make an additional approximation: We assume that the operator λ_L has a simple one-body form. We can then define the initial and final nuclear states in terms of Slater determinants as

$$\Phi_i = \frac{1}{\sqrt{A!}} \det \left[\phi_n^{(i)}(\mathbf{y}_k) \right]_{n=1..A,\, k=1..A}, \tag{2.70}$$
$$\Phi_f = \frac{1}{\sqrt{A!}} \det \left[\phi_m^{(f)}(\mathbf{y}_k) \right]_{m=1..A,\, k=1..A}. \tag{2.71}$$

The action of the operator λ_L, now acting on the i^{th} particle only, can then be written as

$$\int \prod_{j=1, j\neq i}^{A} d^3y_j \, \bar{\Phi}_f \lambda_L^{(i)} \Phi_i = \frac{1}{A!} \sum_{m=1}^{A} \sum_{n=1}^{A} (-1)^{2+m+n}$$
$$\times \int \prod_{j=1, j\neq i}^{A} d^3y_j \, \overline{\det \left[\phi_{g\neq m}^{(f)}(\mathbf{y}_{k\neq i}) \right]} \det \left[\phi_{h\neq n}^{(i)}(\mathbf{y}_{\ell\neq i}) \right]$$
$$\times \bar{\phi}_m^{(f)}(\mathbf{y}_i) \lambda_L^{(i)} \phi_n^{(i)}(\mathbf{y}_i). \tag{2.72}$$

The initial and final nuclear states now differ only by a single one-particle state for example, state number 1. This then becomes

$$\begin{aligned}\int \prod_{j=1,j\neq i}^{A} d^3y_j\ \bar{\Phi}_f \lambda_L^{(i)} \Phi_i &= \frac{(A-1)!}{A!} \sum_{m=1}^{A}\sum_{n=1}^{A} \delta_{m1}\delta_{n1}\ \bar{\phi}_m^{(f)}(\mathbf{y}_i)\lambda_L^{(i)}\phi_n^{(i)}(\mathbf{y}_i) \\ &= \frac{1}{A}\bar{\phi}_1^{(f)}(\mathbf{y}_i)\lambda_L^{(i)}\phi_1^{(i)}(\mathbf{y}_i) \\ &= \frac{1}{A}\langle\Phi_f|\hat{\bar{\phi}}(\mathbf{x})\lambda_L\hat{\phi}(\mathbf{x})|\Phi_i\rangle, \end{aligned} \tag{2.73}$$

where $\hat{\phi}$ is the Heisenberg field operator and $\mathbf{y}_i \rightarrow \mathbf{x}$ from the preceding integrations. Now substituting Eq. (2.73) into Eq. (2.69) gives

$$\mathcal{M} = \sum_{i=1}^{A}\frac{\Delta_i}{A}\sum_{L=S}^{T}\int d^3x\ F_L(\mathbf{k},\mathbf{K}_i,\mathbf{k}')\left[\bar{\psi}^{(-)}(\mathbf{x},\mathbf{k}',\hat{\mathbf{i}}',s')\lambda^L\psi^{(+)}(\mathbf{x},\mathbf{k},\hat{\mathbf{i}},s)\right]$$

$$\langle\Phi_f|\hat{\bar{\phi}}(\mathbf{x})\lambda_L\hat{\phi}(\mathbf{x})|\Phi_i\rangle \tag{2.74}$$

and

$$\Delta_i = 1 \Rightarrow \sum_{i=1}^{A}\Delta_i = A. \tag{2.75}$$

Taking the complex conjugate for $\mathcal{M}$ results in

$$\mathcal{M}^* = \sum_{L'=S'}^{T'}\int d^3y\ F^*_{L'}(\mathbf{k},\mathbf{K}_i,\mathbf{k}')\left[\bar{\psi}^{(+)}(\mathbf{y},\mathbf{k}',\hat{\mathbf{i}}',s')\overline{\lambda^{L'}}\psi^{(-)}(\mathbf{y},\mathbf{k},\hat{\mathbf{i}},s)\right]\langle\Phi_i|\hat{\bar{\phi}}(\mathbf{y})\bar{\lambda}_L\hat{\phi}(\mathbf{y})|\Phi_f\rangle. \tag{2.76}$$

Substituting Eqs. (2.74) and (2.76) into Eq. (2.25) results in

$$\frac{d\sigma}{dE'd\Omega'} = -\frac{1}{\pi}\ K\ \mathrm{Im}\left[\sum_{L,L'=S}^{T} F_L(\mathbf{k},\mathbf{k}',\mathbf{K})F^*_{L'}(\mathbf{k},\mathbf{k}',\mathbf{K})\int d^3x\ d^3y\ \mathcal{H}^{LL'}(\mathbf{x},\mathbf{y})\Pi_{LL'}(\mathbf{x},\mathbf{y},\omega)\right]. \tag{2.77}$$

In Eq. (2.77) the projectile tensor $\mathcal{H}^{LL'}(\mathbf{x},\mathbf{y})$ is defined as

$$\mathcal{H}^{LL'}(\mathbf{x},\mathbf{y}\ ) = \left[\bar{\psi}^{(-)}(\mathbf{x},\mathbf{k}',\hat{\mathbf{i}}',s')\lambda^L\psi^{(+)}(\mathbf{x},\mathbf{k},\hat{\mathbf{i}},s)\right]\left[\bar{\psi}^{(+)}(\mathbf{y},\mathbf{k},\hat{\mathbf{i}},s)\overline{\lambda^{L'}}\psi^{(-)}(\mathbf{y},\mathbf{k}',\hat{\mathbf{i}}',s')\right] \tag{2.78}$$

and the polarization tensor $\Pi_{LL'}(\mathbf{x},\mathbf{y},\omega)$ is defined as

$$\begin{aligned}\Pi_{LL'}(\mathbf{x},\mathbf{y},\omega) &= \sum_n \frac{\langle n|\hat{\bar{\phi}}(\mathbf{x})\lambda_L\hat{\phi}(\mathbf{x})|\ 0\rangle\langle\ 0|\hat{\bar{\phi}}(\mathbf{y})\overline{\lambda_{L'}}\hat{\phi}(\mathbf{y})|n\rangle}{\omega-(E_n-E_0)+i\epsilon} \\ &\quad + \frac{\langle\ n|\hat{\bar{\phi}}(\mathbf{y})\overline{\lambda_{L'}}\hat{\phi}(\mathbf{y})|0\rangle\langle 0|\hat{\bar{\phi}}(\mathbf{x})\lambda_L\hat{\phi}(\mathbf{x})|\ n\rangle}{\omega+(E_n-E_0)-i\epsilon}.\end{aligned} \tag{2.79}$$

In Eq. (2.79)

- The second term has been added in order to write the polarization tensor in terms of the time-ordered product. Since the energy transferred to the nucleus is always positive, it will not contribute [29].
- $|0\rangle$ and $|n\rangle$ represent the initial and final states of the target nucleus, respectively.
- $\overline{\lambda_{L'}} = \gamma^0\lambda_{L'}^\dagger\gamma^0$

As will be shown in a subsequent section, the polarization tensor in the nuclear matter approximation Eq. (2.79) can be written as

$$\Pi_{LL'}(\mathbf{x},\mathbf{y},\omega) = \int \frac{d^3q'}{(2\pi)^3} e^{-i\mathbf{q}'\cdot(\mathbf{x}-\mathbf{y})}\Pi_{LL'}(\mathbf{q}',\omega). \tag{2.80}$$

Substituting Eq. (2.80) into Eq. (2.77) gives

$$\frac{d\sigma}{dE'd\Omega'} = -\frac{1}{\pi}\ K\ \mathrm{Im}\left[\sum_{L,L'=S}^{T} F_L(\mathbf{k},\mathbf{k}',\mathbf{K})F^*_{L'}(\mathbf{k},\mathbf{k}',\mathbf{K})\int\frac{d^3q'}{(2\pi)^3}\mathcal{H}^{LL'}(\mathbf{q}')\Pi_{LL'}(\mathbf{q}',\omega)\right]. \tag{2.81}$$

Eq. (2.81) is our main result for this section. It is the double differential cross section written as a contraction of the hadronic tensor $\mathcal{H}^{LL'}$ and the polarization tensor $\Pi_{LL'}$. The hadronic tensor contains all the information pertaining to the projectile and the ejectile nucleons. The nuclear distortions are built into this quantity and will be discussed in the next section.

In the next section we will look in detail at the calculation of the hadronic tensor, first with plane waves and then distorted waves. The analysis is rather detailed as the computation of the hadronic tensor using eikonal distorted waves is the main focus of the thesis. All we need to do now is write the integral in Eq. (2.81) in the form we will use in the calculations. The integration over the transfer momentum $\mathbf{q}'$ is transformed into spherical coordinates and each integration variable rescaled to lie

within the interval [0,1]. We thus write

$$\frac{d\sigma}{dE'd\Omega'} = -\frac{1}{\pi}\,K\,\mathrm{Im}\left[\sum_{L,L'=S}^{T} F_L(\mathbf{k},\mathbf{k}',\mathbf{K})F_L^*(\mathbf{k},\mathbf{k}',\mathbf{K})\int_0^1 q^2dq\int_0^1 \sin\theta_q d\theta_q\int_0^1 d\phi_q \right.$$
$$\left.\frac{1}{4\pi}(q_{max}-q_{min})\mathcal{H}^{LL'}(q,\theta_q,\phi_q)\;\Pi_{LL'}(q,\theta_q,\phi_q,\omega)\right] \tag{2.82}$$

in which we have made the replacement

$$q' = (q_{max}-q_{min})q + q_{min}, \tag{2.83}$$

$$\theta'_q = \pi\;\theta_q, \tag{2.84}$$

$$\phi'_q = 2\pi\;\phi_q \tag{2.85}$$

2.1.3.1 In summary

To end this section we summarize the development path to Eq. (2.81). We showed in the beginning of this chapter that we can relate the polarized double differential cross section to the product of the invariant matrix element and a kinematic factor. The kinematic factor describe the kinematics for the quasielastic scattering reaction in the center-of-mass frame. The invariant matrix element in turn contain the dynamics of the scattering process.

Starting with the most basic form of the matrix element, we reduced the many-body scattering problem to a two-body scattering problem using the SPVAT representation of the NN scattering operator $\hat{F}$ that was successfully used in proton-nucleus scattering reactions [5, 10, 15, 17, 27]. The scattering operator is formulated in momentum space, however one normally evaluates the NN amplitudes at the asymptotic momenta. These amplitudes are then completely determined by free scattering data [28]. Replacing the amplitudes with their respective asymptotic momenta values allowed us to perform the integrations over the local momenta. The remaining integrations over the space coordinates were performed and the invariant matrix element was written in a form containing a projectile-ejectile part and a target space part. Taking the product of the matrix element and its complex conjugate and applying the nuclear matter approximation to the target tensor resulted in the form of Eq. (2.81).

The compact expression for the double differential cross section given in Eq. (2.82) hides the extreme difficulty of its numerical implementation. Writing the cross section as a contraction of two tensors is analogous to what is normally done in elementary particle physics. It is a standard text book derivation to find that, for example in the case of two-body electron-proton scattering, the cross section is the contraction between a leptonic and hadronic tensor. In that case all the complexity is encoded in the hadronic tensor. Eq. (2.82) has a similar structure but the complexity greatly increases due to a number of reasons:

TABLE 2.1: *Grouping of ranks of target polarizations based on the Lorentz indices needed to specify a particular polarization.*

rank		Polarization tensors			
0	:	Π_{SS}	Π_{SP}	Π_{PS}	Π_{PP}
1	:	Π_{SV}	Π_{SA}	Π_{PV}	Π_{PA}
	:	Π_{VS}	Π_{VP}	Π_{AS}	Π_{AP}
2	:	Π_{ST}	Π_{PT}	Π_{VV}	Π_{VA}
	:	Π_{AV}	Π_{AA}	Π_{TS}	Π_{TP}
3	:	Π_{VT}	Π_{AT}	Π_{TV}	Π_{TA}
4	:	Π_{TT}			

(i) In general the hadronic tensor should be calculated using distorted waves for the projectile and ejectile. The numerical complexity associated with using distorted waves as opposed to plane waves will be further expanded upon in Chapter 3. Here the standard choice that must be made is between a full partial wave expansion or an eikonal approximation.

(ii) The response of the nucleus to an external probe is described by the polarization tensor. This is an extremely complicated many-body quantity, but it can be evaluated systematically using various approximations.

(iii) The calculation of the multidimensional integrals d^3x, d^3y and d^3q significantly increases the numerical burden.

(iv) Even after an integration scheme has been chosen there are still issues related to accuracy and speed associated with any quadrature scheme.

(v) The large number of Lorentz indices which must be contracted. There are 25 in total since $L, L' \in \{S, P, V, A, T\}$. This is in contrast to, for example two-body electron-proton scattering, where one has to contract at most two Lorentz indices. In order to provide a systematic way of evaluating this contraction we classify the tensors according to the number of Lorentz indices they have. This is called the rank of the tensor and the combinations which may be made up from the set $\{S, P, V, A, T\}$ by taking pairs are classified according to the rank in Table 2.1.

The factors mentioned above have been significant in retarding progress in the analysis of quasielastic proton-nucleus scattering using distorted waves. However, the availability of modern software like MATLAB (with its powerful fitting and interpolation functions) together with the use of cluster computing techniques, have made it possible to finally calculate the distorted wave cross sections in a reasonable amount of time. By writing the cross section in a modular fashion each component can

be separately analyzed and studied. Any assumptions which go into the calculation can therefore be easily and honestly identified.

2.1.4 Hadronic tensor

The polarized double differential cross section is given by

$$\frac{d\sigma}{dE'd\Omega'} = -\frac{1}{\pi}K\ \mathrm{Im}\left[\sum_{L,L'=S}^{T} F_L(\mathbf{k},\mathbf{k}',\mathbf{K})F^*_{L'}(\mathbf{k},\mathbf{k}',\mathbf{K})\int\frac{d^3q}{(2\pi)^3}\mathcal{H}^{LL'}(\mathbf{q}),\Pi_{LL'}(\mathbf{q},\omega)\right], \tag{2.86}$$

where

$$\begin{aligned}
\mathcal{H}^{LL'}(\mathbf{q}) &= \int d^3x\ d^3y\ e^{-i\mathbf{q}\cdot(\mathbf{x}-\mathbf{y})}\mathcal{H}^{LL'}(\mathbf{x},\mathbf{y}) \\
&= \int d^3x\ e^{-i\mathbf{q}\cdot\mathbf{x}}\left[\bar{\psi}^{(-)}(\mathbf{x},\mathbf{k}',\hat{\mathbf{i}}',s')\lambda^L\psi^{(+)}(\mathbf{x},\mathbf{k},\hat{\mathbf{i}},s)\right] \\
&\quad\times\int d^3y\ e^{i\mathbf{q}\cdot\mathbf{y}}\left[\bar{\psi}^{(+)}(\mathbf{y},\mathbf{k},\hat{\mathbf{i}},s)\overline{\lambda^{L'}}\psi^{(-)}(\mathbf{y},\mathbf{k}',\hat{\mathbf{i}}',s')\right] \qquad (2.87)\\
&= \mathcal{H}^L(\mathbf{q})[\mathcal{H}^{L'}(\mathbf{q})]^*. \qquad (2.88)
\end{aligned}$$

In this section we will concern ourselves with the calculation of the hadronic tensor $\mathcal{H}^{LL'}$ which is given in the nuclear approximation by Eq. (2.87). The hadronic tensor contains the incoming and outgoing distorted wave functions. To compute one factor of Eq. (2.88) is computationally very demanding in a distorted wave formulation. We will highlight this complexity soon. But first it is important that we are able to use Eq. (2.86) to calculate the polarized double differential cross section. In order to do this, we will first derive an analytical expression for Eq. (2.86) using Dirac plane waves. We will however use as an example only, the scalar-scalar interaction of the full NN-scattering operator for quasielastic scattering.

2.1.4.1 Plane wave limit

We now discuss calculating the polarized double differential cross section in the plane wave limit. The position space representation of the incoming Dirac plane wave is given by

$$\psi^{(+)}(\mathbf{x},\mathbf{k},\hat{\mathbf{i}},s) = U(\mathbf{k},\hat{\mathbf{i}},s)e^{i\mathbf{k}\cdot\mathbf{x}} \tag{2.89}$$

in which the Dirac spinor is

$$U(\mathbf{k},\hat{\mathbf{i}},s) = \sqrt{\frac{E_\mathbf{k}+M}{2M}}\begin{bmatrix}\phi(\hat{\mathbf{i}},s)\\ \dfrac{\vec{\sigma}\cdot\mathbf{k}}{E_\mathbf{k}+M}\phi(\hat{\mathbf{i}},s)\end{bmatrix} \tag{2.90}$$

with $E_{\mathbf{k}}^2 = \mathbf{k}^2 + M^2$. The Pauli spinor $\phi(\hat{\mathbf{i}}, s)$ is defined as

$$\phi(\hat{\mathbf{i}}, s) = \sum_{s_z} \mathcal{D}^{(1/2)}_{s_z s}(\hat{\mathbf{i}})\chi_s \tag{2.91}$$

in which $\mathcal{D}^{(1/2)}_{s_z s}$ is the Wigner-D function. The base spin vectors are for spin-up

$$\chi_{s_z=\frac{1}{2}} = \begin{pmatrix} 1 \\ 0 \end{pmatrix} \tag{2.92a}$$

and spin-down

$$\chi_{s_z=-\frac{1}{2}} = \begin{pmatrix} 0 \\ 1 \end{pmatrix}. \tag{2.92b}$$

The polarized two-component spinor is a linear combination of Eqs. (2.92a) and (2.92b) defined as

$$\chi_s = \chi_{s_z=\frac{1}{2}} + \chi_{s_z=-\frac{1}{2}}. \tag{2.93}$$

The orientation of the spin polarization is obtained by performing a Wigner-D transformation on χ_s. We begin by defining the longitudinal, sideways and normal polarization directions $\hat{\mathbf{l}}$, $\hat{\mathbf{s}}$ and $\hat{\mathbf{n}}$ respectively. The Wigner-D function is a 2×2 matrix given in Ref. [30] as

$$\mathcal{D}^{(1/2)}(\alpha, \beta, \gamma) = \exp\left(\frac{-i\sigma_3\alpha}{2}\right)\exp\left(\frac{-i\sigma_2\beta}{2}\right)\exp\left(\frac{-i\sigma_3\gamma}{2}\right) \tag{2.94}$$

$$= \begin{bmatrix} e^{-i(\alpha+\gamma)/2}\cos\frac{\beta}{2} & -e^{-i(\alpha-\gamma)/2}\sin\frac{\beta}{2} \\ e^{i(\alpha-\gamma)/2}\sin\frac{\beta}{2} & e^{i(\alpha+\gamma)/2}\cos\frac{\beta}{2} \end{bmatrix}, \tag{2.95}$$

in which α, β and γ are the Euler angles and the quantization axis $\hat{\mathbf{i}}$ represent the spin polarizations $\hat{\mathbf{l}}$, $\hat{\mathbf{s}}$ and $\hat{\mathbf{n}}$. These polarizations are related to the Euler angles used in Eq. (2.95) as follows for

$$\hat{\mathbf{l}}: \quad \alpha = 0 \qquad \beta = \theta_{cm} \qquad \gamma = 0, \tag{2.96}$$

$$\hat{\mathbf{s}}: \quad \alpha = 0 \quad \beta = \pi/2 + \theta_{cm} \quad \gamma = 0, \tag{2.97}$$

$$\hat{\mathbf{n}}: \quad \alpha = \pi/2 \qquad \beta = \pi/2 \qquad \gamma = 0. \tag{2.98}$$

Substituting Eqs. (2.96-2.98) into Eq. (2.95) gives

$$\mathcal{D}^{(1/2)}(\hat{\mathbf{l}}) = \begin{bmatrix} \cos\frac{\beta}{2} & -\sin\frac{\beta}{2} \\ \sin\frac{\beta}{2} & \cos\frac{\beta}{2} \end{bmatrix} \tag{2.99}$$

$$\mathcal{D}^{(1/2)}(\hat{\mathbf{s}}) = \begin{bmatrix} \frac{1}{\sqrt{2}}\left(\cos\frac{\beta}{2} - \sin\frac{\beta}{2}\right) & \frac{1}{\sqrt{2}}\left(\sin\frac{\beta}{2} + \cos\frac{\beta}{2}\right) \\ \frac{1}{\sqrt{2}}\left(\sin\frac{\beta}{2} + \cos\frac{\beta}{2}\right) & \frac{1}{\sqrt{2}}\left(\cos\frac{\beta}{2} - \sin\frac{\beta}{2}\right) \end{bmatrix} \tag{2.100}$$

$$\mathcal{D}^{(1/2)}(\hat{\mathbf{n}}) = \begin{bmatrix} \frac{1-i}{2} & -\frac{1-i}{2} \\ \frac{1+i}{2} & \frac{1+i}{2} \end{bmatrix}. \tag{2.101}$$

The outgoing Dirac plane wave is given by

$$\psi^{(-)}(\mathbf{x}, \mathbf{k}', \hat{\mathbf{i}}', s') = U(\mathbf{k}', \hat{\mathbf{i}}', s')e^{i\mathbf{k}'\cdot\mathbf{x}}. \tag{2.102}$$

Substituting Eqs. (2.89) and (2.102) into $\mathcal{H}^L(\mathbf{q})$ gives

$$\mathcal{H}^L(\mathbf{q}) = \int d^3x\, e^{-i\mathbf{q}\cdot\mathbf{x}}\, e^{i\mathbf{k}\cdot\mathbf{x}}\, e^{-i\mathbf{k}'\cdot\mathbf{x}}\, \bar{U}(\mathbf{k}', \hat{\mathbf{i}}', s')\lambda^L U(\mathbf{k}, \hat{\mathbf{i}}, s). \tag{2.103}$$

The only $\mathbf{x}$ dependence resides in the exponentials and thus the d^3x integral can be done and results in

$$\mathcal{H}^L(\mathbf{q}) = (2\pi)^3\delta(\mathbf{k} - \mathbf{k}' - \mathbf{q})\bar{U}(\mathbf{k}', \hat{\mathbf{i}}', s')\lambda^L U(\mathbf{k}, \hat{\mathbf{i}}, s). \tag{2.104}$$

The hadronic tensor in the plane wave case then becomes

$$\mathcal{H}^{LL'}(\mathbf{q}) = \left[(2\pi)^3\delta(\mathbf{k} - \mathbf{k}' - \mathbf{q})\right]^2 \left[\bar{U}(\mathbf{k}', \hat{\mathbf{i}}', s')\lambda^L U(\mathbf{k}, \hat{\mathbf{i}}, s)\right] \left[\bar{U}(\mathbf{k}, \hat{\mathbf{i}}, s)\overline{\lambda^{L'}} U(\mathbf{k}', \hat{\mathbf{i}}', s')\right]. \tag{2.105}$$

As mentioned before, we concern ourselves with only the rank-0 set of polarizations in this work. As an illustration therefore, we derive the analytical expression for the polarized double differential cross section for the SS case. We therefore proceed with the analysis whereby we select $L = S \rightarrow \lambda^{[L=S]} = I_4$. Eq. (2.105) can be computed either numerically or by means of trace techniques. Using the latter we arrive at

$$\mathcal{H}^{SS}(\mathbf{q}) = \left[(2\pi)^3\delta(\mathbf{k} - \mathbf{k}' - \mathbf{q})\right]^2 \frac{1}{16M^2}\left[4k\cdot k' + 4k\cdot s'k'\cdot s - 4s\cdot s'(k\cdot k' + M^2) + 4M^2\right]. \tag{2.106}$$

We substitute Eq. (2.106) into Eq. (2.86) and perform the integration over $\mathbf{q}$. We arrive at

$$\left(\frac{d\sigma}{dE'd\Omega'}\right)_{PW} = -\frac{1}{\pi}K\left(F_S(\mathbf{k},\mathbf{k}',\mathbf{K})F_S^*(\mathbf{k},\mathbf{k}',\mathbf{K})\right)\left(\frac{3\pi^2 A}{2k_F^3}\right)16M^2\left[4k\cdot k' + 4k\cdot s'k'\cdot s - 4s\cdot s'(k\cdot k' + M^2) + 4M^2\right]\left[\mathrm{Im}\left\{\Pi_{SS}(\mathbf{k}-\mathbf{k}',\omega)\right\}\right], \tag{2.107}$$

where k_F^3 is the Fermi momentum. The analytical expression (see derivation in Section 2.1.5) for $\mathrm{Im}\left\{\Pi_{SS}\right\}$ is [29]

$$\mathrm{Im}\ \left\{\Pi_{SS}(q)\right\} = \frac{1}{8\pi q}\left(4M^{*2} - q^2\right)(E_F^* - E^*), \tag{2.108}$$

where the four-vector $q^2 = \omega^2 - \mathbf{q}^2$ and

$$E^* = \min\left(E_F^*, E_{max}\right) \tag{2.109}$$

in which

$$E_{max} = \max\left(E_F^* - \omega, \frac{1}{2}\left[|\mathbf{q}|\left(1 - \frac{4M^{*2}}{q^2}\right)^{\frac{1}{2}} - \omega\right]\right). \tag{2.110}$$

The quantity E_F^* is the energy at the Fermi momentum $\mathbf{k}_F$ given by

$$E_F^* = \sqrt{\mathbf{k}_F^2 + M^{*2}}, \tag{2.111}$$

where M^* is the reduced mass [7]. Eq. (2.107) provides us with an analytical solution to compute the polarized double differential cross section in the plane wave limit where we have included the SS interaction only. We will now turn the attention to the use of distorted wave functions to compute $\mathcal{H}^L$.

2.1.4.2 Distorted partial wave

One of the main goals of this thesis is to use distorted waves for the projectile and ejectile in quasielastic proton-nucleus scattering. In this respect it represents a significant improvement over previous work ([7, 8, 9, 11, 12, 10, 31]) which all utilized the plane wave impulse approximation. When one considers distorted waves then a choice must be made between a full partial wave expansion or some approximation which retains the essentials of distortion effects, whilst still offering a benefit in terms of speed of calculation and accuracy.

In this work we adopted the eikonal approximation as a means to realistically include distortion effects. To put it in perspective we show, below, the expression for the full partial wave expansion of

the projectile wave function [1, 15, 32, 33]

$$\psi^{(+)}(\mathbf{x},\mathbf{k},\hat{\mathbf{i}},s) = \frac{4\pi}{kx}\left(\frac{E(\mathbf{k})+M}{2M}\right)^{\frac{1}{2}}\sum_{ljm_l s_z} i^l e^{i\delta_{lj}}\langle l\tfrac{1}{2}ms_z|j,m+s_z\rangle\,\mathcal{D}^{(\frac{1}{2})}_{s_z s}(\hat{\mathbf{i}})\,Y^*_{lm}(\hat{\mathbf{x}}) \times\begin{bmatrix} g_{lj}(kx)\mathcal{Y}_{lj,m+s_z}(\hat{\mathbf{x}}) \\ if_{2j-l,j}(kx)\mathcal{Y}_{2j-l,j,m+s_z}(\hat{\mathbf{x}})\end{bmatrix}, \tag{2.112}$$

with a similar expression for the ejectile wave function. In the above equation

- $x = |\mathbf{x}|$ and $k = |\mathbf{k}|$,
- $\langle l\frac{1}{2}m_l m_s|jm_j\rangle$ is a Clebsch-Gordon coefficient,
- $Y_{lm}(\hat{\mathbf{x}})$ is a spherical harmonic function,
- $g_{lj}(z)$ and $f_{lj}(z)$ are radial wave function solutions of Schrodinger-like radial differential equations that contain the central, spin-orbit and Darwin potentials [1, 32],
- $\mathcal{Y}_{lj\mu}(\hat{\mathbf{x}})$ is a spin-spherical harmonic function given by

$$\mathcal{Y}_{lj\mu}(\hat{\mathbf{x}}) = \sum_{t'_z}\langle l\frac{1}{2},\mu-t'_z,t'_z|j\mu\rangle Y_{l,\mu-t'_z}(\hat{\mathbf{x}})\chi_{t'_z}, \tag{2.113}$$

- the relativistic Coulomb phase shift δ_{lj} is an implicit function of the projectile and target masses, the projectile and target atomic numbers and the momentum $\mathbf{k}$.

From Eq. (2.112) one can see that the incident projectile has a sum over l up to some l_{max} where typically the amount of partial wave needed to give a relatively accurate description of the distortion effects is a function of the physical size of the target nucleus, the range of the interaction and the energies of the colliding particles. For instance, one or two partial waves will suffice in some scattering problems, whereas others will require hundreds of partial waves. Coupled with this is a sum over $j = |l-\frac{1}{2}|, l+\frac{1}{2}$. However, one has a sum over l in the ejectile wave function as well, together with a sum over j and (the source of considerable increase in computation) over m_l (the projection over l). The projectile and ejectile wave functions are therefore three-dimensional functions which must be evaluated for every combination of quantum numbers. In addition, one has to integrate over all space as well as the final integral over $\mathbf{q}$. Note also that in the distorted wave case the functions g_{lj} and f_{lj} are not analytical functions but must be stored in large arrays (keeping in mind the large number of quantum number combinations) further adding to the numerical burden. Together with the strong oscillatory nature of the integrand and convergence issues of the integral, it quickly becomes clear that a full partial wave expansion is an extremely numerically intensive operation. In contrast, the eikonal approximation offers a semi-analytical form closely resembling the plane wave expression and with the

contribution of distortion effects neatly isolated in a multiplicative factor. The eikonal approximation has also been fruitfully applied to the exclusive $(p, 2p)$ reaction [17, 18] and we will therefore use it in our calculations as well to provide a realistic, yet computationally efficient, method to incorporate distortion effects in quasielastic proton-nucleus scattering. This motivates why we settled on the eikonal approximation discussed below in Section. 2.1.4.3.

2.1.4.3 The Dirac eikonal distorted wave functions

The purpose of this section is to derive expressions for the incoming and outgoing distorted waves $\psi^{(+)}$ and $\psi^{(-)}$ in the eikonal approximation. Eikonal distorted wave functions introduced by Glauber removed the computational burden of dealing with partial waves at high energies and have since been improved upon to apply to a wide range of scattering problems [34, 35, 36, 37, 38, 39, 40, 41, 42]. For our application, we follow the familiar procedure described by Amado to derive the distorted wave functions [43]. We begin by considering the time independent Dirac equation for a projectile with energy $E = \sqrt{k^2 + M^2}$ subject to local Lorentz scalar $V_s(r) \equiv V_s$ and vector $V_v(r) \equiv V_v$ potentials

$$[\vec{\alpha} \cdot \hat{\mathbf{p}} + \beta M + \beta V_s + V_v]\psi^{(+)}_{\mathbf{k},s}(\mathbf{r}) = E\psi^{(+)}_{\mathbf{k},s}(\mathbf{r}), \tag{2.114}$$

where in Eq. (2.114)

$$\hat{\mathbf{p}} = -i\vec{\nabla}, \tag{2.115}$$

$$\vec{\alpha} = \gamma^0 \cdot \vec{\gamma} = \begin{pmatrix} 0 & \vec{\sigma} \\ \vec{\sigma} & 0 \end{pmatrix}, \tag{2.116}$$

$$\beta = \gamma^0 = \begin{pmatrix} I_2 & 0 \\ 0 & -I_2 \end{pmatrix}. \tag{2.117}$$

The four component Dirac spinor is decomposed into its upper, $u^{(+)}_{\mathbf{k},s}(\mathbf{r}) \equiv u_+$, and lower, $l^{(+)}_{\mathbf{k},s}(\mathbf{r}) \equiv l_+$, Pauli spinor components

$$\psi^{(+)}_{\mathbf{k},s}(\mathbf{r}) = \begin{bmatrix} u^{(+)}_{\mathbf{k},s}(\mathbf{r}) \\ l^{(+)}_{\mathbf{k},s}(\mathbf{r}) \end{bmatrix} \equiv \begin{bmatrix} u_+ \\ l_+ \end{bmatrix}. \tag{2.118}$$

Substituting these relationships into Eq. (2.114) produces a pair of coupled differential equations

$$\begin{aligned} (E - M - V_s - V_v)u_+ + i\vec{\sigma} \cdot \vec{\nabla} l_+ &= 0, \\ (E + M + V_s - V_v)l_+ + i\vec{\sigma} \cdot \vec{\nabla} u_+ &= 0. \end{aligned} \tag{2.119}$$

Expressing l_+ in terms of u_+

$$l_+ = \left(\frac{\vec{\sigma} \cdot \hat{\mathbf{p}}}{E + M + V_s - V_v} \right) u_+, \tag{2.120}$$

we can write the Dirac equation in terms of the upper component as

$$(\vec{\sigma} \cdot \hat{\mathbf{p}}) \left(\frac{\vec{\sigma} \cdot \hat{\mathbf{p}}}{E + M + V_s - V_v} \right) u_+ - (E - M - V_s - V_v)\, u_+ = 0. \tag{2.121}$$

It can be shown that we can write Eq. (2.121) as a Schrödinger like equation for the upper component spinor, namely

$$\left[\frac{\hat{\mathbf{p}}^{\,2}}{2M} + V_c + V_{so} \left(\vec{\sigma} \cdot \mathbf{L} - i\mathbf{r} \cdot \hat{\mathbf{p}} \right) \right] u^{(+)}_{\mathbf{k},s}(\mathbf{r}) = \frac{k^2}{2M} u^{(+)}_{\mathbf{k},s}(\mathbf{r}) \tag{2.122}$$

with the central V_c and spin-orbit V_{so} potentials defined as

$$V_c(r) = V_s + \frac{E}{M} V_v + \frac{V_s^2 - V_v^2}{2M}, \tag{2.123}$$

$$V_{so}(r) = \frac{1}{2M[E + M + V_s - V_v]} \frac{1}{r} \frac{d}{dr} [V_v - V_s]. \tag{2.124}$$

At this point the derivation has been completely general and to solve Eq. (2.122) in the 'eikonal limit' the momentum transfer $\mathbf{Q}$ is defined in terms of the initial and final momenta $\mathbf{k}$ and $\mathbf{k}'$ as

$$\mathbf{Q} = \mathbf{k} - \mathbf{k}' \tag{2.125}$$

and the average momentum as

$$\mathbf{K} = \frac{1}{2} \left(\mathbf{k} + \mathbf{k}' \right). \tag{2.126}$$

Following Glauber [34] one makes use of the small angle approximation whereby the quadratic momentum operator $\hat{\mathbf{p}}^2$ in Eq. (2.122) is replaced by

$$\hat{\mathbf{p}}^2 = [(\hat{\mathbf{p}} - \mathbf{K}) + \mathbf{K}]^2 \approx 2\mathbf{K} \cdot \hat{\mathbf{p}} - K^2. \tag{2.127}$$

Replacing $\hat{\mathbf{p}}^2$ in Eq. (2.122) with the expression in Eq. (2.127) results in

$$\left(\mathbf{K} \cdot \hat{\mathbf{p}} - K^2 + M \left[V_c + V_{so} \left(\vec{\sigma} \cdot [\mathbf{r} \times \hat{\mathbf{p}}] - i\mathbf{r} \cdot \hat{\mathbf{p}} \right) \right] \right) u^{(+)}_{\mathbf{k},s}(\mathbf{r}) = 0 \tag{2.128}$$

for the upper component wave function. Next we replace $\hat{\mathbf{p}}$ with $\mathbf{K}$ in the spin-orbit and Darwin terms

$$\left(\mathbf{K} \cdot \hat{\mathbf{p}} - K^2 + M \left[V_c + V_{so} \left(\vec{\sigma} \cdot [\mathbf{r} \times \mathbf{K}] - i\mathbf{r} \cdot \mathbf{K} \right) \right] \right) u^{(+)}_{\mathbf{k},s}(\mathbf{r}) = 0. \tag{2.129}$$

To find a solution to the differential equation above, one normally uses a trial function

$$u(\mathbf{r}) = A(\mathbf{r})e^{i\mathbf{k}\cdot\mathbf{r}}\chi_s,$$

which in the eikonal approximation reads

$$u^{(+)}_{\mathbf{k},s}(\mathbf{r}) = e^{i\mathbf{k}\cdot\mathbf{r}}e^{iS(\mathbf{r})}\chi_s. \tag{2.130}$$

Substituting Eq. (2.130) into Eq. (2.129) and solving for the eikonal phase $S(\mathbf{r})$ results in the differential equation

$$\mathbf{K}\cdot\vec{\nabla}S(\mathbf{r}) = -M\left[V_c + V_{so}\left(\vec{\sigma}\cdot[\mathbf{r}\times\mathbf{K}] - i\mathbf{r}\cdot\mathbf{K}\right)\right]. \tag{2.131}$$

To solve for $S(\mathbf{r})$, we choose our coordinate system in such a way that

$$\mathbf{K} = K\hat{\mathbf{z}}. \tag{2.132}$$

The dot product on the left hand side of Eq. (2.131) will be zero for the $\hat{\mathbf{x}}$ and $\hat{\mathbf{y}}$ directions but

$$K\frac{\partial}{\partial z}S(\mathbf{r}) = K\frac{d}{dz}S(\mathbf{r}) = -M\left[V_c + V_{so}\left(\vec{\sigma}\cdot[\mathbf{r}\times\mathbf{K}] - i\mathbf{r}\cdot\mathbf{K}\right)\right]. \tag{2.133}$$

Also, in the first term of the spin-orbit potential part

$$\mathbf{r}\times\mathbf{K} = (r_x\hat{\mathbf{x}} + r_y\hat{\mathbf{y}} + r_z\hat{\mathbf{z}})\times\mathbf{K} = (r_x\hat{\mathbf{x}} + r_y\hat{\mathbf{y}})\times\mathbf{K} = \mathbf{b}\times\mathbf{K}$$

and for the Darwin term

$$r_x\hat{\mathbf{x}}\cdot\mathbf{K} = r_y\hat{\mathbf{y}}\cdot\mathbf{K} = 0.$$

Using these relations we can solve for the incoming eikonal phase

$$S^{(+)}(\mathbf{b}, z) = -\frac{M}{K}\int_{-\infty}^{z} dz'\left(V_c + V_{so}\left[\vec{\sigma}\cdot(\mathbf{b}\times\mathbf{K}) - iKz'\right]\right). \tag{2.134}$$

It is worth discussing the choice of integration limits used in Eq. (2.134). A quick glance at the trial function indicates that the phase factor $A(\mathbf{r})$ must satisfy the boundary condition

$$A(\pm\infty) \to 1, \tag{2.135}$$

which in turn implies that

$$S(\pm\infty) \to 0. \tag{2.136}$$

This condition simply means that the distorted wave function must be equal to the plane wave in the absence of the scattering potentials far away from the nucleus. However, $S(z) \neq 0$ where the scattering

occurs due to the presence of the potentials. Hence

$$\int_{-\infty}^{z} dS(\mathbf{b}, z') = S(\mathbf{b}, z) - S(\mathbf{b}, -\infty) = S(\mathbf{b}, z) \neq 0. \tag{2.137}$$

It is appropriate at this point to mention the optical potentials used in this work. The complex optical potentials used were calculated using the procedure outlined by Ref. [44]. Here the standard Lorentz scalar-vector optical potential model of Dirac phenomenology is used. The scalar and vector potentials are parameterized by functions of the general form

$$V(r, E) = V_v(E) f_1(r, E, A) + i \left[W_{v1}(E) f_2(r, E, A) + W_{v2}(E) \frac{d}{dr} f_3(r, E, A) \right], \tag{2.138}$$

where the energy E is the total energy of the incident projectile divided by 1000 MeV in the proton-nucleus center-of-mass frame and A the atomic number of the target nucleus. The functions $f(r, E, A)$ are symmetrized Woods-Saxon potentials of the form

$$f(r, E, A) = \left(\left[1 + \exp\left((r - R(E, A))/z(E, A) \right) \right] \left[1 + \exp\left((r - R(E, A))/z(E, A) \right) \right] \right)^{-1} \tag{2.139}$$

in which R and z are E and A dependent geometry parameters. For our calculations we reproduce the scalar, vector, the effective central potential given in Eq. (2.123) and effective spin-orbit potentials given in Eq. (2.124) for ^{40}Ca at 497.5 MeV shown in FIG. 2.3.

The incoming wave function: The upper component Dirac wave function is related to the lower component by Eq. (2.120). We can then immediately write down the solution to Eq. (2.114) for the incoming Dirac distorted wave function $\psi^{(+)}(\mathbf{r})$ with momentum $\mathbf{k}$

$$\psi^{(+)}(\mathbf{r}, \mathbf{k}, \hat{\mathbf{i}}, s) = \sqrt{\frac{E_{\mathbf{k}} + M}{2M}} \begin{bmatrix} \mathbf{I}_2 \\ \dfrac{\vec{\sigma} \cdot \hat{\mathbf{p}}}{E_{\mathbf{k}} + M + V_s - V_v} \end{bmatrix} e^{i\mathbf{k}\cdot\mathbf{r}} e^{iS^{(+)}(\mathbf{r})} \phi(\hat{\mathbf{i}}, s), \tag{2.140}$$

where $\phi(\hat{\mathbf{i}}, s)$ in Eq. (2.140) is given by Eq. (2.91).

The eikonal phase $S^{(+)}(\mathbf{r})$ is a 2×2 matrix that acts on the Pauli spinor $\phi(\hat{\mathbf{i}}, s)$ in Eq. (2.140). The eikonal phase for the incoming distorted wave is given by Eq. (2.134). We can use the identity

$$\exp\left(\frac{-i\vec{\sigma} \cdot \mathbf{n}\alpha}{2} \right) = \mathbf{1} \cos\left(\frac{\alpha}{2} \right) - i\vec{\sigma} \cdot \mathbf{n} \sin\left(\frac{\alpha}{2} \right) \tag{2.141}$$

in Eq. (2.140) and expand the distorted wave function in full to read

$$\begin{aligned}\psi^{(+)}(\mathbf{r},\mathbf{k},\hat{\mathbf{i}},s) &= \sqrt{\frac{E_{\mathbf{k}}+M}{2M}}\begin{bmatrix}\mathbf{I}_2\\ \dfrac{\vec{\sigma}\cdot\hat{\mathbf{p}}}{E_{\mathbf{k}}+M+V_s-V_v}\end{bmatrix}e^{i\mathbf{k}\cdot\mathbf{r}}\\ &\times\exp\left(-\frac{M}{K}\left(i\int_{-\infty}^{z}dz'V_c(\mathbf{b},z')-\int_{-\infty}^{z}dz'V_{so}(\mathbf{b},z')Kz'\right)\right)\\ &\times\left\{\mathbf{I}_2\cos\left(\frac{M}{2K}\int_{-\infty}^{z}dz'V_{so}(\mathbf{b},z')\right)-i\vec{\sigma}\cdot\mathbf{n}\sin\left(\frac{M}{2K}\int_{-\infty}^{z}dz'V_{so}(\mathbf{b},z')\right)\right\}\\ &\times\phi(\hat{\mathbf{i}},s). \end{aligned}\tag{2.142}$$

The outgoing wave function: The outgoing distorted wave function, $\bar{\psi}^{(-)}(\mathbf{r})=\psi^{\dagger(-)}(\mathbf{r})\gamma^0$ is derived from the incoming distorted wave function by applying time reversal on the incoming wave function. If we let $\mathcal{T}$ denote the time reversal operator, we have

$$\psi^{(-)}(\mathbf{r},\mathbf{k}',\hat{\mathbf{i}}',s') = \mathcal{T}\left[\psi^{(+)}(\mathbf{r},\mathbf{k}',\hat{\mathbf{i}}',s')\right]\tag{2.143}$$

$$\begin{aligned}&= \mathcal{T}\left(\sqrt{\frac{E_{\mathbf{k}'}+M}{2M}}\begin{bmatrix}\mathbf{I}_2\\ \dfrac{\vec{\sigma}\cdot\hat{\mathbf{p}}}{E_{\mathbf{k}'}+M+V_s-V_v}\end{bmatrix}\right)\mathcal{T}\left(e^{i\mathbf{k}'\cdot\mathbf{r}}e^{iS^{(+)}(\mathbf{r})}\right)\\ &\quad\times\mathcal{T}\left(\phi(\hat{\mathbf{i}}',s')\right)\end{aligned}\tag{2.144}$$

$$\begin{aligned}&= \sqrt{\frac{E_{\mathbf{k}'}+M}{2M}}\begin{bmatrix}\mathbf{I}_2\\ \dfrac{-\vec{\sigma}\cdot-\hat{\mathbf{p}}}{E_{\mathbf{k}'}+M+V_s^*-V_v^*}\end{bmatrix}e^{(-i)(-\mathbf{k}')\cdot\mathbf{r}}e^{(-i)S^{(-)}(\mathbf{r})}\\ &\quad\times\sum_{s'_z}(-)^{\frac{1}{2}-s'_z}\left(\mathcal{D}^{(1/2)}_{s'_z s'}(\hat{\mathbf{i}}')\right)^*\chi_{-s'_z},\end{aligned}\tag{2.145}$$

which gives for the outgoing distorted wave function

$$\psi^{(-)}(\mathbf{r},\mathbf{k}',\hat{\mathbf{i}}',s')=\sqrt{\frac{E_{\mathbf{k}'}+M}{2M}}\begin{bmatrix}\mathbf{I}_2\\ \dfrac{\vec{\sigma}\cdot\hat{\mathbf{p}}}{E_{\mathbf{k}'}+M+V_s^*-V_v^*}\end{bmatrix}e^{i\mathbf{k}'\cdot\mathbf{r}}e^{-iS^{(-)}(\mathbf{r})}\tilde{\phi}(\hat{\mathbf{i}}',s'),\tag{2.146}$$

where the outgoing eikonal phase with incoming boundary conditions becomes

$$\begin{aligned} S^{(-)}(\mathbf{r}) &= \frac{M}{-K}\int_z^\infty dz' \left(V_c^* + V_{so}^*\left[-\vec{\sigma}\cdot(\mathbf{b}\times -\mathbf{K}) - (-i)(-K)z'\right]\right) \\ &= -\frac{M}{K}\int_z^\infty dz' \left(V_c^* + V_{so}^*\left[\vec{\sigma}\cdot(\mathbf{b}\times \mathbf{K}) - iKz'\right]\right). \end{aligned} \tag{2.147}$$

Finally, we need to take the Hermitian conjugate to get the outgoing distorted wave function in the eikonal limit

$$\left(\psi^{(-)}(\mathbf{r},\mathbf{k}',\hat{\mathbf{i}}',s')\right)^\dagger = \sqrt{\frac{E_{\mathbf{k}'}+M}{2M}}\phi^\dagger(\hat{\mathbf{i}}',s')e^{-i\mathbf{k}'\cdot\mathbf{r}}e^{iS^{(-)}(\mathbf{r})}\left[\mathbf{I}_2, \frac{\vec{\sigma}\cdot\hat{\mathbf{p}}}{E_{\mathbf{k}'}+M+V_s-V_v}\right] \tag{2.148}$$

in which the outgoing eikonal phase is given by

$$S^{(-)}(\mathbf{r}) = -\frac{M}{K}\int_z^\infty dz' \left(V_c + V_{so}\left[\vec{\sigma}\cdot(\mathbf{b}\times\mathbf{K}) + iKz'\right]\right) \tag{2.149}$$

and

$$\phi^\dagger(\hat{\mathbf{i}}',s') = \sum_{s_z'}(-)^{\frac{1}{2}-s_z'}\left[\left(\mathcal{D}^{(1/2)}_{s_z's'}(\hat{\mathbf{i}}')\right)^*\chi_{-s_z'}\right]^\dagger. \tag{2.150}$$

The distorted wave functions in Eq. (2.140) and Eq. (2.148) contain the spin-orbit terms. Including spin-orbit distortions significantly increases the complexity of the calculation. It is common to exclude this contribution to the distortions in a first order calculation. The magnitude of the spin-orbit potential is much smaller than that of the central potential and therefore is assumed to enter as a higher order effect. Various authors using the eikonal wave functions have derived expressions for the scattering amplitude for both relativistic and non-relativistic treatments when spin-orbit distortions are included in the formalism [38, 39, 40, 45]. The formulas are rather complicated and include differentials often undersired from a numerical point of view. For this reason, we take a purely practical approach to derive an expression that include the spin-orbit contribution.

2.1.4.4 Spin-orbit distortions

Before we begin our analysis to include spin-orbit distortions, we mention an important assessment of using the eikonal distorted wave functions in $\mathcal{H}^L(\mathbf{q})$ given by

$$\mathcal{H}^L(\mathbf{q}) = \int d^3r e^{-i\mathbf{q}\cdot\mathbf{r}}\left[\bar{\psi}^{(-)}(\mathbf{r},\mathbf{k}',\hat{\mathbf{i}}',s')\lambda^L\psi^{(+)}(\mathbf{r},\mathbf{k},\hat{\mathbf{i}},s)\right]. \tag{2.151}$$

In general the eikonal phases $S(\mathbf{r})$ contained in the wavefunctions $\psi^{(+)}$ and $\psi^{(-)}$ are 2×2 matrices acting on the Pauli spinors. However, when we neglect the spin-orbit potential, $S(\mathbf{r})$ becomes proportional

to the identity matrix. Consequently

$$H^L(\mathbf{q}) = \left[\bar{U}\lambda^L U\right] \left\{ \int b\, d^2b dz\, e^{i(\mathbf{k}-\mathbf{k}'-\mathbf{q})\cdot(\mathbf{b},z)} \exp\left(-i\frac{M}{K}\int_{-\infty}^{\infty} dz' V_c(\mathbf{b},z')\right)\right\}, \tag{2.152}$$

where $(\mathbf{r}=\mathbf{b},z)$ and we have written the three dimensional spatial integral d^3r in terms of cylindrical coordinates. We can recast Eq. (2.152) in a compact form as

$$H^L(\mathbf{q}) = \left[\bar{U}(\mathbf{k}',\hat{\mathbf{i}}',s')\lambda^L U(\mathbf{k},\hat{\mathbf{i}},s)\right] G(\mathbf{q}), \tag{2.153}$$

where

$$G(\mathbf{q}) = \int d^3r\, e^{i(\mathbf{k}-\mathbf{k}'-\mathbf{q})\cdot\mathbf{r}} \exp\left(-i\frac{M}{K}\int_{-\infty}^{\infty} dz' V_c(\mathbf{b},z')\right). \tag{2.154}$$

Eq. (2.153) illustrates the incredible usefulness of using the eikonal distorted waves. One is able to separate all the effects related to the nuclear distortions from the effects related to the nuclear spin couplings of the particles. This form makes the eikonal approach such a powerful and insightful approximation as it allows one to systematically study these modular structures independently and assess their effects. We are aware that there are limits to the application of each method, nevertheless the eikonal allows to a certain degree, just enough and the necessary flexibility to continue studying complicated physical processes.

However, Eq. (2.153) is yet again an example of where the simplicity of the expression hides the complexity of the numerical implementation. The integrand contained in $G(\mathbf{q})$ is a multidimensional oscillatory integral dependent on six independent variables $b, \phi_b, z, q, \theta_q$ and ϕ_q in the case of cylindrical coordinates. The central potential $V_c(r)$ for instance is not an analytical function and must be re-evaluated numerically for every value of $\mathbf{r}$.

Clearly there are issues connected with speed of evaluation, convergence and accuracy of the integrals. The study of multidimensional oscillatory integration is currently a topic of intense investigations [46] and no "black box" type of application exists to deal effectively with the type of integrals in Eq. (2.154). Indeed, following our investigations of testing alternative numerical integration techniques developed to handle multidimensional oscillatory integrals we have found that they are either too complicated to implement (essentially they provide no speed advantage) or tailored specifically for a test case integrand. We eventually developed a novel integration technique that combines the efficiency of raw FORTRAN 90 and using cluster computing techniques together with the powerful fitting and interpolation algorithms of MATLAB to integrate Eq. (2.154) in a reasonable amount of time.

We now continue with the analysis to include spin-orbit contributions. The distorted waves in the eikonal approximation are given by

$$\psi^{(+)}(\mathbf{r},\mathbf{k},\hat{\mathbf{i}},s) = U(\mathbf{k},E,M)e^{i\mathbf{k}\cdot\mathbf{r}}e^{iS^{(+)}(\mathbf{r})}\phi(\hat{\mathbf{i}},s) \tag{2.155}$$

for the incoming wave function and the outgoing wavefunction

$$\psi^{(-)}(\mathbf{r},\mathbf{k}',\hat{\mathbf{i}}',s') = U(\mathbf{k}',E,M)e^{i\mathbf{k}'\cdot\mathbf{r}}e^{iS^{(-)}(\mathbf{r})}\phi(\hat{\mathbf{i}}',s') \tag{2.156}$$

and has been used to study moderate energy nucleon-nucleus scattering and relativistic effects on spin observables [3]. The lower components of Eqs. (2.155) and (2.156) are related to the upper components by Eq. (2.120). With simpler interaction potentials the action of the differential operators can be avoided in an elegant manner [43, 47]. In this case we can not really go further and we proceed 'in the spirit of the eikonal approximation' and replace the gradient operators in Eqs. (2.155-2.156) to leading order with their respective expectation values. This replacement has proved useful in studying different nucleon-nucleus scattering reactions [16, 15, 17]. We then write

$$U(\mathbf{k},E,M) = U(\mathbf{k},E,M,V_s(r),V_v(r)) = \sqrt{\frac{E+M}{2M}}\begin{bmatrix} I_2 \\ \dfrac{\vec{\sigma}\cdot\mathbf{k}}{E+M+V_s-V_v} \end{bmatrix} \tag{2.157}$$

and

$$U(\mathbf{k}',E,M) = \sqrt{\frac{E+M}{2M}}\begin{bmatrix} I_2 \\ \dfrac{\vec{\sigma}\cdot\mathbf{k}'}{E+M+V_s^*-V_v^*} \end{bmatrix} \tag{2.158}$$

and the eikonal phase $S(\mathbf{r})$

$$S^{(\pm)}(\mathbf{r}) = \mp\frac{M}{k}\int_{\mp\infty}^{z} dz'\left(V_c(\mathbf{b},z) + V_{so}(\mathbf{b},z)[\vec{\sigma}\cdot(\mathbf{b}\times\mathbf{k}) \mp ikz']\right), \tag{2.159}$$

where we have replaced the gradient operator with the incoming momentum $\mathbf{k}$ in the eikonal phases. Also, in the eikonal approximation, we assume that the magnitudes of $\mathbf{k}$ and $\mathbf{k}'$ are the same. We can now proceed by substituting the 'eikonal-modified' distorted waves in Eqs. (2.155) and (2.156) into Eq. (2.151). This results in

$$\begin{aligned}
\mathcal{H}^L(\mathbf{q}) \;=\; & \int d^3r e^{-i\mathbf{q}\cdot\mathbf{r}} \\
& \times\phi^\dagger(\hat{\mathbf{i}}',s')\exp\left(-i\frac{M}{k}\int_z^\infty dz'\left(V_c(r)+V_{so}(r)[\vec{\sigma}\cdot(\mathbf{b}\times\mathbf{k})+ikz']\right)\right) \\
& \times e^{-i\mathbf{k}'\cdot\mathbf{r}}U^\dagger(\mathbf{k}',E,M)\begin{bmatrix} I_2 & 0 \\ 0 & -I_2 \end{bmatrix}\begin{bmatrix} \lambda_{11} & \lambda_{12} \\ \lambda_{21} & \lambda_{22} \end{bmatrix}U(\mathbf{k},E,M)e^{i\mathbf{k}\cdot\mathbf{r}} \\
& \times\exp\left(-i\frac{M}{k}\int_{-\infty}^z dz'\left(V_c(r)+V_{so}(r)[\vec{\sigma}\cdot(\mathbf{b}\times\mathbf{k})-ikz']\right)\right)\phi(\hat{\mathbf{i}},s).
\end{aligned} \tag{2.160}$$

The 'λ' matrix is the IA1 or SPVAT representation of the NN scattering matrix [4, 25] where $\lambda^L \in$

$\left(I_4, \gamma^5, \gamma^\mu, \gamma^5\gamma^\mu, \sigma^{\mu\nu}\right)$ represented here in 2×2 component form. These 2×2 λ matrices have the values

$$\lambda_{mn} \in 0, I_2, \sigma^i, \qquad\qquad i = 1, 2, 3.$$

The 4×4 matrix element for the SS-case is written in 2×2 form; we use $a(r) = E + M + V_s(r) - V_v(r)$

$$\bar{U} I_4 U = U^\dagger(\mathbf{k}', E, M) \begin{bmatrix} I_2 & 0 \\ 0 & -I_2 \end{bmatrix} \begin{bmatrix} I_2 & 0 \\ 0 & I_2 \end{bmatrix} U(\mathbf{k}, E, M) \tag{2.161}$$

$$= U^\dagger(\mathbf{k}', E, M) \begin{bmatrix} I_2 & 0 \\ 0 & -I_2 \end{bmatrix} U(\mathbf{k}, E, M) \tag{2.162}$$

$$= I_2 - \frac{\vec{\sigma}\cdot\mathbf{k}'\vec{\sigma}\cdot\mathbf{k}}{a^2(r)} \tag{2.163}$$

$$= \left(I_2 - \frac{\mathbf{k}'\cdot\mathbf{k}}{a^2(r)}\right) + \frac{i\vec{\sigma}\cdot(\mathbf{k}\times\mathbf{k}')}{a^2(r)} = \alpha_S + \vec{\sigma}\cdot\vec{\beta}_S \tag{2.164}$$

and the 4×4 matrix element for the PP-case is written in 2×2 form; we use $a(r) = E+M+V_s(r)-V_v(r)$

$$\bar{U}\gamma^4 U = U^\dagger(\mathbf{k}', E, M) \begin{bmatrix} I_2 & 0 \\ 0 & -I_2 \end{bmatrix} \begin{bmatrix} 0 & I_2 \\ I_2 & 0 \end{bmatrix} U(\mathbf{k}, E, M) \tag{2.165}$$

$$= U^\dagger(\mathbf{k}', E, M) \begin{bmatrix} 0 & I_2 \\ -I_2 & 0 \end{bmatrix} U(\mathbf{k}, E, M) \tag{2.166}$$

$$= \frac{\vec{\sigma}\cdot\mathbf{k}}{a(r)} - \frac{\vec{\sigma}\cdot\mathbf{k}'}{a(r)} = \frac{\vec{\sigma}\cdot(\mathbf{k}-\mathbf{k}')}{a(r)} = \vec{\sigma}\cdot\vec{\beta}_P \tag{2.167}$$

where we have

$$\alpha_S = I_2 - \frac{\mathbf{k}\cdot\mathbf{k}'}{\left(E + M + V_s(r) - V_v(r)\right)^2}, \tag{2.168}$$

$$\vec{\beta}_S = i\frac{(\mathbf{k}\times\mathbf{k}')}{\left(E + M + V_s(r) - V_v(r)\right)^2}, \tag{2.169}$$

$$\vec{\beta}_P = \frac{(\mathbf{k}-\mathbf{k}')}{E + M + V_s(r) - V_v(r)}. \tag{2.170}$$

For the scalar-scalar case, we have a spin-independent α_S and spin-dependent $\vec{\sigma}\cdot\vec{\beta}_S$ term. We concen-

trate on the first term of the spin-independent term whereby the first term of Eq. (2.164) reads

$$\begin{aligned}\mathcal{H}^S(\mathbf{q})^i_{t_1} &= \phi^\dagger(\hat{\mathbf{i}}', s') \int d^3r e^{-i\mathbf{q}\cdot\mathbf{r}} \\ &\times e^{-i\mathbf{k}'\cdot\mathbf{r}} \exp\left(-i\frac{M}{k}\int_z^\infty dz' \left(V_c(r) + V_{so}(r)[\vec{\sigma}\cdot(\mathbf{b}\times\mathbf{k}) + ikz']\right)\right) \\ &\times I_2 \\ &\times e^{i\mathbf{k}\cdot\mathbf{r}} \exp\left(-i\frac{M}{k}\int_{-\infty}^z dz' \left(V_c(r) + V_{so}(r)[\vec{\sigma}\cdot(\mathbf{b}\times\mathbf{k}) - ikz']\right)\right)\phi(\hat{\mathbf{i}}, s)\end{aligned}$$

which becomes

$$\begin{aligned}\mathcal{H}^S(\mathbf{q})^i_{t_1} &= \phi^\dagger(\hat{\mathbf{i}}', s') \int d^3r e^{i(\mathbf{Q}-\mathbf{q})\cdot\mathbf{r}} \exp\left(-i\frac{M}{k}\left[\int_z^\infty dz' V_c + \int_{-\infty}^z dz' V_c\right]\right) \\ &\times \exp\left(-i\frac{M}{k}\left[\int_z^\infty dz' V_{so}(r)[\vec{\sigma}\cdot(\mathbf{b}\times\mathbf{k})] + \int_{-\infty}^z dz' V_{so}(r)[\vec{\sigma}\cdot(\mathbf{b}\times\mathbf{k})]\right]\right) \\ &\times \exp\left(-i\frac{M}{k}\left[\int_z^\infty dz'\ ikz' V_{so} - \int_{-\infty}^z dz'\ ikz' V_{so}\right]\right)\phi(\hat{\mathbf{i}}, s). \qquad (2.171)\end{aligned}$$

Eq. (2.171) reduces to

$$\mathcal{H}^S(\mathbf{q}) = \phi^\dagger(\hat{\mathbf{i}}', s') \int d^3r e^{i(\mathbf{Q}-\mathbf{q})\cdot\mathbf{r}} e^{i\chi_c(\mathbf{b})} e^{S_D} e^{i\chi_{so}(\mathbf{b})[\vec{\sigma}\cdot\hat{\mathbf{n}}]}\phi(\hat{\mathbf{i}}, s), \qquad (2.172)$$

where

$$\chi_c(\mathbf{b}) = -\frac{M}{k}\int_{-\infty}^{+\infty} dz' V_c(\mathbf{b}, z') \qquad (2.173)$$

and

$$\chi_{so}(\mathbf{b}) = -Mb\int_{-\infty}^{+\infty} dz' V_{so}(\mathbf{b}, z'), \qquad (2.174)$$

and the exponential related to the Darwin term

$$e^{S_D} = \exp\left(-i\frac{M}{k}\left[\int_z^\infty dz'\ ikz' V_{so} - \int_{-\infty}^z dz'\ ikz' V_{so}\right]\right) \qquad (2.175)$$

simplifies to [47]

$$e^{S_D} = \frac{E + M + V_s - V_v}{E + M}. \qquad (2.176)$$

Using the identity given by Eq. (2.141) we have that

$$e^{-i\chi_{so}(b)[\vec{\sigma}\cdot\hat{\mathbf{n}}]} = \cos(\chi_{so}(b))\ I_2 - i[\vec{\sigma}\cdot\hat{\mathbf{n}}]\sin(\chi_{so}(b)). \qquad (2.177)$$

Substituting Eqs. (2.176) and (2.177) into Eq. (2.172) gives

$$\begin{aligned}\mathcal{H}^S(\mathbf{q})^i_{t_1} &= \phi^\dagger(\hat{\mathbf{i}}', s') \int d^3r e^{i(\mathbf{Q}-\mathbf{q})\cdot\mathbf{r}} e^{i\chi_c(\mathbf{b})} \frac{E+M+V_s-V_v}{2M} \\ &\times \left[\cos(\chi_{so}(b))\ I_2 - i[\vec{\sigma}\cdot\hat{\mathbf{n}}]\sin(\chi_{so}(b))\right]\phi(\hat{\mathbf{i}}, s).\end{aligned} \tag{2.178}$$

The second term of the spin-independent term is then

$$\begin{aligned}\mathcal{H}^S(\mathbf{q})^i_{t_2} &= -\phi^\dagger(\hat{\mathbf{i}}', s') \int d^3r e^{i(\mathbf{Q}-\mathbf{q})\cdot\mathbf{r}} e^{i\chi_c(\mathbf{b})} \frac{\mathbf{k}\cdot\mathbf{k}'}{2M(E+M+V_s-V_v)} \\ &\times \left[\cos(\chi_{so}(b))\ I_2 - i[\vec{\sigma}\cdot\hat{\mathbf{n}}]\sin(\chi_{so}(b))\right]\phi(\hat{\mathbf{i}}, s).\end{aligned} \tag{2.179}$$

For the spin-dependent portion of the scalar-scalar matrix element, inserting the vector $\vec{\beta_S}$, the spin-dependent part reads

$$\begin{aligned}\mathcal{H}^S(\mathbf{q})^d_{t_3} &= \int d^3r e^{i(\mathbf{Q}-\mathbf{q})\cdot\mathbf{r}} e^{i\chi_c(\mathbf{b})} \frac{1}{2M(E+M+V_s-V_v)} \\ &\times \exp\left(-iMb\int_z^\infty dz' V_{so}(r)[\vec{\sigma}\cdot\hat{\mathbf{n}}]\right)\left(i\vec{\sigma}\cdot\vec{\beta}_S\right)\exp\left(-iMb\int_{-\infty}^z dz' V_{so}(r)[\vec{\sigma}\cdot\hat{\mathbf{n}}]\right).\end{aligned} \tag{2.180}$$

The most important contribution of the spin-orbit potential to the integral in Eq. (2.180) comes from values where the impact parameter $b \approx R$, where R is the nuclear radius, or equivalently from small values of z [16, 38]. Using this and the fact that the spin-orbit potential is even in z allows us to make the following approximation. The dz' integral in Eq. (2.180) is written as

$$\int_z^\infty dz' V_{so} \simeq \int_0^\infty dz' V_{so} = \frac{1}{2}\int_{-\infty}^\infty dz' V_{so}. \tag{2.181}$$

Also,

$$\int_{-\infty}^z dz' V_{so} \simeq \int_{-\infty}^0 dz' V_{so} = \frac{1}{2}\int_{-\infty}^\infty dz' V_{so} \tag{2.182}$$

and Eq.(2.180) becomes

$$\begin{aligned}\mathcal{H}^S(\mathbf{q})^d_{t_3} &= i\int d^3r e^{i(\mathbf{Q}-\mathbf{q})\cdot\mathbf{r}} e^{i\chi_c(\mathbf{b})} \frac{1}{2M(E+M+V_s-V_v)} \\ &\times \exp\left(-i\frac{\chi_{so}}{2}[\vec{\sigma}\cdot\hat{\mathbf{n}}]\right)\left(\vec{\sigma}\cdot\vec{\beta}_s\right)\exp\left(-i\frac{\chi_{so}}{2}[\vec{\sigma}\cdot\hat{\mathbf{n}}]\right).\end{aligned} \tag{2.183}$$

Expanding the last factor in Eq. (2.183)

$$\begin{aligned} e^{\left(-i\frac{\chi_{so}}{2}[\vec{\sigma}\cdot\hat{\mathbf{n}}]\right)}\left(\vec{\sigma}\cdot\vec{\beta}_s\right)e^{\left(-i\frac{\chi_{so}}{2}[\vec{\sigma}\cdot\hat{\mathbf{n}}]\right)} &= (\cos(\chi_{so}(b)/2) - i[\vec{\sigma}\cdot\hat{\mathbf{n}}]\sin(\chi_{so}(b)/2))\left(\vec{\sigma}\cdot\vec{\beta}_s\right) \\ &\quad \times(\cos(\chi_{so}(b)/2) - i[\vec{\sigma}\cdot\hat{\mathbf{n}}]\sin(\chi_{so}(b)/2)) \\ &= (\vec{\sigma}\cdot\vec{\beta}_S)\cos(\chi_{so}(b)) - i\left(\hat{\mathbf{n}}\cdot\vec{\beta}_S\right)\sin(\chi_{so}(b)). \end{aligned} \tag{2.184}$$

Plugging this result into Eq. (2.183) gives

$$\mathcal{H}^S(\mathbf{q})^d_{t_3} = \int d^3r e^{i(\mathbf{Q}-\mathbf{q})\cdot\mathbf{r}}e^{i\chi_c(\mathbf{b})}\left[\frac{\left(\hat{\mathbf{n}}\cdot\vec{\beta}_S\right)\sin(\chi_{so}(b)) + i(\vec{\sigma}\cdot\vec{\beta}_S)\cos(\chi_{so}(b))}{2M(E+M+V_s-V_v)}\right]. \tag{2.185}$$

For the PP case the result is analogous to Eq. (2.185). We replace $\vec{\beta}_S \longrightarrow \vec{\beta}_P$ and also $1/[2M(E+M+V_s-V_v)] \longrightarrow 1/2M$ and the complex term becomes real and the real term complex, that is

$$\mathcal{H}^P(\mathbf{q}) = \int d^3r e^{i(\mathbf{Q}-\mathbf{q})\cdot\mathbf{r}}e^{i\chi_c(\mathbf{b})}\left[\frac{(\vec{\sigma}\cdot\vec{\beta}_P)\cos(\chi_{so}(b)) - (i\hat{\mathbf{n}}\cdot\vec{\beta}_P)\sin(\chi_{so}(b))}{2M}\right]. \tag{2.186}$$

If we let

$$\mathcal{Q}(\mathbf{r}) = e^{i(\mathbf{Q}-\mathbf{q})\cdot\mathbf{r}}e^{i\chi_c(\mathbf{b})}, \tag{2.187}$$

we can combine these equations and separate the spin independent components from the spin dependent ones. Doing this with

$$\varphi_{so} = \chi_{so}(b)$$

results in

$$\mathcal{H}^S(\mathbf{q}) = \phi^\dagger(\hat{\mathbf{i}}', s')\int d^3r\mathcal{Q}(\mathbf{r})\left[\mathcal{F}_1^S + (\vec{\sigma}\cdot\hat{\mathbf{n}})\mathcal{F}_2^S + (\vec{\sigma}\cdot\vec{\beta}_S)\mathcal{F}_3^S\right]\phi(\hat{\mathbf{i}}, s) \tag{2.188}$$

where

$$\mathcal{F}_1^S = \frac{(E+M+V_s-V_v)\cos\varphi_{so}}{2M} + \frac{(\hat{\mathbf{n}}\cdot\vec{\beta}_s)\sin\varphi_{so} - (\mathbf{k}\cdot\mathbf{k}')\cos\varphi_{so}}{2M(E+M+V_s-V_v)}, \tag{2.189}$$

$$\mathcal{F}_2^S = i\left(\frac{\mathbf{k}\cdot\mathbf{k}'}{2M(E+M+V_s-V_v)} - \frac{(E+M+V_s-V_v)}{2M}\right)\sin\varphi_{so}, \tag{2.190}$$

$$\mathcal{F}_3^S = \frac{i\cos\varphi_{so}}{2M(E+M+V_s-V_v)}. \tag{2.191}$$

For the PP case Eq. (2.188) reads

$$\mathcal{H}^P(\mathbf{q}) = \phi^\dagger(\hat{\mathbf{i}}', s')\int d^3r\mathcal{Q}(\mathbf{r})\left[\mathcal{F}_1^P + (\vec{\sigma}\cdot\vec{\beta}_P)\mathcal{F}_2^P\right]\phi(\hat{\mathbf{i}}, s) \tag{2.192}$$

where

$$\mathcal{F}_1^P = -\frac{i(\hat{\mathbf{n}}\cdot\vec{\beta}_P)\sin\varphi_{so}}{2M}, \tag{2.193}$$

$$\mathcal{F}_2^P = \frac{\cos\varphi_{so}}{2M}. \tag{2.194}$$

The analysis above is a way of including spin-orbit distortions in a numerically convenient way. Interpretation of the expressions however is rather cumbersome and one would have to resort to numerical evaluations of $\mathcal{H}^S$ and $\mathcal{H}^P$. In addition, the derived expressions above are only for the rank-0 case of polarizations and similar expressions for the other ranks will have to be derived in a similar fashion.

The big difference however, when including the spin-orbit contribution is the fact that $\mathcal{H}^L$'s factorized property as in Eq. (2.153) is now broken and no simple interpretation of this quantity is possible anymore. Whereas in Eq. (2.153) the distortion effects are well separated from that of the spinors, in the above analysis with spin-orbit contributions, the spin evolution of the incident and outgoing particles are hidden and obscured by the complicated expressions. To end this section we test whether we recover the plane wave case given in Eq. (2.105).

Plane wave limit: In using plane waves the scalar and vector potentials become zero. The complex $\cos\varphi_{so}$ and $\sin\varphi_{so}$ become 1 and zero respectively. Consequently $\mathcal{F}_2^S$ and $\mathcal{F}_1^P$ become zero. $\mathcal{F}_1$ reduces to

$$\mathcal{F}_1^S = \frac{E+M}{2M}\left(1-\frac{\mathbf{k}\cdot\mathbf{k}'}{(E+M)}\right) \tag{2.195}$$

and

$$\mathcal{F}_3^S = \frac{E+M}{2M}\left(\frac{i\vec{\sigma}\cdot(\mathbf{k}\times\mathbf{k}')}{(E+M)}\right). \tag{2.196}$$

Combining $\mathcal{F}_1^S$ and $\mathcal{F}_3^S$

$$\phi^\dagger(\hat{\mathbf{i}}',s')(\mathcal{F}_1^S+\mathcal{F}_3^S)\phi(\hat{\mathbf{i}},s) = U^\dagger(\mathbf{k}',\hat{\mathbf{i}}',s')\gamma^0 U(\mathbf{k},\hat{\mathbf{i}},s). \tag{2.197}$$

The eikonal phase proportional to the effective central potential $\chi_c \to 0$ resulting in e^0. Subsequently the function $\mathcal{Q}(\mathbf{r})$ becomes

$$\mathcal{Q}(\mathbf{r}) = e^{i(\mathbf{k}-\mathbf{k}'-\mathbf{q})\cdot\mathbf{r}}. \tag{2.198}$$

Using the results of the above and substituting Eqs. (2.197) and (2.198) into Eq. (2.188), we recover $\mathcal{H}^S(\mathbf{q})$ for the plane wave case

$$\begin{aligned}\mathcal{H}^S(\mathbf{q}) &= \int d^3r e^{i(\mathbf{k}-\mathbf{k}'-\mathbf{q})\cdot\mathbf{r}}\bar{U}(\mathbf{k}',\hat{\mathbf{i}}',s')\lambda^S U(\mathbf{k},\hat{\mathbf{i}},s)\\ &= (2\pi)^3\delta\left(\mathbf{k}-\mathbf{k}'-\mathbf{q}\right)\bar{U}(\mathbf{k}',\hat{\mathbf{i}}',s')\lambda^S U(\mathbf{k},\hat{\mathbf{i}},s).\end{aligned} \tag{2.199}$$

In a similar vein

$$\mathcal{F}_2^P = \frac{\vec{\sigma}\cdot(\mathbf{k}-\mathbf{k}')}{2M} \tag{2.200}$$

and

$$\phi^\dagger(\hat{\mathbf{i}}',s')(\mathcal{F}_2^P)\phi(\hat{\mathbf{i}},s) = U^\dagger(\mathbf{k}',\hat{\mathbf{i}}',s')\gamma^0\gamma^5 U(\mathbf{k},\hat{\mathbf{i}},s). \tag{2.201}$$

Substituting Eq. (2.201) into Eq. (2.192) we recover

$$\begin{aligned}\mathcal{H}^S(\mathbf{q}) &= \int d^3r e^{i(\mathbf{k}-\mathbf{k}'-\mathbf{q})\cdot\mathbf{r}}\bar{U}(\mathbf{k}',\hat{\mathbf{i}}',s')\lambda^P U(\mathbf{k},\hat{\mathbf{i}},s)\\ &= (2\pi)^3\delta\left(\mathbf{k}-\mathbf{k}'-\mathbf{q}\right)\bar{U}(\mathbf{k}',\hat{\mathbf{i}}',s')\lambda^P U(\mathbf{k},\hat{\mathbf{i}},s).\end{aligned} \tag{2.202}$$

2.1.5 Polarization tensor

In this section we discuss the polarization tensor which describes the nuclear response of the target to an external probe. Even though this is a complex many-body quantity, it can be evaluated in a systematic manner [48]. The polarization tensor based on the relativistic free Fermi-gas model (FGM) treats the nuclear ground state as a system of non-interacting fermions at finite density. The free Fermi-gas model is expressed in terms of the free non-interacting nucleon propogator $\mathcal{G}_0(k)$ which is given as

$$\mathcal{G}(k) = (\not{k}+M)\frac{1}{k^2-M^2+i\epsilon} + (\not{k}+M)\frac{i\pi}{E_k}\delta(k_0-E_k)\theta(k_F-|\mathbf{k}|), \tag{2.203}$$

where the first term is the familiar free propagator of baryons and anti-baryons and the second term incorporates the Pauli exclusion principle.

$$i\Pi_{LL'}(q) = \int \frac{d^4k}{(2\pi)^4}\mathrm{Tr}\left[\mathcal{G}(k)\lambda^L\mathcal{G}(k+q)\overline{\lambda^{L'}}\right]. \tag{2.204}$$

In this work we will only consider the rank-0 contribution to the polarization tensor (see Table. 2.1) and consequently the derivation will be done explicitly for the scalar-scalar case alone, where

$$\lambda^{L=S} = \overline{\lambda^{L'=S}} = I_4$$

and $\Pi_{LL'}$ above becomes

$$i\Pi_{SS}(q) = \int \frac{d^4k}{(2\pi)^4}\mathrm{Tr}\left[\mathcal{G}(k)\mathcal{G}(k+q)\right]. \tag{2.205}$$

The nucleon propogator is written in terms of the Feynman (F) and density dependant (D) terms, i.e

$$\begin{aligned}\mathcal{G}(k) &= (\not{k}+M)\frac{1}{k^2-M^2+i\epsilon} + (\not{k}+M)\frac{i\pi}{E_k}\delta(k_0-E_k)\theta(k_F-|\mathbf{k}|),\\ \mathcal{G}(k) &= \mathcal{G}_F^k + \mathcal{G}_D^k.\end{aligned}$$

Similarly

$$\begin{aligned}\mathcal{G}(k+q) &= (\not{k}+\not{q}+M)\left[\frac{1}{(k+q)^2-M^2+i\epsilon}+\frac{i\pi}{E_{k+q}}\delta(k_0-E_{k+q})\theta(k_F-|\mathbf{k}+\mathbf{q}|)\right],\\ \mathcal{G}(k+q) &= \mathcal{G}_F^{k+q}+\mathcal{G}_D^{k+q}.\end{aligned}$$

Eq. (2.205) is then written as

$$\Pi_{SS}(q) = -i\int\frac{d^4k}{(2\pi)^4}\mathrm{Tr}\left[\mathcal{G}_F^k\mathcal{G}_F^{k+q}+\mathcal{G}_F^k\mathcal{G}_D^{k+q}+\mathcal{G}_D^k\mathcal{G}_F^{k+q}+\mathcal{G}_D^k\mathcal{G}_D^{k+q}\right] \tag{2.206}$$

where

$$\mathcal{G}_F(k)\mathcal{G}_F(k+q) = \frac{(\not{k}+M)(\not{k}+\not{q}+M)}{(\mathbf{k}^2-M^2+i\epsilon)((\mathbf{k}+\mathbf{q})^2-M^2+i\epsilon)}, \tag{2.207}$$

$$\begin{aligned}\mathcal{G}_F(k)\mathcal{G}_D(k+q) &= \frac{(\not{k}+M)(\not{k}+\not{q}+M)(i\pi)}{(\mathbf{k}^2-M^2+i\epsilon)E_{k+q}}\delta(k_0+q_0-E_{k+q})\theta(k_F-|\mathbf{k}+\mathbf{q}|)\\ &\quad\times\theta(k_0+q_0),\end{aligned} \tag{2.208}$$

$$\mathcal{G}_D(k)\mathcal{G}_F(k+q) = \frac{(\not{k}+M)(\not{k}+\not{q}+M)(i\pi)}{((\mathbf{k}+\mathbf{q})^2-M^2+i\epsilon)E_k}\delta(k_0-E_k)\theta(k_F-|\mathbf{k}|)\theta(k_0), \tag{2.209}$$

$$\begin{aligned}\mathcal{G}_D(k)\mathcal{G}_D(k+q) &= -\frac{(\not{k}+M)(\not{k}+\not{q}+M)\pi^2}{E_kE_{k+q}}\delta(k_0-E_k)\delta(k_0+q_0-E_{k+q})\\ &\quad\times\theta(k_F-|\mathbf{k}|)\theta(k_F-|\mathbf{k}+\mathbf{q}|)\theta(k_0)\theta(k_0+q_0).\end{aligned} \tag{2.210}$$

We make the replacement $k\to k-q$ in the second term of Eq. (2.206) and Eq. (2.208) becomes

$$\mathcal{G}_F(k-q)\mathcal{G}_D(k) = \frac{(\not{k}-\not{q}+M)(\not{k}+M)(i\pi)}{((\mathbf{k}-\mathbf{q})^2-M^2+i\epsilon)E_k}\delta(k_0-E_{k+q})\theta(k_F-|\mathbf{k}|)\theta(k_0).$$

Eq. (2.206) becomes

$$\begin{aligned}
\Pi_{SS}(q) &= -i\int \frac{d^4k}{(2\pi)^4}\mathrm{Tr}\left[G_F^k G_F^{k+q} + G_F^{k-q}G_D^k + G_D^k G_F^{k+q} + G_D^k G_D^{k+q}\right] \\
&= -i\int \frac{d^4k}{(2\pi)^4}\frac{\mathrm{Tr}\left((\not{k}+M)(\not{k}+\not{q}+M)\right)}{(\mathbf{k}^2-M^2+i\epsilon)((\mathbf{k}+\mathbf{q})^2-M^2+i\epsilon)} \\
&\quad -i\int \frac{d^4k}{(2\pi)^4}\frac{\mathrm{Tr}\left((\not{k}-\not{q}+M)(\not{k}+M)\right)(i\pi)}{((\mathbf{k}-\mathbf{q})^2-M^2+i\epsilon)E_k}\delta(k_0-E_{k+q})\theta(k_F-|\mathbf{k}|)\theta(k_0) \\
&\quad -i\int \frac{d^4k}{(2\pi)^4}\frac{\mathrm{Tr}\left((\not{k}+M)(\not{k}+\not{q}+M)\right)(i\pi)}{((\mathbf{k}+\mathbf{q})^2-M^2+i\epsilon)E_k}\delta(k_0-E_k)\theta(k_F-|\mathbf{k}|)\theta(k_0) \\
&\quad -i\int \frac{d^4k}{(2\pi)^4}\frac{\mathrm{Tr}\left((\not{k}+M)(\not{k}+\not{q}+M)\right)\pi^2}{E_kE_{k+q}}\delta(k_0-E_k)\delta(k_0+q_0-E_{k+q}) \\
&\qquad \times\theta(k_F-|\mathbf{k}|)\theta(k_F-|\mathbf{k}+\mathbf{q}|)\theta(k_0)\theta(k_0+q_0). \qquad (2.211)
\end{aligned}$$

Regrouping Eq. (2.211) and designating

$$\mathcal{T}_{SS}(k,k+q) = \mathrm{Tr}\left((\not{k}+M)(\not{k}+\not{q}+M)\right), \qquad (2.212)$$

$$\mathcal{T}_{SS}(k-q,k) = \mathrm{Tr}\left((\not{k}-\not{q}+M)(\not{k}+M)\right) \qquad (2.213)$$

we arrive at

$$\begin{aligned}
\Pi_{SS}(q) &= -i\int \frac{d^4k}{(2\pi)^4}\frac{\mathcal{T}_{SS}(k,k+q)}{(\mathbf{k}^2-M^2+i\epsilon)((\mathbf{k}+\mathbf{q})^2-M^2+i\epsilon)} \\
&\quad +\int \frac{d^4k}{(2\pi)^4}\frac{\pi\delta(k_0-E_k)\theta(k_F-|\mathbf{k}|)\theta(k_0)}{E_k}\left[\frac{\mathcal{T}_{SS}(k-q,k)}{(\mathbf{k}-\mathbf{q})^2-M^2+i\epsilon}\right. \\
&\qquad \left. +\frac{\mathcal{T}_{SS}(k,k+q)}{(\mathbf{k}+\mathbf{q})^2-M^2+i\epsilon}\right] \\
&\quad +i\int \frac{d^4k}{(2\pi)^4}\frac{\pi^2\theta(k_F-|\mathbf{k}|)\theta(k_F-|\mathbf{k}+\mathbf{q}|)\theta(k_0)\theta(k_0+q_0)}{E_kE_{k+q}} \\
&\qquad \times\delta(k_0-E_k)\delta(k_0+q_0-E_{k+q})\mathcal{T}_{SS}(k,k+q). \qquad (2.214)
\end{aligned}$$

The first term $\Pi_{SS}^{(FF)}$ in Eq. (2.214), also known as the vacuum polarization, diverges. Also, the imaginary part of this term makes no contribution to the quasielastic cross section and is therefore

dropped. We can then derive the imaginary part of the remaining three terms, $\Pi_{SS}^{(D)}$

$$\begin{aligned}
\Pi_{SS}^{D}(q) &= \left[\Pi_{SS}^{FD} + \Pi_{SS}^{DF}\right] + \Pi_{SS}^{DD} \\
&= \int \frac{d^4k}{(2\pi)^4} \frac{\pi\delta(k_0 - E_k)\theta(k_F - |\mathbf{k}|)\theta(k_0)}{E_k} \left\{ \frac{\mathcal{T}_{SS}(k-q,k)}{(\mathbf{k}-\mathbf{q})^2 - M^2 + i\epsilon)} + \frac{\mathcal{T}_{SS}(k,k+q)}{(\mathbf{k}+\mathbf{q})^2 - M^2 + i\epsilon)} \right\} \\
&\quad + i \int \frac{d^4k}{(2\pi)^4} \frac{\pi^2\theta(k_F - |\mathbf{k}|)\theta(k_F - |\mathbf{k}+\mathbf{q}|)\theta(k_0)\theta(k_0+q_0)}{E_k E_{k+q}} \\
&\quad \times\delta(k_0 - E_k)\delta(k_0 + q_0 - E_{k+q})\mathcal{T}_{SS}(k,k+q), \qquad (2.215)
\end{aligned}$$

by applying the Cauchy principal value

$$\mathrm{Im}\left\{\frac{1}{\omega \pm i\epsilon}\right\} = \mp\pi\delta(\omega) \qquad (2.216)$$

to Eq. (2.215). The result is

$$\mathrm{Im}\left\{\Pi_{SS}^{D}\right\} = \mathrm{Im}_1 + \mathrm{Im}_2,$$

where

$$\begin{aligned}
\mathrm{Im}_1 &= -\frac{1}{4}\int \frac{d^4k}{(2\pi)^2} \frac{\delta(k_0 - E_k)\theta(k_F - |\mathbf{k}|)\theta(k_0)}{E_k} \\
&\quad \times \left\{\delta\left[(\mathbf{k}-\mathbf{q})^2 - M^2\right]\mathcal{T}_{SS}(k-q,k) + \delta\left[(\mathbf{k}+\mathbf{q})^2 - M^2\right]\mathcal{T}_{SS}(k,k+q)\right\}, \qquad (2.217) \\
\mathrm{Im}_2 &= \int \frac{d^4k}{(2\pi)^2} \frac{\theta(k_F - |\mathbf{k}|)\theta(k_F - |\mathbf{k}+\mathbf{q}|)\theta(k_0)\theta(k_0+q_0)}{4E_k E_{k+q}} \\
&\quad \times\delta(k_0 - E_k)\delta(k_0 + q_0 - E_{k+q})\mathcal{T}_{SS}(k,k+q). \qquad (2.218)
\end{aligned}$$

It can be shown that

$$\delta\left[(\mathbf{k}\pm\mathbf{q})^2 - M^2\right] = \frac{\delta\left(k_0 \pm q_0 - E_{k\pm q}\right)}{2E_{k\pm q}} \qquad (2.219)$$

with which we make the replacements

$$\delta\left[(\mathbf{k}-\mathbf{q})^2 - M^2\right]\mathcal{T}_{SS}(k-q,k) = \frac{\delta\left(k_0 - q_0 - E_{k-q}\right)}{2E_{k-q}}\mathcal{T}_{SS}(k-q,k) \qquad (2.220)$$

$$\delta\left[(\mathbf{k}+\mathbf{q})^2 - M^2\right]\mathcal{T}_{SS}(k,k+q) = \frac{\delta\left(k_0 + q_0 - E_{k+q}\right)}{2E_{k+q}}\mathcal{T}_{SS}(k,k+q) \qquad (2.221)$$

in Eq. (2.217). Then Eqs. (2.217) and (2.218) become

$$\begin{aligned}\mathrm{Im}_1 &= -\frac{1}{8}\int \frac{d^4k}{(2\pi)^2}\frac{\delta(k_0-E_k)\theta(k_F-|\mathbf{k}|)\theta(k_0)}{E_k} \\ &\quad\times\left\{\frac{\delta\left(k_0-q_0-E_{k-q}\right)}{E_{k-q}}\mathcal{T}_{SS}(k-q,k)+\frac{\delta\left(k_0+q_0-E_{k+q}\right)}{E_{k+q}}\mathcal{T}_{SS}(k,k+q)\right\}. \qquad (2.222)\end{aligned}$$

We split Eq. (2.218) into two equal parts

$$\begin{aligned}\mathrm{Im}_2 &= \int \frac{d^4k}{(2\pi)^2}\frac{\theta(k_F-|\mathbf{k}|)\theta(k_F-|\mathbf{k}+\mathbf{q}|)\theta(k_0)\theta(k_0+q_0)}{4E_kE_{k+q}} \\ &\quad\times\delta(k_0-E_k)\delta(k_0+q_0-E_{k+q})\mathcal{T}_{SS}(k,k+q) \\ &= \frac{1}{4}\int \frac{d^4k}{(2\pi)^2}\theta(k_F-|\mathbf{k}|)\theta(k_0)\delta(k_0-E_k)\left\{\frac{1}{2E_k}+\frac{1}{2E_k}\right\} \\ &\quad\times\theta(k_0+q_0)\theta(k_F-|\mathbf{k}+\mathbf{q}|)\delta(k_0+q_0-E_{k+q})\left\{\frac{1}{2E_{k+q}}+\frac{1}{2E_{k+q}}\right\}\mathcal{T}_{SS}(k,k+q)\end{aligned}$$

and make the replacement of $k\to k-q$ in the second term

$$\begin{aligned}\mathrm{Im}_2 &= \frac{1}{8}\int \frac{d^4k}{(2\pi)^2}\left\{\frac{\theta(k_F-|\mathbf{k}|)\theta(k_0)\theta(k_F-|\mathbf{k}+\mathbf{q}|)\theta(k_0+q_0)}{E_kE_{k+q}}\right\} \\ &\quad\times\delta(k_0-E_k)\delta(k_0+q_0-E_{k+q})\mathcal{T}_{SS}(k,k+q) \\ &\quad+\int \frac{d^4k}{8(2\pi)^2}\left\{\frac{\theta(k_F-|\mathbf{k}-\mathbf{q}|)\theta(k_0-q_0)\theta(k_F-|\mathbf{k}|)\theta(k_0)}{E_kE_{k-q}}\right\} \\ &\quad\times\delta(k_0-q_0-E_{k-q})\delta(k_0-E_k)\mathcal{T}_{SS}(k-q,k) \\ &= \frac{1}{8}\int \frac{d^4k}{(2\pi)^2}\left(\frac{\theta(k_F-|\mathbf{k}|)\theta(k_0)\delta(k_0-E_k)}{E_k}\right) \\ &\qquad\times\{\frac{\theta(k_F-|\mathbf{k}+\mathbf{q}|)\theta(k_0+q_0)\delta(k_0+q_0-E_{k+q})}{E_{k+q}}\mathcal{T}_{SS}(k,k+q) \\ &\qquad+\frac{\theta(k_F-|\mathbf{k}-\mathbf{q}|)\theta(k_0-q_0)\delta(k_0-q_0-E_{k-q})}{E_{k-q}}\mathcal{T}_{SS}(k-q,k)\}. \qquad (2.223)\end{aligned}$$

Next we add Eqs. (2.222) and (2.223) and integrate over k_0. This results in

$$\mathrm{Im}\left\{\Pi^D_{SS}\right\}=\mathrm{Im}_A+\mathrm{Im}_B \qquad (2.224)$$

where

$$\begin{aligned}
\mathrm{Im}_A &= -\frac{1}{8}\int \frac{d^3k}{(2\pi)^2}\frac{\theta(k_F-|\mathbf{k}|)\theta(E_{k+q}-q_0)\theta(|\mathbf{k}+\mathbf{q}|-k_F)}{E_kE_{k+q}} \\
&\quad \times\delta(E_{k+q}-q_0-E_k)\mathcal{T}_{SS}(k,k+q)_{k_0=E_{k+q}-q_0}, \qquad (2.225)\\
\mathrm{Im}_B &= -\frac{1}{8}\int \frac{d^3k}{(2\pi)^2}\frac{\theta(\theta(k_F-|\mathbf{k}|)\theta(E_{k-q})\theta(|\mathbf{k}-\mathbf{q}|-k_F)}{E_kE_{k-q}} \\
&\quad \times\delta(E_{k-q}-q_0-E_k)\mathcal{T}_{SS}(k-q,k)_{k_0=E_{k-q}+q_0}. \qquad (2.226)
\end{aligned}$$

We have that

$$E_k^2 = \mathbf{k}^2 + M^2 \qquad (2.227)$$

and also

$$\begin{aligned}
E_{k\pm q}^2 &= (\mathbf{k}\pm\mathbf{q})^2 + M^2 \qquad (2.228)\\
&= E_k^2 \pm 2|\mathbf{k}||\mathbf{q}|\cos\theta_\pm + \mathbf{q}^2 \qquad (2.229)\\
\Rightarrow \cos\theta_\pm &= \frac{\pm E_{k\pm q}^2 \pm E_k^2 - \mathbf{q}^2}{2|\mathbf{k}||\mathbf{q}|} \qquad (2.230)\\
\Rightarrow d\cos\theta &= \frac{E_{k+q}dE_{k+q}}{|\mathbf{k}||\mathbf{q}|}. \qquad (2.231)
\end{aligned}$$

The three-dimensional momentum integral is rewritten as

$$\begin{aligned}
\int d^3k &= \int |\mathbf{k}|^2 dk \int \sin\theta d\theta \int d\phi \\
&= \frac{2\pi}{|\mathbf{q}|}\int E_k dE_k \int E_{k\pm q}dE_{k\pm q} \qquad (2.232)
\end{aligned}$$

where we have substituted $|\mathbf{k}| \to E_k$. Finally, we impose the integration limits on $|\cos\theta_\pm| \leq 1$ by means of the Heavyside step function

$$\begin{aligned}
\int_{-1}^{1} d|\cos\theta_\pm| &= \int E_{k\pm q}dE_{k\pm q}\theta\left[4|\mathbf{k}|^2|\mathbf{q}|^2 - \left(E_{k+q}^2 - E_k^2 - |\mathbf{q}|^2\right)^2\right] \qquad (2.233)\\
\Rightarrow \int d^3k &= \pm\frac{2\pi}{|\mathbf{q}|}\int E_k dE_k \int E_{k\pm q}dE_{k\pm q}\theta\left[4|\mathbf{k}|^2|\mathbf{q}|^2 - \left(\pm E_{k+q}^2 \mp E_k^2 \mp |\mathbf{q}|^2\right)^2\right]. \qquad (2.234)
\end{aligned}$$

Substituting the equation above into Eqs. (2.225) and (2.226) and performing the integration over $E_{k\pm q}$ results in

$$\begin{aligned}\mathrm{Im}_A &= -\frac{1}{16\pi|\mathbf{q}|}\int dE_k\theta(E_F-E_k)\theta(E_k)\theta(-E_F+E_k+q_0)\\ &\quad\times\theta\left(-E_k^2q_\mu^2-M^2|\mathbf{q}|^2-E_kq_0q_\mu^2-\frac{q_\mu^4}{4}\right)\mathcal{T}_{SS}(k,k+q)_{k_0=E_k},\end{aligned}\tag{2.235}$$

$$\begin{aligned}\mathrm{Im}_B &= -\frac{1}{16\pi|\mathbf{q}|}\int dE_k\theta(E_F-E_k)\theta(E_k-q_0)\theta(-E_F+E_k-q_0)\\ &\quad\times\theta\left(-E_k^2q_\mu^2-M^2|\mathbf{q}|^2+E_kq_0q_\mu^2-\frac{q_\mu^4}{4}\right)\mathcal{T}_{SS}(k-q,k)_{k_0=E_k}.\end{aligned}\tag{2.236}$$

The integral in Eq. (2.236) equates to zero because the step functions require E_k to be larger and smaller than the Fermi energy, E_F, i.e.

$$E_k+q_0<E_k<E_F.\tag{2.237}$$

This requirement is unphysical, hence

$$\mathrm{Im}_B \Rightarrow 0 \text{ contribution.}$$

We therefore have that

$$\begin{aligned}\mathrm{Im}\{\Pi_{SS}\} &= -\frac{1}{16\pi|\mathbf{q}|}\int dE_k\theta(E_F-E_k)\theta(E_k)\theta(-E_F+E_k+q_0)\\ &\quad\times\theta\left(-E_k^2q_\mu^2-M^2|\mathbf{q}|^2-E_kq_0q_\mu^2-\frac{q_\mu^4}{4}\right)\mathcal{T}_{SS}(k,k+q)_{k_0=E_k}.\end{aligned}\tag{2.238}$$

We solve Eq. (2.238) analytically for the scalar-scalar (SS) case. Here

$$\begin{aligned}\mathcal{T}_{SS}(k,k+q) &= 8M^2+4(k_0q_0-\mathbf{k}\cdot\mathbf{q})\\ &= 8M^2+4(E_kq_0-E_kq_0-\frac{q_\mu^2}{2})\\ &= 8M^2-2q_\mu^2.\end{aligned}\tag{2.239}$$

Substituting Eq. (2.239) into Eq. (2.238) and performing the integration over E_k results in

$$\mathrm{Im}\left\{\Pi_{SS}(q)\right\} = -\frac{1}{8\pi|\mathbf{q}|}\left(4M^2 - q^2\right)\left(E_{upper} - E_{lower}\right) \tag{2.240}$$

where

$$E_{upper} = \sqrt{k_F^2 + M^2} \tag{2.241}$$

$$E_{max} = \max\left[M, E_{upper} - q_0, \frac{|\mathbf{q}|}{2}\left(\sqrt{1 - \frac{4M^2}{q_\mu^2}} - q_0\right)\right] \tag{2.242}$$

$$E_{lower} = \min\left[E_{max}, E_{upper}\right] \tag{2.243}$$

are derived from the limits imposed by the $\theta-$functions on the integral in Eq. (2.238). Eq. (2.240) is our main result for this section. To conclude we have that the polarization tensors for $\mathrm{Im}\left\{\Pi_{SP}\right\} = \mathrm{Im}\left\{\Pi_{PS}\right\} = 0$ and

$$\mathrm{Im}\left\{\Pi_{PP}(q)\right\} = \frac{q^2}{8\pi|\mathbf{q}|}(E_F^* - E^*). \tag{2.244}$$

In Summary

In this chapter we systematically presented our fully relativistic formalism to calculate the double differential cross section for the inclusive quasielastic proton nucleus scattering reaction using distorted wave functions. Starting with the definition of the double differential cross section we derived an expression whereby the differential cross section was related to the matrix element. The matrix element contains all the dynamics that describe the reaction under consideration.

The matrix element describes the initial and final state of the reaction connected to each other by means of the scattering operator. For our purposes, we used the IA1 representation of the scattering operator. Evaluating the amplitudes of the scattering operator at the asymtotic momenta, allowed us to remove the local momentum dependence after which we were able to continue with our analysis. Furthermore, making use of the nuclear matter approximation, made it possible to separate the projectile/ejectile part from the nuclear structure part. We were then able to write the double differential cross section as a contraction between the projectile or hadronic tensor and the polarization tensor.

To include distortions in our formalism, we employed the eikonal approximation to describe the nuclear distortions on the incoming and outgoing particles. Finally, we showed that one can derive an analytical expression for the polarization tensor using a Fermi gas model of the nuclear response.

In the next chapter we will look at the numerical work related to the successful calculation of the double differential cross section using Eq. (2.82).

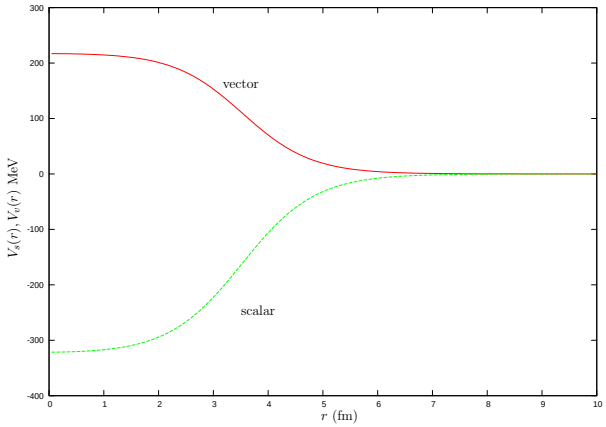

(a) Real part of the scalar and vector Dirac optical potentials

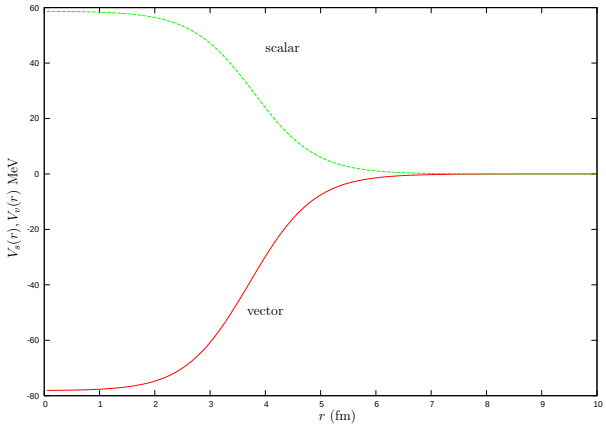

(b) Imaginary part of the scalar and vector Dirac optical potentials

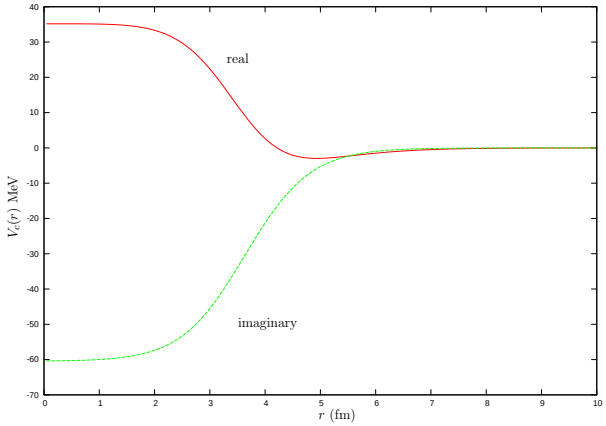

(c) Effective central potential (real and imaginary components)

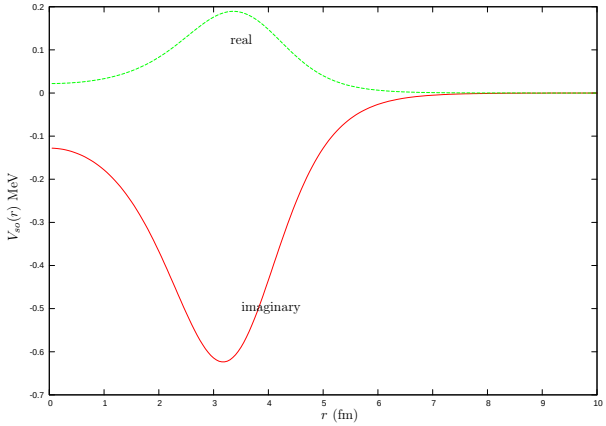

(d) Effective spin-orbit potential (real and imaginary components)

FIG. 2.3: *Dirac optical potentials and equivalent Schrödinger central and spin-orbit potentials for* ^{40}Ca *at 497.5 MeV. Notice that at around 6 fm the optical potentials are already close to zero. Also take note of the shape of the spin-orbit potential which is the derivative of the central potential.*

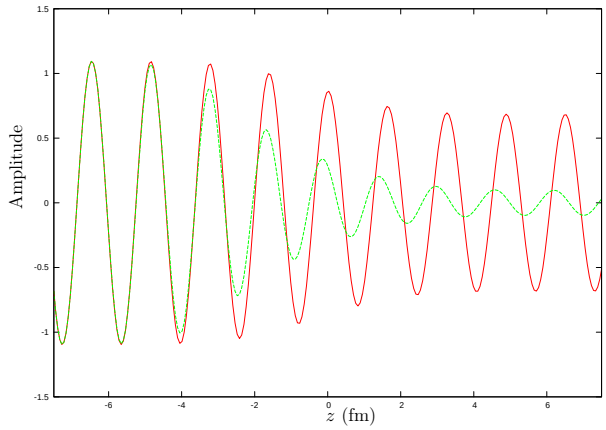

(a) Real part of the incoming upper 1st component Dirac eikonal distorted wave for a wave passing close to the center of the scattering potential (green) and for one a further distance away from the scattering center (red).

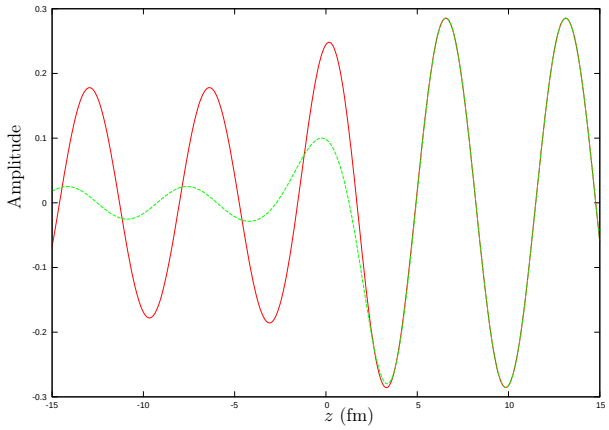

(b) Real part of the outgoing 3rd component Dirac eikonal distorted wave for a wave passing close to the center of the scattering potential (green) and for one a further distance away from the scattering center (red).

FIG. 2.4: *Incoming and outgoing Dirac eikonal distorted waves for an incident proton with $T_{lab} = 400$ MeV. The target nucleus is ^{40}Ca. Notice how the incoming wave function's wavelength changes relative to (a) its left side, the condition where the potentials are zero and (b) the wave function of a particle further away from the scattering center. Also notice the attenuation of the amplitudes of the two wave functions. Similarly the outgoing wave functions (on the right) have much longer wavelengths from the incoming wave functions. Their amplitudes are altered to that of plane waves outside of the nuclear boundary ($\pm$ 6 fm).*

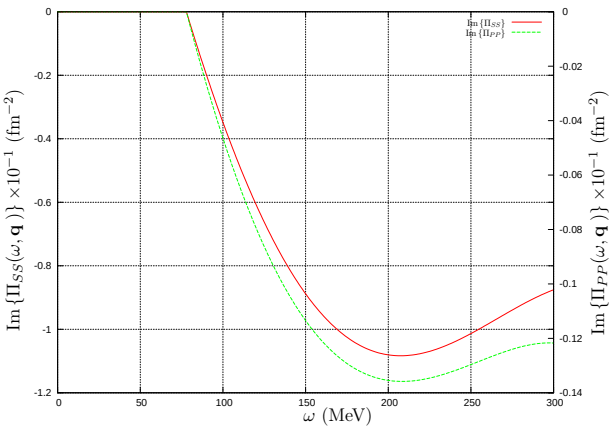

(a) $\mathrm{Im}\Pi_{SS}(\omega, \mathbf{q})$

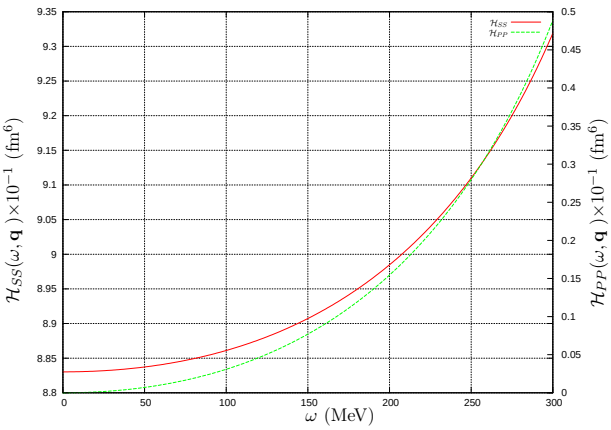

(b) $\mathcal{H}^{SS}(\mathbf{q})$ for longitudinally polarized protons

FIG. 2.5: *The hadronic and polarization tensors in the plane wave limit with incident projectile energy of $T_{lab} = 400$ MeV on ^{40}Ca, $\theta_{cm} = 40°$. The red curves indicate the cases for the scalar interaction and the green dashed curve indicates the pseudovector interaction.*

Chapter 3

Numerical Analysis

In this chapter we discuss the numerical analysis which accompanies the theoretical development outlined in the previous chapter. The numerical implementation of the formalism presented in this thesis is one of the pillars of this project. It often happens that the discussion of the numerical aspect of a certain research project is not given as much attention as the theoretical development. One reason for this is that generations of physicists have used codes which have been freely available and basically just modified them to suite the particular problem they were studying. This is surely the case in Nuclear Physics. The code then becomes a "black box" and the researcher then feels justified in mentioning as little as possible (or in some cases nothing at all) about the numerical aspects of the project. This philosophy is in no way applicable to the problem studied in this thesis. Indeed, all codes were written from scratch to ensure compatibility and the optimal use of resources. As mentioned earlier, and further expanded upon in this chapter, speed of execution is one of the primary factors which must be considered in the numerical implementation of the formalism. In the painstaking process of writing a code which balances accuracy with speed of execution, we have developed a novel method which combines FORTRAN and the powerful fitting and interpolation function of Matlab with cluster computing techniques to obtain results in a reasonable amount of time.

It is appropriate at this stage to define terms and concepts in the context of this thesis:

Code/Compiler Code refers to a computer program written for this project. The programming language used is primarily FORTRAN 90 with some FORTRAN 77 subroutines included. The compiler that was used to generate the executables is the Intel 'ifort' 11.0.083 compiler. Also, the free gFortran compiler was used as well and the Fujitsu Lahey compiler. Apart from minor irritations with the Lahey and gFortran compilers, they gave the exact same results.

Precision/Convergence In conventional computational physics text books, the 'accuracy' refers to the error term in which the error is the difference between the exact analytical result and the numerically computed result, usually presented as $I_{exact} = I_{numerical} + \epsilon$. In our case I_{exact} **does not exist**! Accuracy or precision therefore refers to the convergence value computed with two

or more different numerical integration tools or schemes.

Speed/Time These are used interchangeableably unless explicitly stated. The terms will refer to the CPU usage clock time. The speed at which a particular code runs is measured in seconds based on the time the CPU uses to carry out the instructions.

Operating systems The operating system used is openSUSE 11.1. On the cluster system that we used Mandriva vers.10 was the operating system.

Machines Machine refers to the physical computer used to perform the calculations. CPU clock times shown is on a Intel Core2Duo 2.8 GHz processor with 2 GB of RAM[1]. Clearly not the top of the line, but sufficiently fast for our purposes.

In our case, new code was written from the ground up except for the calculation of the scattering amplitudes F_L. Our aim is to be able to compute the differential cross section in a reasonable amount of time (without sacrificing accuracy) and preferably using a desktop or laptop computer. We have shown in the previous chapter that we can write the differential cross section for quasielastic proton-nucleus scattering as a contraction of two tensors

$$\frac{d\sigma}{dE'd\Omega'} = -\frac{1}{\pi}K \text{ Im}\left[\sum_{L,L'=S}^{T} F_L F^*_{L'} \int d^3q d^3x d^3y \; e^{-i\mathbf{q}\cdot(\mathbf{x}-\mathbf{y})}\mathcal{H}^{LL'}(\mathbf{x},\mathbf{y})\Pi_{LL'}(\mathbf{q},\omega)\right]. \tag{3.1}$$

The most elegant feature of Eq. (3.1) remains its complete separation of the hadronic (projectile) part $\mathcal{H}^{LL'}$ from the polarization (target) part $\Pi_{LL'}(\mathbf{q})$. We stress again that this is a first attempt to calculate the distorted wave differential cross section for inclusive proton-nucleus quasielastic scattering.

Previous calculations of quasielastic cross sections used plane waves, but there was always a need to include distorted wave functions into the RPWIA formalism [1]. We choose to describe the nuclear distortions on the incoming and outgoing wave functions in terms of Dirac eikonal distorted waves derived in the previous chapter. This choice is motivated on the grounds of its simplicity but effectiveness of including distortions as opposed to a full partial wave expansion, where one finds that usually 30 or more partial waves are needed to compute the incoming full distorted wave function alone. A distorted partial wave expansion [1] adds an additional set of summations (l, j, m, s_z) **per distorted wave** within the three dimensional integral that describes $\mathcal{H}^L(\mathbf{q}\ )$. In contrast, the eikonal distorted wave function only contains an additional integration variable z' in the three dimensional integral $\mathcal{H}^L(\mathbf{q}\ )$ to compute the magnitude of the force that acts in on the projectile and the ejectile. This results in a frequency change and an attenuated amplitude of the incoming plane wave and outgoing plane wave. The frequency change is brought about by the real part of the effective optical potential whereas the

[1]Note: The cluster computer system we used to run parallel algorithms used Intel Pentium 4 3.0 GHz processors with each box having 2 GB of RAM onboard. We also used two older 'linux boxes' fitted with AMD 3200 2.2GHz 64-bit processors. These were comparable in speed to that of the Pentium 4 cluster machines.

amplitude attenuation of the plane wave is due to the imaginary part of the effective optical potential. Additionally we were able to include spin orbit distortions in the formalism which is often dropped in applications using distorted waves described by the Dirac eikonal distorted wave function. In our calculations we set this parameter equal to zero.

Although the formalism uses less integration variables, it is still a multidimensional integral. Keep in mind that the distorted wave functions are computed in a three dimensional integral over space d^3x. This integral is nested in a three dimensional momentum integral d^3q. Multidimensional integrals are not studied extensively [46] and one will in general resort to integration product rules expanded upon in Sec. 3.1.1.2. However, from a numerical point of view, Monte Carlo and quasi-Monte Carlo methods prove to be the more convenient integration methods to employ provided the integrand is relatively smooth. The question is then which of the two numerical approaches is best suited to our problem and why? This question we address in the immediate section following. Then, based on the method of choice, we develop a workable procedure to do the integration in an efficient manner from which we are able to compute the differential cross section in a reasonable amount of time. The next question to answer is if the eikonal distorted wave provide the necessary qualities to extract the relevant inclusive quasielastic scattering observables? Based on the arguments above, we implicitly assume that the Dirac eikonal formalism will provide a significant speed advantage when it comes to computing the double differential cross section. This chapter aims to measure that advantage.

3.1 Numerical quadrature

In this section we discuss the numerical integration method best suited to calculate the integrals in Eq. (3.1). Normally one would use two alternate but complementary integration techniques to draw confidence from a numerically computed result. In general, both methods should give results within a margin of each other. Initially, we wanted to compute the differential cross section using Gaussian integration, Monte Carlo integration and quasi-Monte Carlo integration however due to the time penalty related to the convergence rate of each method we had to choose one. Secondly, having to maintain different codes proved to be problematic because errors creep in easily and distinguishing between human error or 'software' errors proved to be tremendously time consuming. We did however, compare the different quadrature schemes. Before we present our results, we quickly review each method [49, 50, 51].

3.1.1 Gaussian quadrature

Gaussian quadrature is a numerical integration technique in which the integral is evaluated by means of a sum of finite terms. Each term is a product of an interpolation function evaluated at specific function values known as roots x_i's and the associated weights $w(x_i) = w_i$'s for each point. The interpolation function $p(x_i)$ is normally a polynomial. This scheme is also known as an interpolation quadrature

scheme.

3.1.1.1 One-dimensional integration

The integral is given as

$$I = \int_a^b dx\ f(x). \tag{3.2}$$

The function $f(x)$ is interpolated by a weighted function $p(x)$ as follows

$$f(x) \approx w(x)p(x). \tag{3.3}$$

The integral is then evaluated as

$$I \ \approx \ I_{GQ} = \int_a^b dx\ w(x)p(x) = (b-a)\sum_{i=1}^{N} w_i p(x_i) \tag{3.4}$$

in which $w(x)p(x)$ is integrated exactly.

3.1.1.2 Multidimensional integration

The integration rule given by Eq. (3.4) becomes a 'product rule' in multiple dimensions where each dimension is integrated using the one-dimensional rule. Eq. (3.4) then becomes

$$I_{GQ} = \int_a^b \int_c^d dx\ dy\ f(x,y) = (b-a)(d-c)\sum_{i=1}^{N}\sum_{j=1}^{N} w_i w_j\ p(x_i, y_j) \tag{3.5}$$

in the case of two dimensions. Extending Eq. (3.5) for many dimensions highlights the 'dimensional curse'. The integrand $p(x_i, y_j, \ldots, z_r)$ is sampled N^r times where r is the number of dimensions that need to be integrated over. It is clear from this that if N is large, the computation will take a long time to complete. In general smooth functions require fewer function evaluations.

3.1.2 Monte Carlo integration

To bypass the dimensionality curse, the Monte Carlo integration technique is used. For reasonably **smooth** functions, Monte Carlo integration works just as well and sometimes better than interpolation techniques [51]. Instead of sampling the function at pre-determined equally spaced points between the integration limits, the Monte Carlo method samples the integrand at random points within the integration limits. The function values are subsequently summed and then the average is computed.

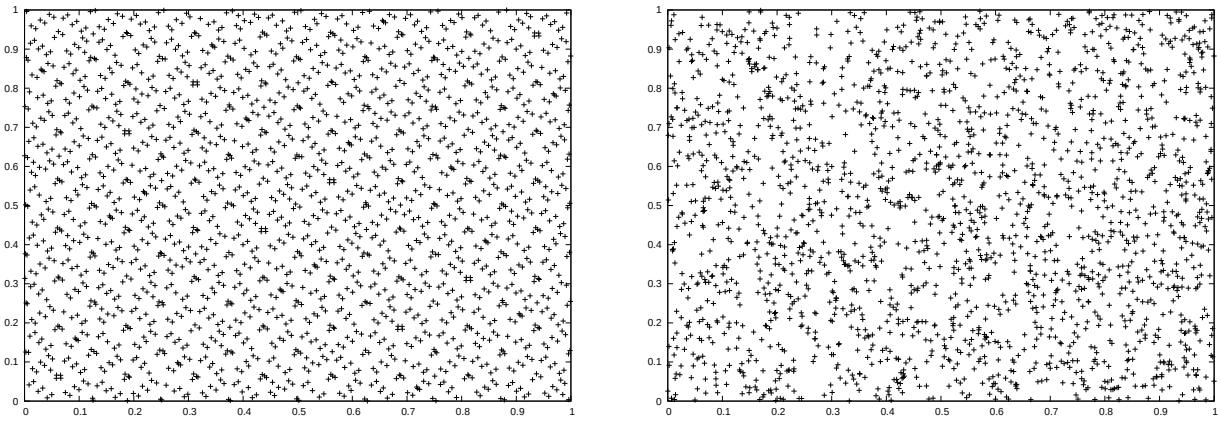

(a) Sobol sequence in 2-D

(b) Random numbers in 2-D

FIG. 3.1: *Sobol sequence and random number sampling of an [0,1]×[0,1] area with N = 2048 points. Notice the 'pattern' of the quasirandom sequence.*

The general formula to calculate Eq. (3.2) using Monte Carlo integration is given by

$$I_{MC} = (b-a)\frac{1}{N}\sum_{i=1}^{N} f(x_i), \tag{3.6}$$

where (a, b) mark the integration limits and the i-th point $x_i = (b-a) \times r_i + a$ is computed from the random number set $r_i \in (0, 1)$.

Additionally one can compute an 'error' of the computed integral's value from the 'absolute or correct' value with the Monte Carlo integration method. The formula to compute the error or 'variance' of Eq. (3.6) is given as

$$\sigma \approx \pm\sqrt{\frac{I_{MC}^2 - (I_{MC})^2}{N}}, \tag{3.7}$$

where

$$I_{MC}^2 = (b-a)^2\frac{1}{N}\sum_{i=1}^{N} f^2(x_i). \tag{3.8}$$

3.1.2.1 Multidimensional integration

In the case of interpolation quadrature techniques, we see that each dimension or degree of freedom that needs to be summed over generates a nested one-dimensional sum. However, in the case where the Monte Carlo method is used, Eq. (3.6) becomes

$$I_{MC} = (b-a)(d-c)\frac{1}{N}\sum_{i=1}^{N} f(x_i, y_i), \tag{3.9}$$

where $y_i = (d-c) \times r_i + c$ and the random number $r_i \in (0,1)$. Monte Carlo integration is always appealing for multidimensional integration problems because the single sum can easily and effectively be parallelized.

3.1.3 Quasi-Monte Carlo integration

As the name suggests, quasi-Monte Carlo integration is based on Monte Carlo integration, i.e. the integral is evaluated with the same formula as Eq. (3.6). The difference however is with the evaluation of the points r_i. Whereas the points in Monte Carlo routines are random points between the (0,1) interval, quasi-Monte Carlo routines make use of *low discrepancy* sequences shown in FIG. 3.1. Common sequences are Sobol, Halton and Nieddereiter sequences [52, 53, 54]. As mentioned, the numbers comprising the sequence are termed low discrepancy and refers to the magnitude difference in distance between successive points in the sequence. The smaller the difference, the lower the 'discrepancy'. 'Quasirandom sequences' then are deterministic points that are uniformly spread across the integration interval [55].

The advantage of using quasirandom sequences is based on their perceived rapid error decrease which is considered superior to the Monte Carlo error term. Whereas the error term of Monte Carlo integration decreases as $N^{-\frac{1}{2}}$ and is independent of the number of dimensions, that of quasi-Monte Carlo decreases as $(\log N)^d/N$ where N is the number of function evaluations and d the number of dimensions. The latter reason was the motivation to test the quasi-Monte Carlo integration scheme. However, we must point out here too that quasirandom sequences are generated at will by researches for a variety of applications [56].

3.2 Numerical checks

The complete calculations for the double differential cross section is far from trivial and this work is the first attempt to include distorted wave functions, consequently we will only focus on the rank-0 contribution to $\Pi_{LL'}$, i.e. Π_{SS} and Π_{PP}. Due to the fact that we are attempting the computation, we need a system of numerical checks with which we could measure the accuracy of our programming.

The method discussed in the previous section formed the basis of our numerical checks. This is because the quantity $\mathcal{H}^S(\mathbf{q})$ has not been computed before for distorted waves and we used two complementary numerical methods as confirmation of the results. However, the constituents of $\mathcal{H}^S$ namely, the wave functions had to be computed correctly. We identified the main building blocks or constituents of the double differential cross section and computed these individually.

Eq. (3.1) contains three major ingredients. These are:

1. The distorted wave functions $\psi^{(+)}_{\mathbf{k},s}, \bar{\psi}^{(-)}_{\mathbf{k}',s}$ contained in $\mathcal{H}_{LL'}(\mathbf{q},\omega)$,

2. The form of the polarization $\Pi_{LL'}(\mathbf{q},\omega)$,

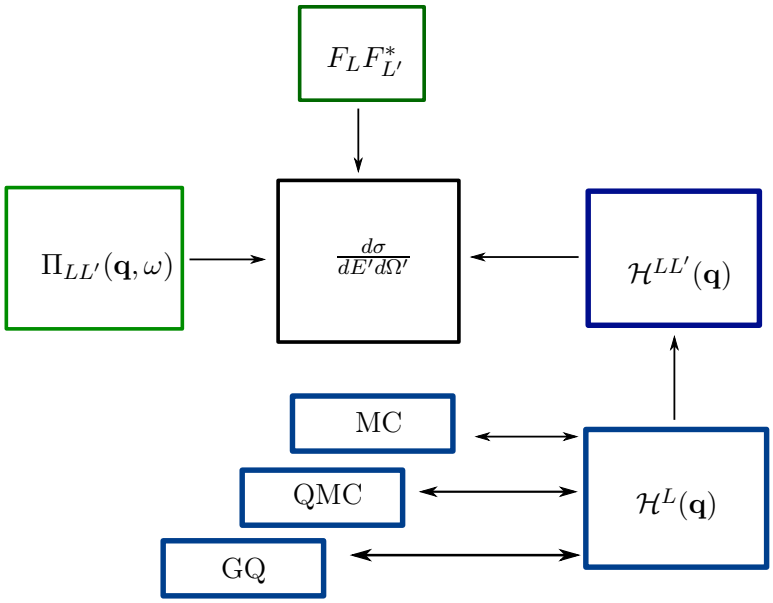

FIG. 3.2: *General flow diagram of numerical inputs to the proper calculation of the polarized double differential cross section for inclusive quasielastic proton-nucleus scattering reactions. The major computational complexity lies in the hadronic tensor $\mathcal{H}^L(\boldsymbol{q})$ and we use three different numerical quadrature schemes to confirm our computed result as a measure of numerical accuracy and convergence.*

3. The complex scattering amplitudes $F_L(\mathbf{k},\mathbf{k}',\mathbf{K})$.

3.3 Application of numerical methods

Using the IA1 representation of the NN interaction allows us to write the double differential cross section proportional to the contraction of the hadronic and polarization tensors. The modular nature of Eq. (3.10) allows us to systematically compute each factor individually knowing their precise components.

$$\frac{d\sigma}{dE'd\Omega'} \propto \int d^3q\, \mathcal{H}^{SS}(\mathbf{q})\, \mathrm{Im}\left\{\Pi_{SS}(\mathbf{q},\omega)\right\}. \tag{3.10}$$

We take advantage of this to test the performance of the three integration methods. We write

$$\begin{aligned}\int d^3q\, \mathrm{Im}\left\{\Pi_{SS}(\mathbf{q},\omega)\right\} \int d^3x \mathcal{H}^S(\mathbf{q}) \int d^3y \mathcal{H}^S(\mathbf{q}) &= \int d^3x\, d^3y \mathcal{H}^{SS}(\mathbf{x},\mathbf{y}) \int d^3q\, e^{-i\mathbf{q}\cdot(\mathbf{x}-\mathbf{y})} \\ &\quad \times \mathrm{Im}\left\{\Pi_{SS}(\mathbf{q},\omega)\right\} \\ &= \int d^3x\, d^3y\, \mathcal{H}^{SS}(\mathbf{x},\mathbf{y}) F(\mathbf{z},\mathbf{q},\omega) \end{aligned} \tag{3.11}$$

where

$$F(\mathbf{z},\mathbf{q},\omega) = \int d^3q\, e^{-i\mathbf{q}\cdot\mathbf{z}}\, \mathrm{Im}\left\{\Pi_{SS}(\mathbf{q},\omega)\right\} \tag{3.12}$$

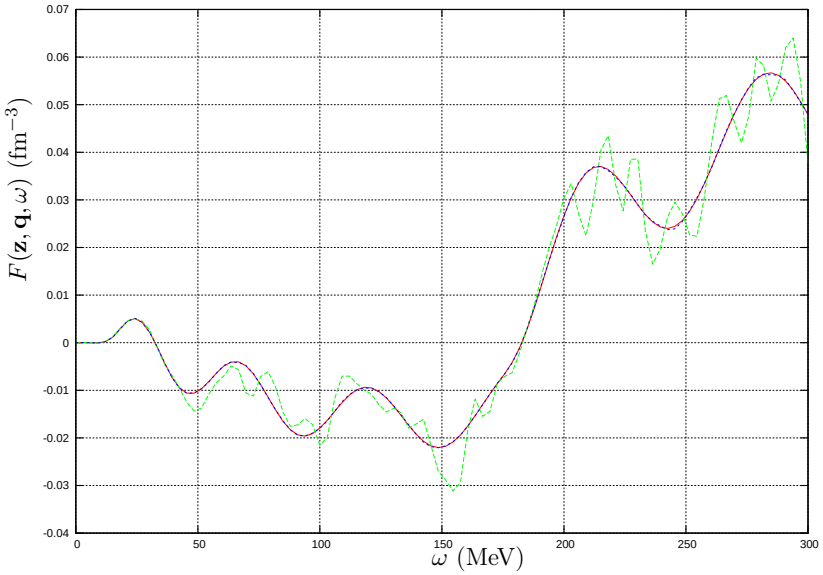

FIG. 3.3: *Real part of* $F(\boldsymbol{z},\boldsymbol{q},\omega)$ *(Gaussian Quadrature (GQ), quasi-Monte Carlo (QMC) and Monte Carlo (MC) integration where* $F(\boldsymbol{z},\boldsymbol{q},\omega) = \int d^3q\; e^{-i\boldsymbol{q}\cdot\boldsymbol{z}}\,\mathrm{Im}\{\Pi_{SS}(\boldsymbol{q},\omega)\}$*. GQ used 200 Gaussian points, QMC -* 10^7 *points and MC -* 10^7 *points). The red curve is for GQ, the blue curve for QMC and the green curve for MC.*

with $\mathbf{z} = \mathbf{x} - \mathbf{y}$ and

$$\mathcal{H}^{SS}(\mathbf{x},\mathbf{y}) = \left[\bar{\psi}^{(-)}(\mathbf{x},\mathbf{k}',\hat{\mathbf{i}}',s')\lambda^S\psi^{(+)}(\mathbf{x},\mathbf{k},\hat{\mathbf{i}},s)\right]\left[\bar{\psi}^{(+)}(\mathbf{y},\mathbf{k},\hat{\mathbf{i}},s)\overline{\lambda^S}\psi^{(-)}(\mathbf{y},\mathbf{k}',\hat{\mathbf{i}}',s')\right]. \tag{3.13}$$

The benefit of this form (Eq. (3.11)) is that the six dimensional integral $\int d^3x\; d^3y$ can easily be transformed to dimensionless variables and integrated with the equation similar to Eq. (3.9) using either random variables or quasirandom sequences. However, the integral $F(\mathbf{z},\mathbf{q},\omega)$ is still nested within this sum. Before we proceed we mention that all integration variables are transformed using the transformation equation

$$x' = (b-a)x + a \tag{3.14}$$

where a and b are the old integration limits and the transformed variable now lies between the new integration limits [0,1]. Additionally, the integrand is scaled by $(b-a)$ when dx' is substituted for dx because

$$dx' = (b-a)dx. \tag{3.15}$$

Therefore, for all the integrations we performed the transformation

$$\int_a^b f(x')\,dx' \;\rightarrow \int_0^1 f((b-a)x+a)(b-a)dx. \tag{3.16}$$

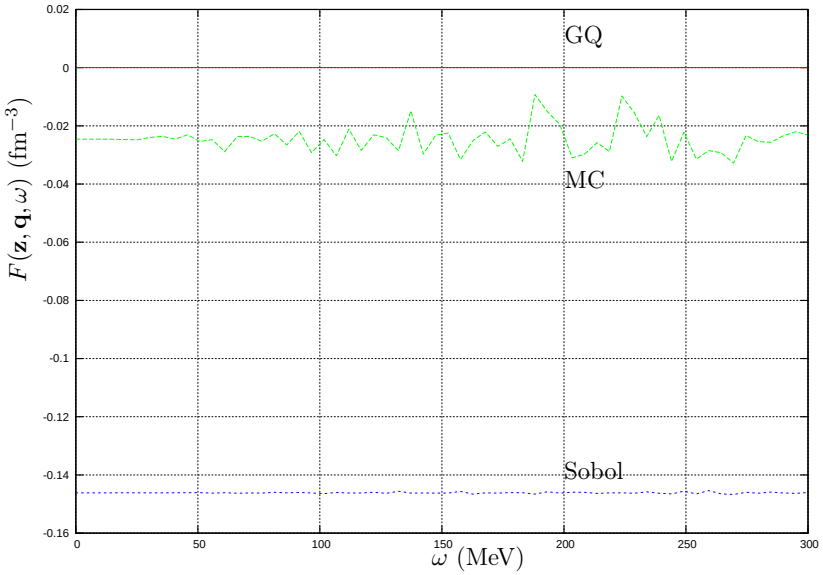

FIG. 3.4: *Imaginary part of* $F(\boldsymbol{z},\boldsymbol{q},\omega)$ *(Gaussian Quadrature (GQ), quasi-Monte Carlo (QMC) and Monte Carlo (MC) integration where* $F(\boldsymbol{z},\boldsymbol{q},\omega) = \int d^3q\, e^{-i\boldsymbol{q}\cdot\boldsymbol{z}}\, \mathrm{Im}\,\{\Pi_{SS}(\boldsymbol{q},\omega)\}$*. GQ used 200 Gaussian points, QMC -* 10^7 *points and MC -* 10^7 *points).*

We now look at the convergence properties of Eq. (3.12).

The integral in Eq. (3.12) is a function of the space coordinate $\mathbf{z}$ and the energy transfer ω. For a fixed coordinate in space $\mathbf{z} = (z_x, z_y, z_z)$ we computed the integral in spherical momentum space as a function of ω in the region where $\mathrm{Im}\,\{\Pi_{SS}(\mathbf{q},\omega)\} \neq 0$. Even though $\mathrm{Im}\,\{\Pi_{SS}(\mathbf{q},\omega)\}$ is a function of $|\mathbf{q}|$ only, the dot product in the exponential of Eq. (3.12) is not and the integration over the polar coordinates (θ_q, ϕ_q) must be performed explicitly.

The result of the comparison of the three methods is summarized in FIG. 3.3 and 3.4. For the Gaussian integration method (GQ), $F(\mathbf{z},\mathbf{q},\omega)$ needed 200 Gaussian points to converge. In the case of using Sobol random sequences (QMC) the function needed 1 048 576 points for the real part to agree exactly with the real part for the GQ case. The Monte Carlo (MC) case did not fare too well with respect to the other two methods. It did not reach exactly the same value for the real part relative to the other two methods. In contrast, the imaginary parts of the integral shown in FIG. 3.6 was of particular interest. It is clear that GQ performs the best in computing a zero imaginary component for F as opposed to the QMC and MC methods. From a computational view, the integral value of F is programmed as a complex data type. Although the imaginary part of F returns zero in the case of GQ, when computing the contraction with the hadronic tensor the imaginary component will have a negligible contribution to the numerically computed matrix element. This will not be the case with the other two methods. Here a contribution from the imaginary component will be carried into the computed value of the matrix element. This is important to keep in mind because it does influence

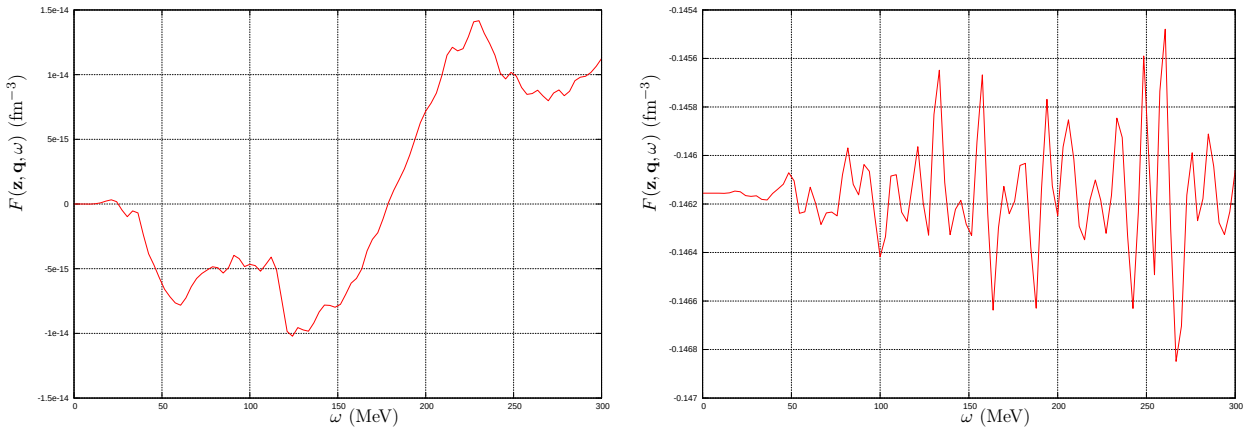

(a) GQ: Imaginary part of $F(\mathbf{z},\mathbf{q},\omega)$

(b) Sobol: Imaginary part of $F(\mathbf{z},\mathbf{q},\omega)$

FIG. 3.5: *The imaginary parts of $F(\boldsymbol{z},\boldsymbol{q},\omega)$ for Gaussian Quadrature (GQ) and QMC (GQ used 200 points and QMC used 10^7 points). Notice that the value computed with GQ is zero however QMC the imaginary component is non-zero. In fact, it is larger in magnitude than the real part of the integral for QMC. Therefore in the latter case this component is non-negligible.*

the rate of convergence. The fact that the imaginary components computed using the quasirandom sequences where not converging to negligible small values (e.g. $\tilde{1}0^{-15}$), implimentation of Eq. (3.11) using the quasi-Monte Carlo integration scheme was a particular source of frustration. Although the use of the quasi-Monte Carlo integration technique using Eq. (3.11) never hinted at converging and took a large amount of time to run, the approach was abandoned because even with a very large number of quasirandom points the computed results at times returned negative cross sections.

In summary then we see that GQ is better suited for the integration of F, however this is hardly unexpected as GQ trumps other quadrature methods when the dimensions are typically small ($d < 4$). The application of any of the three methods to Eq. (3.12) is however impractical. Computing $F(\mathbf{z},\mathbf{q},\omega)$ typically takes 90 seconds on a Intel 2.8GHz Core2Duo to complete for 30 values of ω, i.e. approximately 3 seconds per ω. Even if only a 100 000 QMC or MC random points are needed to converge Eq. (3.11), it takes more than 83 hours to compute $F(\mathbf{z},\mathbf{q},\omega)$ for one ω.

3.4 Speed and convergence

In the previous section we established the use of Gaussian integration as the preferred numerical quadrature method to use. We have shown that for our application, Monte Carlo and quasi-Monte Carlo integration schemes do not provide a significant advantage over the Gaussian technique. However, the example of Eq. (3.12) is not conclusive because one can always parallelize the six-dimensional part in Eq. (3.11) and power through with brute force. Secondly, our preferred method had to converge as fast as possible and with the three methods giving similar speeds in computation for Eq. (3.12) we used another discriminator. Also note, that if one is to compute the integral given as in Eq. (3.11),

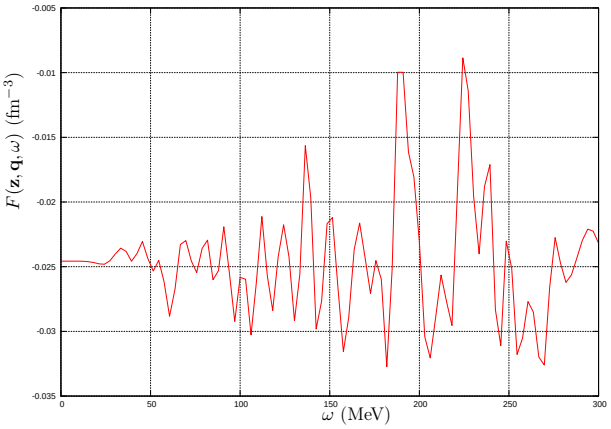

(a) MC: Imaginary part of $F(\mathbf{z},\mathbf{q},\omega)$

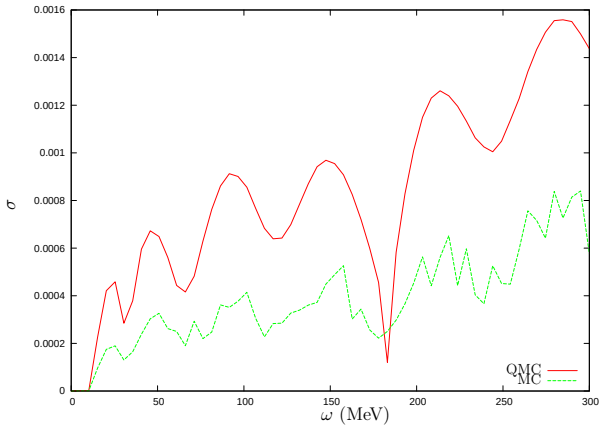

(b) Comparison of error between QMC and MC integration. Notice that the MC error is less than that for QMC.

FIG. 3.6: *The imaginary parts of $F(\boldsymbol{z},\boldsymbol{q},\omega)$ for MC (MC used 10^7 points). Notice that the value computed with GQ is zero however for MC and QMC the imaginary component is non-zero. Here the magnitude of the real part of the integral for MC is of the same order as the imaginary part. On the right, the computed 'error' of the MC and QMC integrals are compared. Notice that the error for QMC is in actual fcat worse than that for MC.*

one is limited to applying the Monte Carlo integration technique because it will be impractical to compute the six-dimensional part using interpolatory integration. This will lead to 9 nested sums in the implimentation according to Eq. (3.5).

The test that highlighted the differences between the Gaussian approach and that of the quasi-Monte Carlo integration approach for this application was when we computed the three dimensional integral $\mathcal{H}^S(\mathbf{q})$ given by Eq. (2.87)

$$\mathcal{H}^S(\mathbf{q}) = \int bdbd\phi_b dz\ e^{-i\mathbf{q}\cdot\mathbf{x}} \left[\bar{\psi}^{(-)}(\mathbf{x},\mathbf{k}',\hat{\mathbf{i}}',s')\lambda^S\psi^{(+)}(\mathbf{x},\mathbf{k},\hat{\mathbf{i}},s)\right] \tag{3.17}$$

where we have set the spin-orbit potential to zero and $\mathbf{x} = (b\sin\phi_b, b\cos\phi_b, z) = (\mathbf{b}, z)$. The momentum transfer $\mathbf{q} = (q,\theta_q,\phi_q)$ is fixed and we compared the speed of Gaussian integration and quasi-Monte Carlo integration using a Sobol sequence.

The result is summarized in Table 3.1 for Gaussian convergence and quasi-Monte Carlo convergence. One sees that the interpolatory method fares much better that that for the quasi-Monte Carlo method in computing $\mathcal{H}^L$. For the Gaussian method one sees that convergence of this integral occurs with 48 Gaussian integration points. Furthermore, this process only lasts a little more than 5 seconds. This was truly encouraging even if it was only for a single point $\mathbf{q}$. At the very least, we now know that the integral converges with at least 50 Gaussian points.

In contrast to this, the quasi-Monte Carlo procedure produced some puzzling results. By using more the 260 000 quasirandom sequence points, it seemed as if the integral converged and also that the time taken for the computation was comparable to that for Gaussian integration. The figures

TABLE 3.1: *Gaussian and quasi-Monte Carlo convergence rate for calculating* $\mathcal{H}^S(\boldsymbol{q})$*, where* $\boldsymbol{q} = (q = 2.64\ \text{fm}^{-1}, \theta_q = 4.58^o, \phi_q = 40.39^\circ)$

No. of Gaussian Points	$\Re(\mathcal{H}^S(\mathbf{q}))$	$\Im(\mathcal{H}^S(\mathbf{q}))$	CPU time
8	-14.6935776686482438	12.7180990798847127	0m0.040s
16	7.4873272525696679	-10.3481646259305933	0m0.264s
24	7.0065493101990333	6.3702518354898912	0m0.704s
32	0.7732524762914023	0.8145888635534635	0m1.688s
48	0.7254198392816334	0.5947267402101690	0m5.524s
56	0.7254136385888407	0.5947187766001918	0m8.725s
64	**0.7254136271728993**	**0.5947187570677752**	**0m13.041s**
76	0.7254136271638945	0.5947187570464221	0m21.597s
No. of Sobol Points	$\Re(\mathcal{H}^S(\mathbf{q}))$	$\Im(\mathcal{H}^S(\mathbf{q}))$	CPU time
1 000	24.7999621247402686	-1.0427836073954766	0m0.084s
30 000	0.6985742400722832	0.2718130347088967	0m1.552s
100 000	0.8969084601044238	0.7650375559647634	0m5.140s
262 144	**0.7273516067647386**	**0.6491917554795898**	**0m13.165s**
300 000	0.6109629901255518	0.5684414514297973	0m15.685s
500 000	0.7594351800169689	0.6144078393118674	0m25.010s
1 000 000	0.7214241330198518	0.6023587407567709	0m50.115s
1 500 000	0.7455002136332319	0.6073048357448024	1m15.141s

in bold in Table 3.1 highlight this scenario. Both methods evaluate or probe the integrand an equal amount of times, i.e. $64^3 = 262\ 144$. **Incidently**, both methods 'converged' to the same value taking an equal amount of time, however, in absolute contradiction to logical thought, using more quasirandom sequence points produced values that were not converging. This was more severe using the Monte Carlo routine. Doing the integral for more and more points up to 1 500 000 for this illustration, indicated that the quasi-Monte Carlo method will converge to the value calculated using Gaussian integration. However, as is clear, the time it takes to compute the integral using more than a million quasirandom points took more than a minute to complete. Another way to view this process is to compare the 'convergence rates' of the two methods shown in FIG. 3.7. As can be seen, the 'dimensional curse' for interpolatory methods is shown quite clearly. As the number of integration points increase per dimension, then time start increasing dramatically. In contrast to this the quasi-Monte Carlo integration method has a linear time increase. For this reason, Monte Carlo methods are very attractive as their estimated time is linear to the amount of sampling points, hence, with enough time, the Monte Carlo method will converge.

Oscillatory integrals: The high number of integration points needed for convergence needs to be clarified. The integrand in Eq. (3.12) is oscillatory. This is a particular problem to deal with in multidimensional integrals and is an area of active research [46, 57, 58, 59]. The general form of an

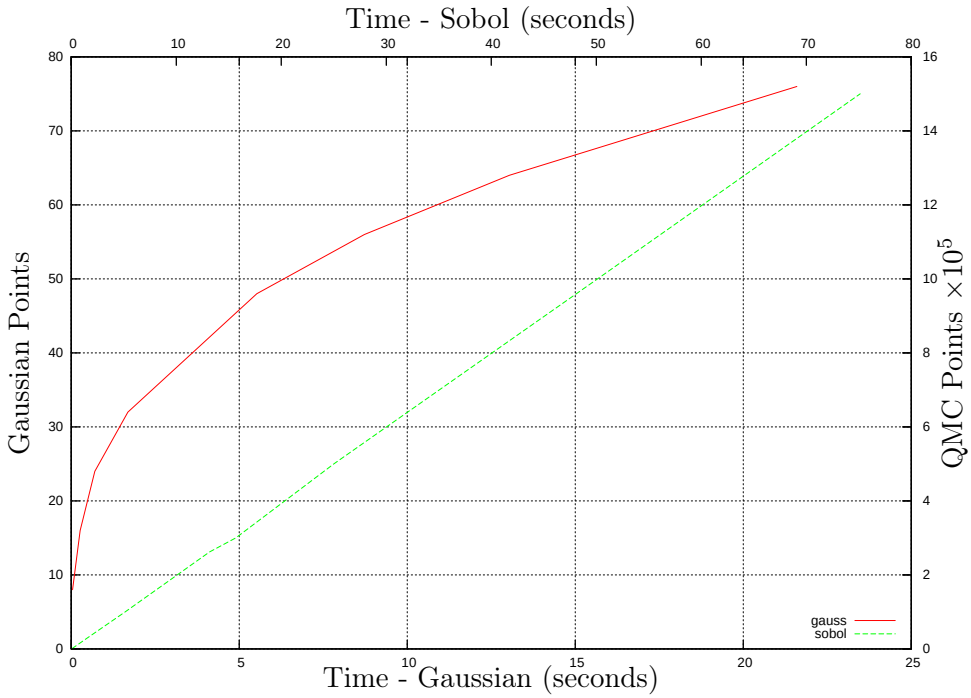

FIG. 3.7: *Convergence rate for GQ and QMC. It is clear from this plot that above 80 GQ points, the time to evaluate the integral grows astronomically, whereas for the (Q)MC schemes the execution time increases linearly.*

oscillatory integral is

$$I(f) \;=\; \int_a^b f(x)\, e^{i\omega g(x)} dx \tag{3.18}$$

where $f(x)$ and $g(x)$ are relatively smooth functions and ω is typically large (100+ say!). In recent years, this type of integrand has received much attention because of its wide recurrance in the natural sciences. Filon [60] and Levin [61] proposed two different methods to deal with this form of integrals. Filon's approach is to find an appropriate polynomial interpolant $p(x)$ for $f(x)$ and doing the integral using $p(x)$ rather than $f(x)$. Levin's approach has a wider application base than the Filon method. Levin transformed the integration problem into an ordinary differential equation problem where he solves

$$f(x) = p'(x) + i\omega\; g'(x)p(x) \tag{3.19}$$

for $p(x)$. The integral is then straightforward to compute

$$I(f) = \int_a^b (p'(x) + i\omega\; g'(x)p(x)) = p(b)e^{i\omega\; g(b)} - p(a)e^{i\omega\; g(a)}. \tag{3.20}$$

The benefit of using these methods rests in the magnitude of ω and much of the research is more geared to the one dimensional aspect of the integration as opposed to its multidimensional counterpart.

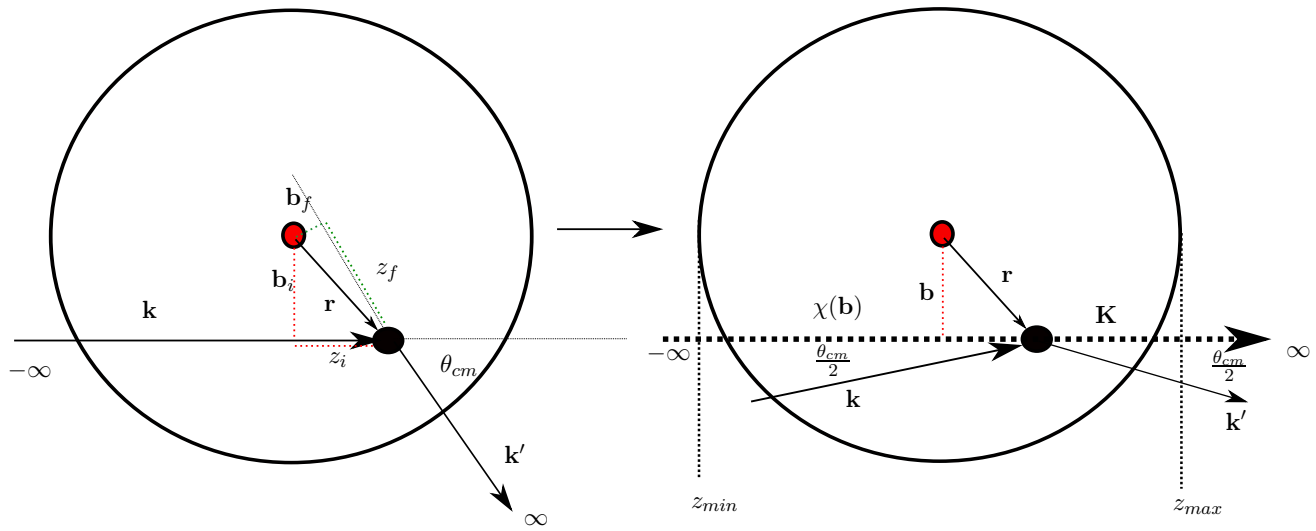

FIG. 3.8: *Impact parameters in the eikonal approximation. The figure on the left shows the different impact parameters for the incoming and outgoing particles, whereas the figure on the right shows the 'penetration depth' or the impact parameter* $\boldsymbol{b}$ *of the eikonal phase* $\chi(\boldsymbol{b})$ *taken to be perpendicular to the average momentum direction*

3.5 Integration limits - Eikonal

From the above analysis the quantity $\mathcal{H}^L$ can be computed in a reasonable amount of time with Gaussian integration. However, the eikonal phase, or 'integral', represents the effect that the potential has on the incoming and outgoing wave functions. Theoretically, the integration limits for the eikonal wave function for the incoming particle with outgoing boundary conditions is $-\infty$ and z, however for the calculation the lower limit must be fixed. The distorted waves only 'exist' in the presence of the potentials whereas outside of these, the distorted wave becomes a plane wave. To establish the limits for infinity we decompose the incoming$(+)$ distorted wave,

$$\psi^{(+)}(\mathbf{x},\mathbf{k},\hat{\mathbf{i}},s)=\left(\frac{E+M}{2M}\right)^{\frac{1}{2}}U_{(+)}(\mathbf{k},\hat{\mathbf{i}},s)f_{(+)}(\mathbf{x},\mathbf{k})g_{(+)}(\mathbf{x},\mathbf{k},\mathbf{k}'), \tag{3.21}$$

and outgoing$(-)$ distorted wave,

$$\bar{\psi}^{(-)}(\mathbf{x},\mathbf{k}',\hat{\mathbf{i}}',s')=\left(\frac{E+M}{2M}\right)^{\frac{1}{2}}U_{(-)}(\mathbf{k}',\hat{\mathbf{i}}',s')\gamma_0 f_{(-)}(\mathbf{x},\mathbf{k}')g_{(-)}(\mathbf{x},\mathbf{k},\mathbf{k}'), \tag{3.22}$$

to separate the integration-variable-dependent functions from the matrix components. Eq. (3.17) can then be written as

$$\mathcal{H}^S(\mathbf{q})=\left(\frac{E+M}{2M}\right)\left[U^{\dagger}_{(-)}\gamma_0 I_4 U_{(+)}\right]\int d^3\mathbf{x}\; e^{-i\mathbf{q}\cdot\mathbf{x}}f_{(-)}g_{(-)}f_{(+)}g_{(+)}. \tag{3.23}$$

In Eq. (3.23), the matrices multiply and reduce to a constant

$$\left[U^{\dagger}_{(-)}\gamma_0 I_4 U_{(+)}\right] \longleftrightarrow [1\times 4]\times[4\times 4]\times[4\times 4]\times[4\times 1] \Rightarrow \text{value},$$

and the three dimensional integral

$$I(\mathbf{q},\mathbf{x}) \approx \int d^3x\; e^{-i\mathbf{q}\cdot\mathbf{x}} f_{(-)} g_{(-)} f_{(+)} g_{(+)} \tag{3.24}$$

we need to compute is an oscillatory integrand. The Dirac spinors U and $\bar{U}$ are strictly functions of $\mathbf{x}$ due to the presence of the optical potentials in the lower components of the spinors and should strictly be confined under the integral sign, but the contributions from the scalar and vector potentials, which approximately cancel each other out, are dominated by the sum of the energy and mass terms. That is $E + M >> V_s - V_v$ and one can safely make the replacement $E + M + V_s - V_v \rightarrow E + M$. Making this replacement, the spinors factor out from under the integral sign and the integrand above contains all the components that are required for the integral. In Eq. (3.24), the 'short-hand' multidimensional integrand

$$e^{-i\mathbf{q}\cdot\mathbf{x}} f_{(-)} g_{(-)} f_{(+)} g_{(+)} \tag{3.25}$$

represents the functions in $\mathbf{x} = (\mathbf{b}, z)$

$$f_{(-)} = e^{-i\mathbf{k}'\cdot\mathbf{x}}, \tag{3.26}$$

$$g_{(-)} = \exp\left(-i\frac{M}{k_f}\int_{z_f}^{\infty} dz'_f V_c(\mathbf{b}_f, z_f)\right), \tag{3.27}$$

$$f_{(+)} = e^{i\mathbf{k}\cdot\mathbf{x}}, \tag{3.28}$$

$$g_{(+)} = \exp\left(-i\frac{M}{k_i}\int_{-\infty}^{z_i} dz'_i V_c(\mathbf{b}_i, z'_i)\right) \tag{3.29}$$

in which we have set the spin-orbit potential, $V_{so}(\mathbf{x})$, to zero and the potential, $V_c(\mathbf{x})$, is the parameterization of the scalar and vector Dirac optical potentials given in Hama *et al.* [44], M is the mass of the projectile and $\mathbf{K} = \frac{1}{2}\left(\mathbf{k} + \mathbf{k}'\right)$ the average momentum. In Eqs. (3.27) and (3.29) the i and f subscripts refer to the position coordinates of the projectile and ejectile respectively at the collision point relative to each particle's position from the scattering center as shown in FIG. 3.8. In this way the distortion effect on the incoming particle is differentiated from that of the outgoing particle. However, if we were to compare the integrand of Eq. (3.25) with that given in Eq. (2.187), namely

$$G(\mathbf{x},\mathbf{q}) = e^{i(\mathbf{Q}-\mathbf{q})\cdot\mathbf{x}} e^{i\chi_c(\mathbf{b})} \tag{3.30}$$

the difference in the two is the evaluation of the eikonal phases, namely $i(\mathbf{Q}-\mathbf{q})\cdot\mathbf{x}+i\chi_c(\mathbf{b})$. In Eq. (3.25) the two eikonal phases are two multiplicative factors to the 'plane wave' part of the integrand. The

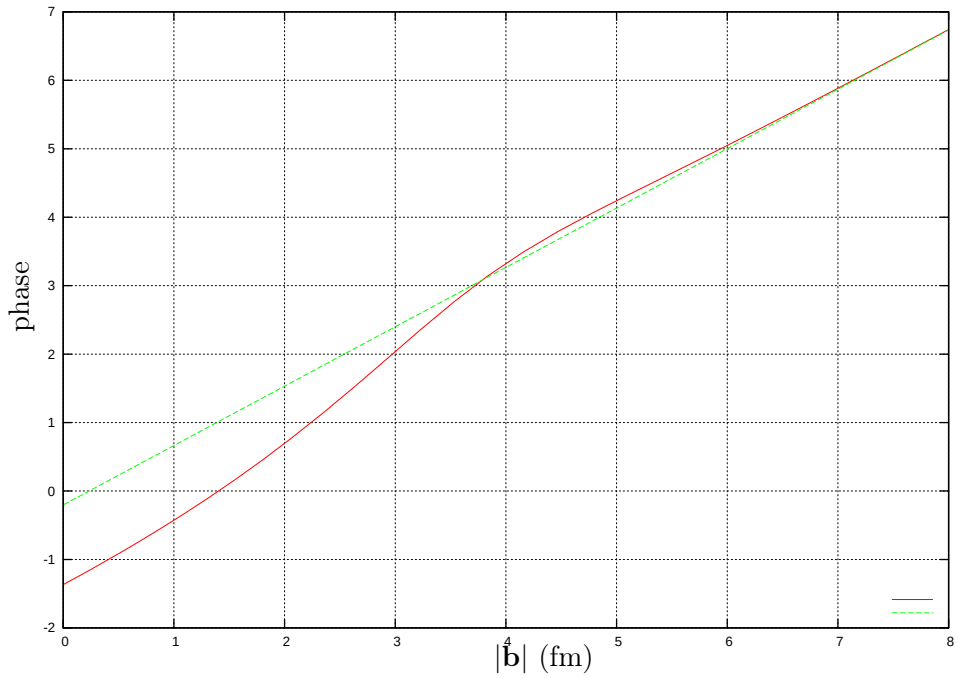

FIG. 3.9: *Distorted wave phase with eikonal phase (red) compared to that of a plane wave phase (green) for a proton with* $T_{lab} = 500$ *MeV on* ^{40}Ca.

eikonal phase now has to be evaluated separately for the incoming wave function and then again for the outgoing wave function. This has a computational cost as the integrals $g_{(+)}$ and $g_{(-)}$ have to be reevaluated for every $(\mathbf{b}, z)$ integration point.

We, however, follow the approach where the eikonal phase is computed along the path of the average momentum $\mathbf{K}$ across the range of the potential. This means that for every $\mathbf{b}$ vector, we compute the eikonal phase from z_{min} to z_{max}. In FIG. 3.9 one sees that the phase with the distortions becomes almost equal to the phase without the distortions when $|\mathbf{b}|$ approaches 4 fm. From 4 fm the phase is almost the same as for that of a plane wave. At approximately 8 fm, the two phases are equal. This indicates that the distortion on the phase is only 'effective' within the range of the potential [30, 34]. This is indicated in FIG. 3.8 by z_{min} and z_{max}. Taking the infinity limits as z_{min} and z_{max} is justified as the potential $V_c(z_{min}) = V_c(z_{max}) = 0$ and therefore there will be no contribution to the integral $\chi_c(\mathbf{b})$ given in Eq. (2.173) in areas outside of these limits. In our calculations, we therefore set the z' integration limits equal to the maximum range of the potential which is 7 fm.

3.6 Integrand characteristics - d^3q

Up to this point, we have established that we can compute the three dimensional $d^3x\ G(\mathbf{x}, \mathbf{q})$ integral for fixed q, θ_q and ϕ_q using traditional Gaussian integration. For the ^{40}Ca nucleus, the 'effective' range of the potential is of the order of 4 fm, however, we have set this parameter as 7 fm. As mentioned,

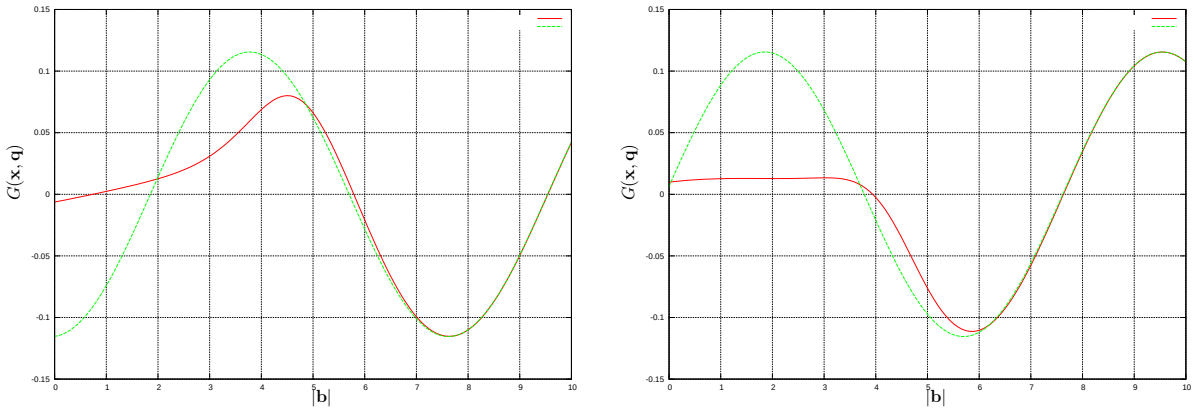

(a) The real part of the integrand for the d^3x integral with the central potential switched on (red) and with the central potential switched off (green)

(b) The imaginary part of the integrand for the d^3x integral with the central potential switched on (red) and with the central potential switched off (green)

FIG. 3.10: *The d^3x integrand as a function of $|\boldsymbol{b}|$ with the potential switched on (red) for the real and imaginary components compared to the case when the potentials are switched off (green). The function is for a fixed $q, \theta_q, \phi_q, \phi_b$ and $z = 0$. Also notice that the two functions become equal at around $|\boldsymbol{b}| = 6$ fm. The functions are for the pseudoscalar interaction for incoming particle with spin down and outgoing particle spin up and projection axis $\hat{\boldsymbol{i}}$ in the normal direction $\hat{\boldsymbol{n}}$.*

the choice of limits are dictated by physical arguments based on the volume in which the eikonal phase is non-zero. In this volume, distortions are in effect, whereas outside of this boundary, plane wave conditions apply.

Having established the limits of the three dimensional space integral d^3x, the attention moved to that of the outer d^3q integral. At this point, it was still impractical to compute the full integral using Gaussian integration because the nested d^3x integral needed no less than 50 Gaussian points to converge. This would then amount to increasing the integration points in each dimension of the d^3q integral up to a point where the full integral converges. This resulted in a trial and error method to test for convergence, but to no avail.

3.6.1 $F(\theta_q)$

The way that we were able to make any progress was to generate functions in the $\mathbf{q}$ integral by integrating over one or two of the three integration variables. Integrating over one variable would generate a surface whereas integrating over two variables will lead to a function in the final integration variable. We then set

$$F(\theta_q) = \int dq\, d\phi_q \mathcal{H}^{SS} \mathrm{Im}\left\{\Pi_{SS}(\mathbf{q}, \omega)\right\}. \tag{3.31}$$

Doing the five dimensional integral above generated the function shown in FIG. 3.11. On the left of the figure is a normal plot whereas the right figure shows a log plot for the function $F(\theta_q)$. We must add that it is difficult and even dangerous to attach an interpretation to the generated functions. We

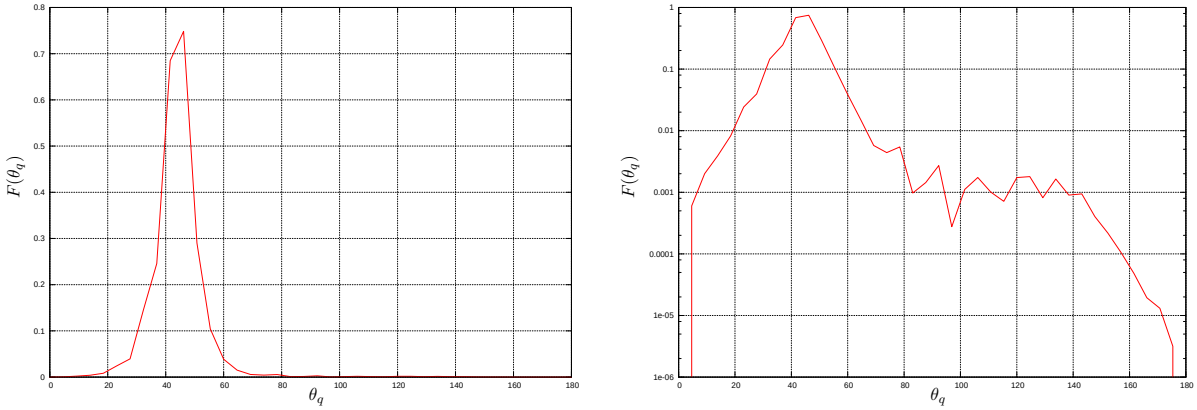

(a) Regular (b) Logplot

FIG. 3.11: *Integration of $dq\,d\phi_q$ to generate the function $F(\theta_q)$*

treated them as mere functions and used their profiles as an indicator of their numerical characteristics. The θ_q function shows a single spike. The log plot indicates that to the right of the spike the function is numerically unstable.

3.6.2 $F(\phi_q)$

We followed the same process for the integral over the variables q and θ_q. Similar to the previous profile, there is a numerical profile to the function $F(\phi_q)$ where the only contribution to the computed differential cross section will come from an area where the ϕ_q variable is at π. As mentioned, it is dangerous to attach any type of physical interpretation to this figure apart from it indicating its numerical character.

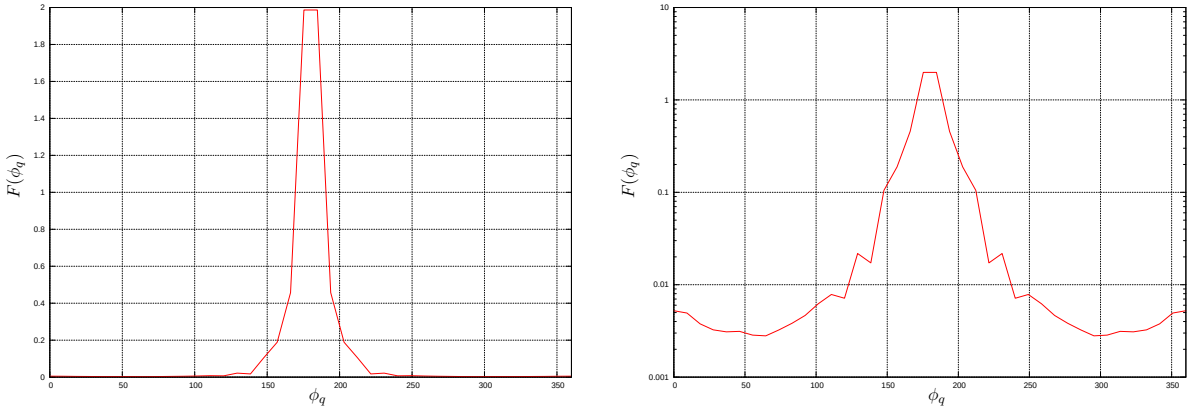

(a) Regular (b) Logplot

FIG. 3.12: *Integration of $dq\,d\theta_q$ to generate the function $F(\phi_q)$*

3.6.3 $F(q)$

The final integration was over the polar angles θ_q and ϕ_q whereby we generated the function $F(q)$ for different values of q. Here

$$F(q) = \int d\theta_q d\phi_q \mathcal{H}^{SS} \mathrm{Im}\left\{\Pi_{SS}(\mathbf{q}, \theta_q, \phi_q, \omega)\right\}. \tag{3.32}$$

The profile function for $F(q)$ is shown in FIG. 3.13 and has a much smoother profile than the other two profile functions. This function has the numerical smoothness character which one can either

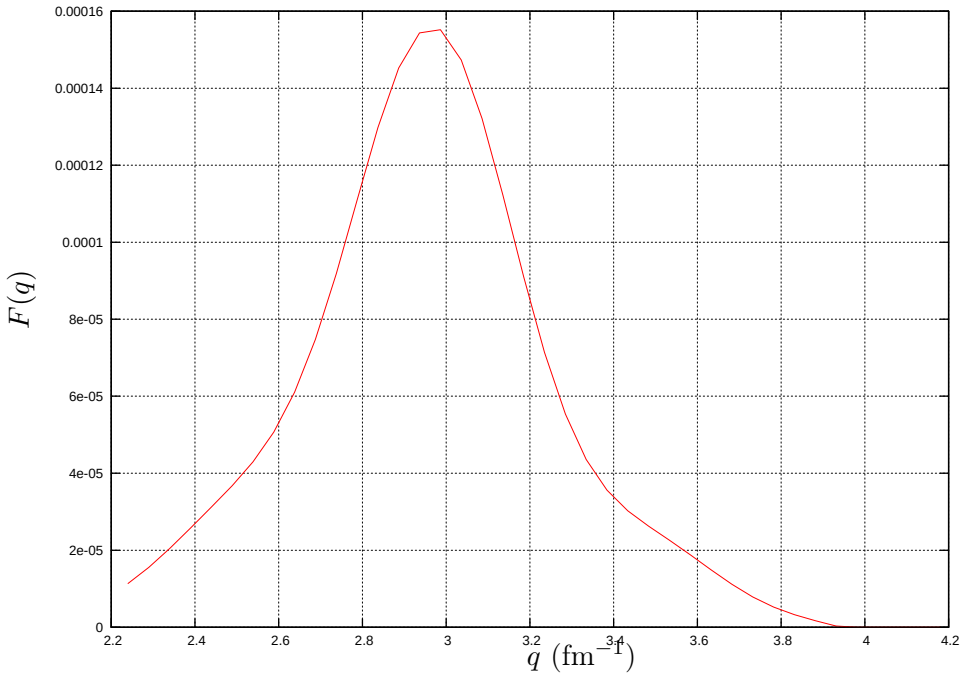

FIG. 3.13: *Integration of $d\theta_q\, d\phi_q$ to generate the function $F(q)$*

interpolate and then use the interpolant to integrate with. Furthermore, powerful numerical software such as MATLAB is available to interpolate such a function. As mentioned before, we attached no physical interpretation to the function $F(q)$ other than it allowing us to compute the differential cross section.

3.6.4 Convergence - d^3q

We generated the function

$$F(q, \omega) = \int d\theta_q d\phi_q \mathcal{H}^{SS} \mathrm{Im}\left\{\Pi_{SS}(q, \theta_q, \phi_q, \omega)\right\} \tag{3.33}$$

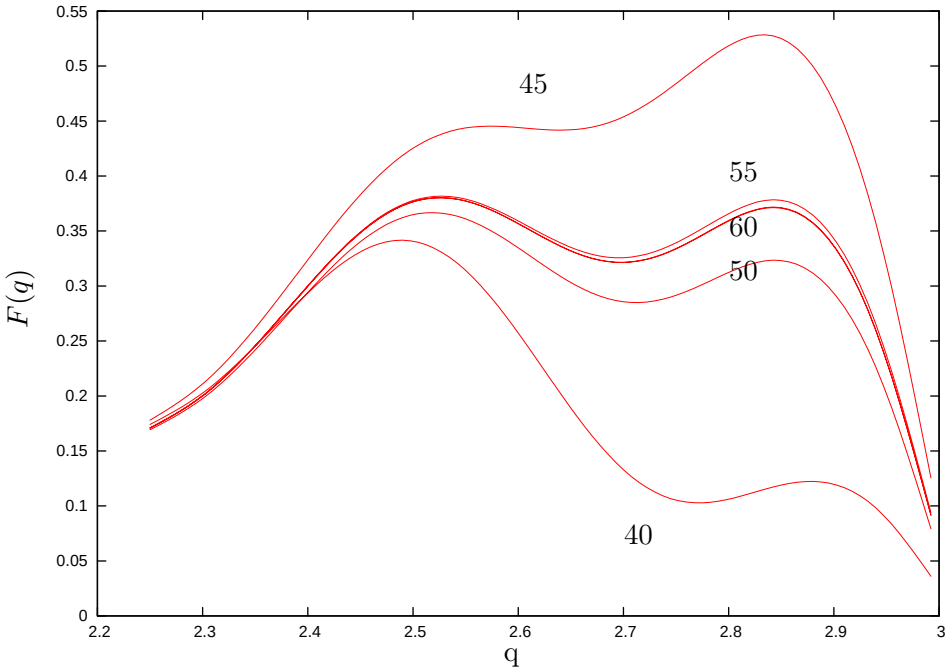

FIG. 3.14: *Gaussian convergence of the $F(q,\omega)$ integral for different Gaussian integration points. Notice how the general shape, with the two humps, of the function is preserved but not the area under the graph. This varies dramatically for different integration points. The energy transfer value ω was set at 75 MeV for this example. The projectile has $T_{lab} = 400$ MeV and the target is ^{40}Ca and $\theta_{cm} = 40^{\circ}$*

for a fixed ω between the momentum transfer values q_{min} and q_{max} with regular spaced intervals on a one-dimensional grid. To perform the integrations over $d\theta_q d\phi_q$ we had to test for convergence of the 5 dimensional integral. As is shown in FIG. 3.14, convergence over the polar integration variables $d\theta_q$ and $d\phi_q$ need more than 60 integration points. For the calculations we used 60 Gaussian integration points to generate $F(q)$ and we used 40 intervals on the one-dimensional q-grid.

We are now in a position to introduce our quadrature method that we employed to compute the polarized double differential cross section using eikonal distorted waves for quasielastic proton nucleus scattering using Eq. (2.82). As a reminder, we highlight the main points so far:

(i) We established that the three dimensional space integral d^3x required no less than 50 Gaussian integration points per dimension for convergence.

(ii) The oscillatory nature of the integrand is very much determined by the input parameter **b** which is the impact parameter. Choosing this value too large will result in an integral that will need an enormous amount of integration points to converge due to the violent oscillations that occur when the distorted wave 'becomes' a plane wave.

(iii) We compute the eikonal phase along the direction of the average momentum in a straight line through the target nucleus and set the limits of infinity to the maximum range in which $V_c(r) \neq 0$.

(iv) We are able to integrate over two of the three d^3q integration variables, however, both the polar and azimuthal functions display dramatic characteristics such as spikes at specific intervals.

The space integral is nested inside the d^3q integral. In this section we showed that we needed at least 60 Gaussian integration points per dimension to guarantee convergence integrating the polar coordinates out.

3.7 Quadrature procedure

In the previous section we established that we can integrate over two of the three integration variables present in the outer momentum transfer integral d^3q and generate functions of one variable. For this reason, the $F(q)$ integral had the smoothest profile of the three possible variables. We let

$$\frac{d\sigma}{dE'd\Omega'} = \int_{q_{min}}^{q_{max}} dq\ F(q,\omega). \tag{3.34}$$

For each value of ω we find that for this specific calculation the function in Eq. (3.34) is well reproduced by the following Fourier series

$$F(q,\omega) = \frac{a_0}{2} + \sum_{n=1}^{5} \left[a_n \cos(nwq) + b_n \sin(nwq)\right], \tag{3.35}$$

where the ω-dependent coefficients for our calculation are given in Table 3.2. For the specific example shown in FIGs. 3.16-3.17 ten functions $F(q)$ for each ω was generated. The one dimensional $q-$grid contains 40 grid points and the $d\theta_q d\phi_q$ integrals needed 60 Gaussian integration points for convergence. The laboratory energy of the incoming particle is $T_{lab} = 400$ MeV, the target ^{40}Ca and the center-of-mass scattering angle $\theta_{cm} = 40^\circ$. The incoming particle has spin quantization and projection $(\hat{\mathbf{n}}, \frac{1}{2})$ and outgoing particle $(\hat{\mathbf{n}}, \frac{1}{2})$.

We can compute double differential cross section analytically as follows

$$\begin{aligned}
\frac{d\sigma}{dE'd\Omega'} &= \sum_{n=1}^{5} \int_{q_{min}}^{q_{max}} dq\ \left(\frac{a_0}{2} + \left[a_n \cos(nwq) + b_n \sin(nwq)\right]\right) \\
&= \frac{a_0(\omega)}{2}(q_{max} - q_{min}) + \sum_{n=1}^{5} \left\{ \frac{b_n(\omega)}{nw} \left[\cos(nwq_{min}) - \cos(nwq_{max})\right] \right. \\
&\qquad \left. + \frac{a_n(\omega)}{nw} \left[\sin(nwq_{max}) - \sin(nwq_{min})\right] \right\}.
\end{aligned} \tag{3.36}$$

Using MATLAB to do the integration using Eq. (3.36) we compute the polarized differential cross section for quasielastic proton-nucleus scattering. The result is shown if FIG. 3.15. The quasielastic

peak is well reproduced in this sample calculation.

TABLE 3.2: *Fourier coefficients for Eq. (3.35) used to interpolate the function $F(q)$. The result of the interpolations are shown in FIGs. 3.16-3.17*

ω	a_0		$n=1$	$n=2$	$n=3$	$n=4$	$n=5$	w
75	0.004798	a_n	0.2246	-0.07723	0.009182	0.001712	-0.0126	2.821
		b_n	0.1098	0.001151	-0.03368	0.04606	-0.009644	
100	0.1853	a_n	-0.2096	0.1054	-0.04718	0.04304	-0.003087	3.174
		b_n	0.2323	-0.005559	0.01143	-0.01069	0.0008471	
125	0.3012	a_n	-0.002143	-0.1335	0.09079	-0.007971	-0.01921	2.797
		b_n	0.4091	-0.1192	-0.0002197	0.05805	-0.01696	
150	0.3918	a_n	-0.2712	-0.01373	0.07594	-0.06597	0.01598	2.902
		b_n	0.4534	-0.2029	0.09222	-0.007007	-0.01004	
175	0.4199	a_n	-0.3609	-0.02922	0.09189	-0.06786	0.01887	2.874
		b_n	0.4586	-0.223	0.09257	-0.003499	-0.01109	
200	0.4153	a_n	-0.4845	0.07271	0.02189	-0.03825	0.01499	2.909
		b_n	0.3133	-0.226	0.1131	-0.04817	0.009294	
225	0.382	a_n	-0.5271	0.2177	-0.0857	0.04091	-0.009284	3.006
		b_n	0.005177	-0.06416	0.03843	-0.01847	0.004432	
250	0.3157	a_n	-0.4063	0.1814	-0.06474	0.0199	-0.004281	3.036
		b_n	-0.1786	0.08986	-0.04264	0.02192	-0.004418	
275	0.9568	a_n	-0.2865	-0.934	0.3436	0.05794	-0.06808	2.189
		b_n	-1.088	0.7291	0.4096	-0.245	-0.04082	
300	6.977	a_n	-12.24	9.047	-4.893	1.886	-0.446	1.693
		b_n	-0.3726	0.2234	-0.1646	-0.08791	-0.01425	

In Summary

The essence of this chapter summarizes the numerical challenges that we faced in finding a workable method to calculate the polarized double differential cross section for quasielastic proton-nucleus scattering reactions. Gaussian quadrature rules and (quasi-) Monte Carlo integration methods proved invaluable in the implimentation of Eq. (3.1). The modular nature of the differential cross section allowed us to test different quadrature schemes. In addition, we got invaluable understanding of the nature and character of specifically the hadronic tensor. More importantly, the simplicity of the eikonal formulation of distorted waves aided in keeping the physics and numerics separate and we could identify numerical instability from unphysical parameter choices. We were then able to use the powerful interpolation tools of MATLAB, specifically the **cftool** package to interpolate our function. This interpolated function, was then integrated and the differential cross section was subsequently calculated. The classic quasielastic peak is clearly visible from the computed cross section. This chapter illustrates the need for reliable quadrature methods that are straightforward to implement. We have relied on tried

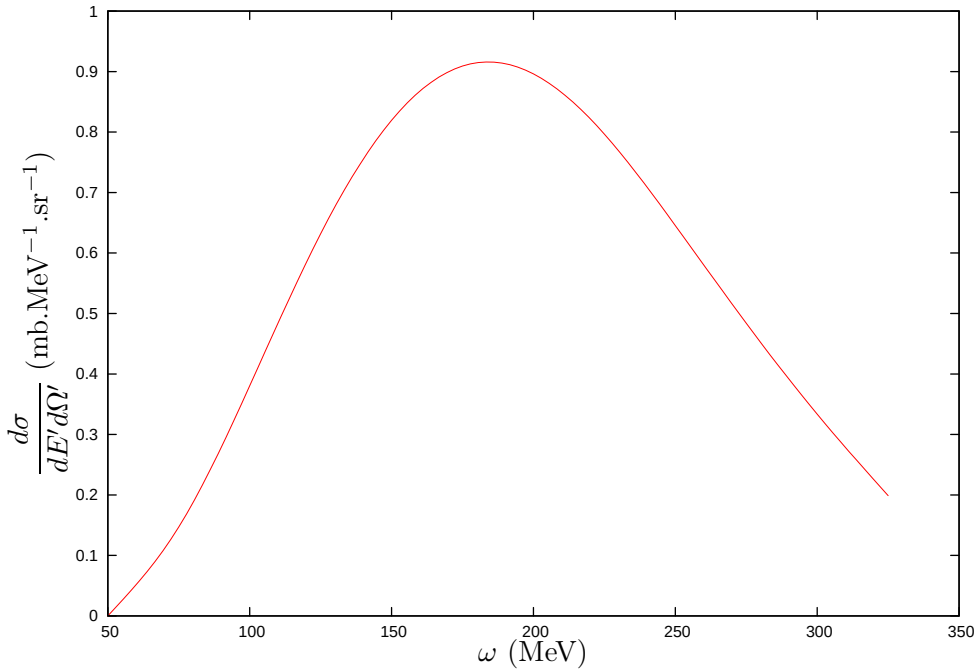

FIG. 3.15: *Numerically computed distorted wave polarized double differential cross section for inclusive quasielastic scattering for a proton with incident energy of* $T_{lab} = 400$ *MeV on a* ^{40}Ca *target at* $\theta_{cm} = 40°$. *The incoming quantization direction and spin* $(\hat{\boldsymbol{n}}, \frac{1}{2})$ *and outgoing* $(\hat{\boldsymbol{n}}, \frac{1}{2})$

and tested product rule formulas to accomplish the numerical integration of a complicated function, primarily because other quadrature methods available on the market have shown to be complicated to implement (they lead to no speed advantage) or too problem specific. This chapter highlights the necessary analysis that goes into choosing an efficient quadrature scheme to perform the integrations.

We have also showed that there are significant physics related considerations when making choices that directly influence the convergence properties of an integrand, for example choosing the impact parameter value larger than the range of the potential. For this specific example it is clear that if a large value for the impact parameter is set, you not only increase the likelihood of divergence due to the violent oscillations outside of the potential, but also the risk of overestimating observables is increased.

Another extremely valuable insight gained from this exercise was the difficulty (quasi-) Monte Carlo integration methods have in evaluating small valued integrals. Using automated Monte Carlo integration routines where one provides a minimum error or variance value can directly influence the rate of convergence. Even though this may sound as stating the obvious, we stress that both the real and imaginary part of the integrand carries valuable information directly related to convergence. One can clearly see in the example we used in Section 3.3, that even though the imaginary part of the integral has become zero using Gaussian integration, the other two methods showed no sign of convergence to zero.

In the next chapter we present our results using the tools and methods we outlined in this chapter.

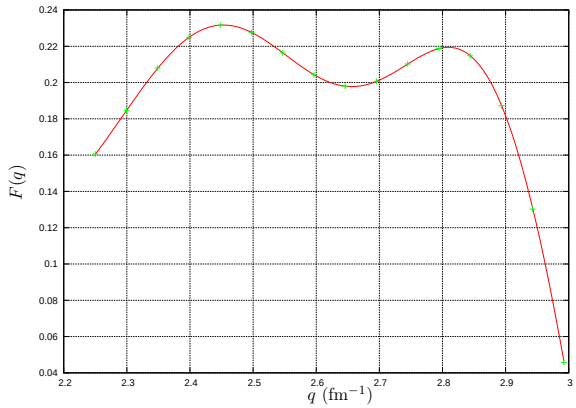

(a) $\omega = 75$ MeV

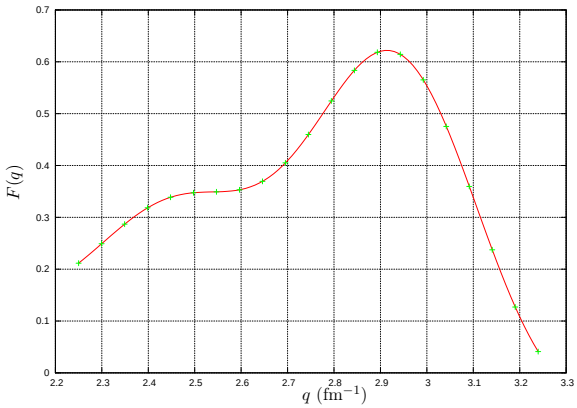

(b) $\omega = 100$ MeV

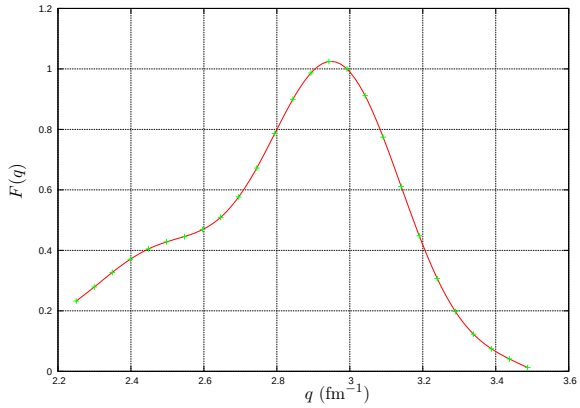

(c) $\omega = 125$ MeV

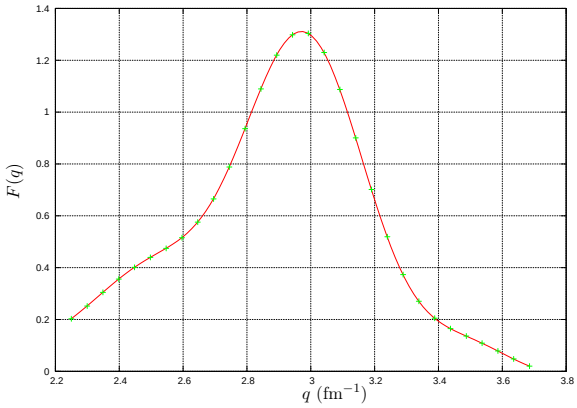

(d) $\omega = 150$ MeV

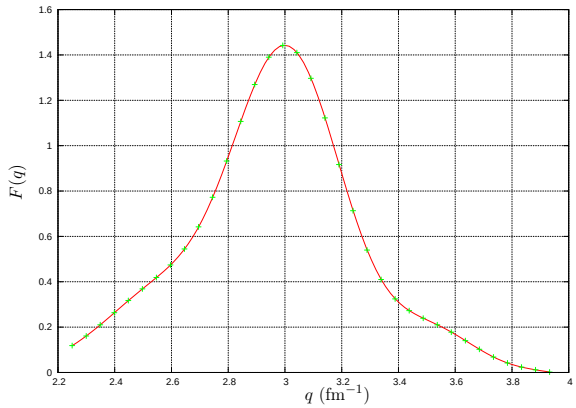

(e) $\omega = 175$ MeV

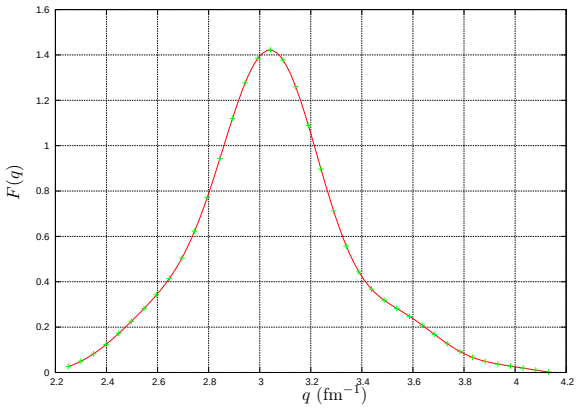

(f) $\omega = 200$ MeV

FIG. 3.16: *Interpolated functions using Eq. (3.35) with coefficients given in Table 3.2. The function values $F(q)$ were generated with the incoming particle which has $T_{lab} = 400$ MeV, the target ^{40}Ca and the center-of-mass scattering angle $\theta_{cm} = 40°$. The incoming particle has spin quantization and projection $(\hat{\boldsymbol{n}}, \frac{1}{2})$ and outgoing particle $(\hat{\boldsymbol{n}}, \frac{1}{2})$.*

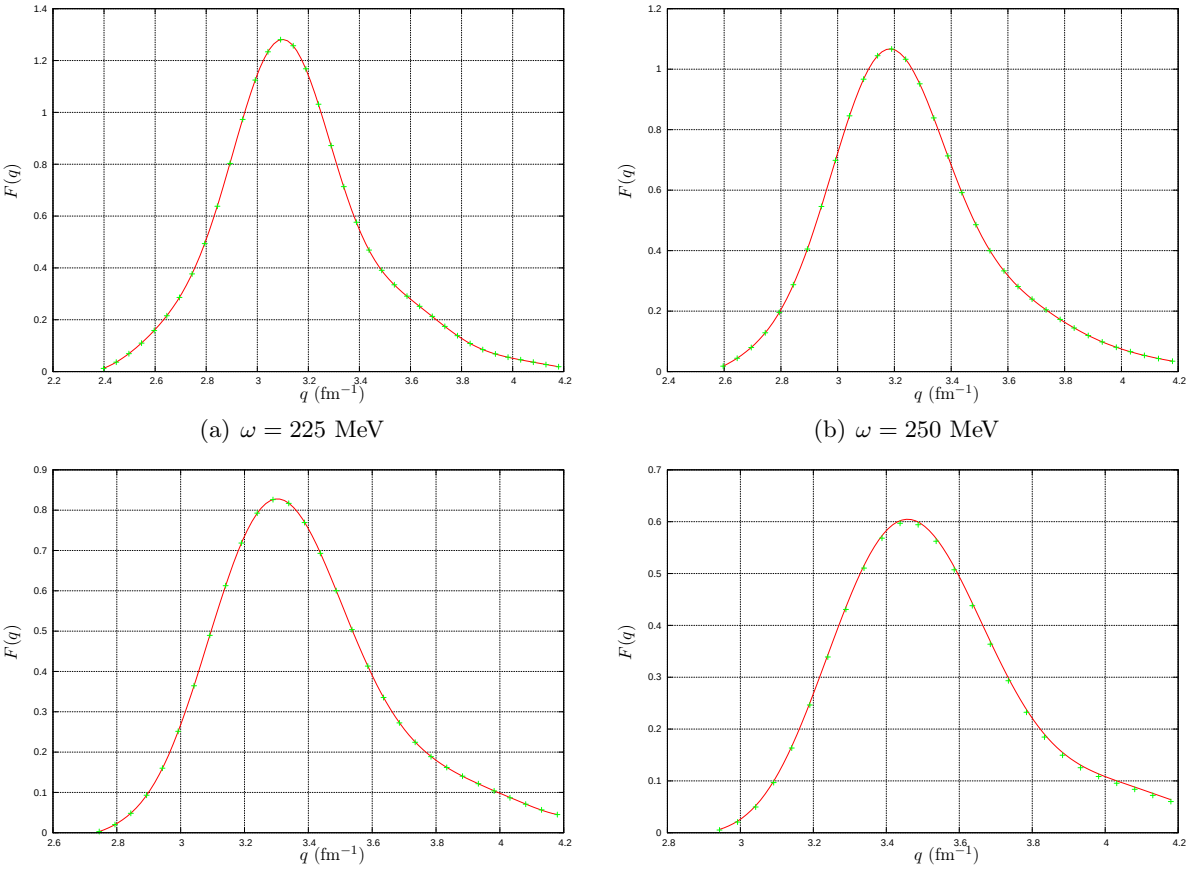

(a) $\omega = 225$ MeV

(b) $\omega = 250$ MeV

(c) $\omega = 275$ MeV

(d) $\omega = 300$ MeV

FIG. 3.17: *Interpolated functions using Eq. (3.35) with coefficients given in Table 3.2. The function values $F(q)$ were generated with the incoming particle which has $T_{lab} = 400$ MeV, the target ^{40}Ca and the center-of-mass scattering angle $\theta_{cm} = 40°$. The incoming particle has spin quantization and projection $(\hat{\boldsymbol{n}}, \frac{1}{2})$ and outgoing particle $(\hat{\boldsymbol{n}}, \frac{1}{2})$.*

Chapter 4

Results and Discussion

In this chapter we present the results based on the formalism developed in this thesis. In chapter two we derived an analytical expression in which we are able to calculate the polarized double differential cross section for the inclusive quasielastic proton nucleus scattering reaction in the plane wave case. This formula is given by Eq. (2.107). Following the plane wave calculations we give the calculations of the distorted waves which are similar in profile to that of the plane wave calculations. We then compare the distorted wave double differential cross section calculations with that of the plane wave calculations. Finally, we compare the spin observables for the plane wave and the distorted wave cases.

4.1 Plane wave limit

With Eq. (2.107) we can calculate the double differential cross section numerically for the scalar-scalar (SS) case in the plane wave limit for the inclusive quasielastic proton-nucleus scattering reaction. A similar formula is used for the PP case, but where we replace Im Π_{SS} with Im Π_{PP}, as well as the relevant trace factor. Using an incident proton energy of 400 MeV impinging on a ^{40}Ca target the polarized double differential cross sections are shown in FIGs. 4.2 and 4.3 for different spin quantization directions. We can see that the quasielastic peak is well represented for both the SS case and for the PP case.

The polarized differential cross section for all polarization directions are shown in FIG. 4.2. The main features for the plane wave calculations for the different polarization directions are as follows:

Polarization directions $l'l$: In the polarized double differential cross sections we find that the quasielastic peak for the uu and dd states are equal and one order of magnitude larger than that for the du and ud directions for the SS interaction. The du and ud states also have equal magnitudes. Also, the position of the two peaks are at the same energy transfer position ω. For the PP interaction the cross sections are reversed with the du and ud states larger than that for the uu and dd states. Here we also see that the quasielastic peak is shifted to a higher ω with respect

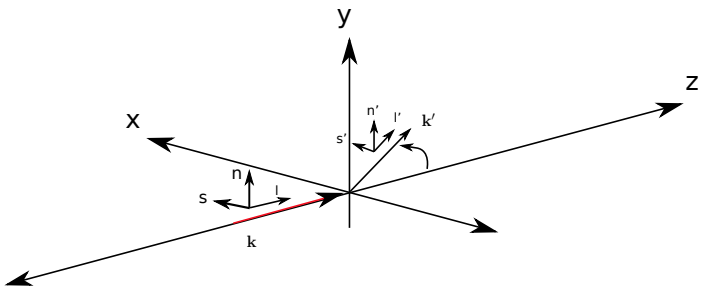

FIG. 4.1: *Quantization axes - $\hat{l}$, $\hat{s}$ and $\hat{n}$ for a particle with incoming momentum* $\mathbf{k}$ *(red arrow) and $\hat{l}'$, $\hat{s}'$ and $\hat{n}$ for the ejectile with outgoing momentum* $\mathbf{k}'$.

to that of the du and ud states and also to that of the SS interaction. Also the uu and dd states are equal in magnitude and the du and ud are equal in magnitude.

Polarization directions $s's$: In the polarized double differential cross sections we find that the quasielastic peak for the uu and dd states are equal and one order of magnitude larger than that for the du and ud directions which are in turn equal to each other for the SS interaction. Also, the position of the two peaks are at the same energy transfer position ω. For the PP interaction the cross sections are reversed with the du and ud states larger than that for the uu and dd states. Here we also see that the quasielastic peak is shifted to a higher ω with respect to that of the du and ud states and also to that of the SS interaction. This is the same as the case for the $l'l$ quantization directions in the previous case.

Polarization directions $l's$: In the polarized double differential cross sections we find that the quasielastic peak for the uu and dd states are one order of magnitude larger than that for the du and ud directions for the SS interaction. Also, the position of the two peaks are at the same energy transfer position ω. For the PP interaction the polarized cross sections are the same as in the SS case with the uu and dd states larger than that for the du and ud states. Here we also see that the quasielastic peak is shifted to a lower ω with respect to that of the du and ud states and also to that of the SS interaction.

Polarization directions $s'l$: In the polarized double differential cross sections we find that the quasielastic peak for the uu and dd states are one order of magnitude smaller than that for the du and ud directions for the SS interaction. Also, the position of the two peaks are at the same energy transfer position ω. For the PP interaction the polarized cross sections are the same as in the SS case with the uu and dd states smaller than that for the du and ud states. Here we also see that the quasielastic peak is shifted to a lower ω with respect to that of the du and ud states and also to that of the SS interaction.

Polarization directions nn: For this case, we see that the polarized cross sections for the ud and du

states are zero for the SS case. They are also zero in the PP case for the uu and dd polarization directions. For the SS case the uu and dd states are equal and in turn for the PP case, the magnitudes of the du and ud states are equal.

4.2 Distorted wave differential cross section

The major result of this work is presented in FIG. 4.4. It is the distorted wave unpolarized double differential cross section shown in red for the inclusive quasielastic proton-nucleus scattering reaction for a proton with an incident laboratory energy of 400 MeV calculated at 40° center-of-mass scattering angle. The distortions were generated in the eikonal approximation. The quasielastic peak occurs at an energy transfer ω of 175 MeV. This curve is compared to that of the unpolarized double differential cross section for the plane wave case and one can immediately see the effect of the distortions. This manifests itself as a reduction in the magnitude of the cross section for the distorted wave case. In this calculation, the two peaks of the distorted wave and that of the plane wave calculation coincide at the same energy transfer of 175 MeV.

Similar profiles for the distorted wave calculated cross sections are seen to that of the plane wave cases. This is to be expected as in the case of central potential scattering because the eikonal phase appears as a multiplicative factor in the differential cross section, very separate from the spin components. The following features are evident from the calculations shown in FIGs 4.5 and 4.6:

Polarization directions $l'l$: In the polarized double differential cross sections we find that the quasielastic peak for the uu and dd states are one order of magnitude larger than that for the du and ud directions for the SS interaction. Also, the maxima positions of the two peaks are at the same energy transfer position ω. For the PP interaction the cross sections are reversed with the du and ud states larger than that for the uu and dd states. Here we also see that the quasielastic peak is shifted to a higher ω with respect to that of the du and ud states and also to that of the SS interaction. This we saw in the plane wave case as well.

Polarization directions $s's$: In the polarized double differential cross sections we find that the quasielastic peak for the uu and dd states are one order of magnitude larger than that for the du and ud directions for the SS interaction. Also, the position of the two peaks are at the same energy transfer position ω. For the PP interaction the cross sections are the same with the uu and dd states larger than that for the du and ud states. Here we also see that the quasielastic peak for the du and ud is shifted to a higher ω with respect to that of the uu and dd states and also to that of the SS interaction. This is opposite to the case for the $l'l$ quantization directions in the previous case.

Polarization directions $l's$: In the polarized double differential cross sections we find that the quasielastic peak for the uu and dd states are one order of magnitude larger than that for the du and

ud directions for the SS interaction. Also, the position of the two peaks are at the same energy transfer position ω. For the PP interaction the polarized cross sections are the opposite to the SS case with the uu and dd states smaller than that for the du and ud states. Here we also see that the quasielastic peak is shifted to a lower ω with respect to that of the du and ud states and also to that of the SS interaction.

Polarization directions $s'l$: In the polarized double differential cross sections we find that the quasielastic peak for the uu and dd states are one order of magnitude smaller than that for the du and ud directions for the SS interaction. Also, the position of the two peaks are at the same energy transfer position ω. For the PP interaction the polarized cross sections are the same as in the SS case with the uu and dd states smaller than that for the du and ud states. Here we also see that the quasielastic peak is shifted to a lower ω with respect to that of the du and ud states and also to that of the SS interaction.

Polarization directions nn: For this case, we see that the polarized cross sections for the ud and du states are zero for the SS case. They are also zero in the PP case for the uu and dd polarization directions.

4.3 Spin observables

The spin observables are one of the most interesting physical quantities to study. In our calculations we see dramatic differences in the spin observables. Normally, the spin observables are displayed between limits that tend to hide the dramatic structures of the observables. As a matter of fact, the spin observables seem structureless between the -1 and 1 limits. However, we notice that each spin observable is different from the next. The following features are prominent when viewing these observables:

Spin observable A_y: The polarized cross sections for the uu and dd states are equal and that for the du and ud states are zero. This results in the numerator of Eq. (2.38) becoming zero making the analyzing power zero.

Spin observable $D_{l'l}$: This observable increases from about 0.5 to 0.66. for both the plane wave and distorted wave calculations. At 200 MeV, the two lines cross with the distorted wave calculation now lying below that of the plane wave calculation. Also, the magnitude difference between the two curves is very small and suggests that distortions have little influence on this observable.

Spin observable $D_{s's}$: In the plot that ranges between -0.5 and 1.0 there seems to be no structure to the spin observable. However, 'zoomed-in' we see that the distorted wave calculations lie below that for the plane wave calculation and both curves have a parabolic structure. This is in

stark contrast to that for the previous case, even though their respective double differential cross sections look very similar.

Spin observable $D_{l's}$: This observable decreases almost linearly from a ratio of about 0.73 to 0.57 for both the distorted wave and plane wave calculations. The distorted wave curve crosses the plane wave curve at 200 MeV where the distorted wave calculation lies below that of the plane wave curve.

Spin observable $D_{s'l}$: We see here that the distorted wave and the plane wave curves touch at 200 MeV and both increase to a lesser ratio for higher ω. At lower values of ω the two curves move away from each other.

Spin observable D_{nn}: For this observable, we see that the two curves for the plane wave and distorted wave cases differ the most from each other if one considers the 'zoomed-in' plot in FIG. 4.7. The observable however does not vary much in terms of the ratio across the energy range. In this case we also see again that the two curves cross at around 200 MeV whereby the distorted wave curve lies below that of the plane wave case for higher values of ω.

4.4 Summary and conclusions

We now summarise our findings for the goals we set for this thesis.

1. *Develop a consistent and fully relativistic formalism in order to calculate the double differential cross section for quasielastic proton-nucleus scattering.*

   Starting from fundamental principles (Eq. (2.25)) we derived an expression for the polarized double differential cross section (Eq. (2.82)). In contrast to previous models the transition matrix element was first written in a full many-body form and then we showed systematically how this reduces to a two-body form. One advantage of this derivation is the ease with which we can incorporate distortion effects. The cross section is written as a contraction of two very complex tensors, namely the hadronic tensor $\mathcal{H}^{LL'}$ and the polarization tensor $\Pi_{LL'}$. The hadronic tensor describes the distortion effects on the projectile and ejectile and the polarization tensor describes the properties of the target nucleus. The cross section is written in modular form where each component can be separately computed allowing a systematic investigation of the relevant factors influencing quasielastic proton-nucleus scattering.

2. *Include, for the first time, the use of relativistic distorted waves to describe the projectile and ejectile.*

   This thesis represents the first calculation for quasielastic proton-nucleus scattering which employs relativistic distorted waves for the projectile and ejectile. The calculation was done in

the context of the eikonal formalism as motivated in Section 2.1.4.2. What makes the eikonal approach such a powerful approximation tool to use in medium to high energy nuclear physics is the fact that the distortion effect on the particle is well isolated in a multiplicative factor. The direct consequence of this factor is to reduce the double differential cross section. Another major benefit of the eikonal formalism is (in the case of central potential scattering only) that the hadronic tensor is a product of two factors; one describing the distortion effects and the second one describing the spin of the particle.

3. *Investigate the use of a quadrature scheme to efficiently handle multidimensional integrals where the integrand has a strong oscillatory character.*

   The numerical implementation of the formalism is a significant challenge. This is primarily due to the multidimensional integrals and the very strong oscillatory character of the integrand. To our dismay we discovered that none of the methods available for such integrals were of any real practical use, primarily since they are geared towards one dimensional integrals and are often very integrand specific. In fairness we should mention that this field of numerical analysis is currently very active and more efficient methods may well be available in the future. Instead of being stymied by an impenetrable numerical problem we relied on the tried-and-tested method of Gaussian quadrature, but combined it with modern computer languages such as Matlab as well as cluster computing techniques. The use of the eikonal formalism also has the major benefit of being much simpler to implement numerically (as opposed to a full partial wave expansion) even though one still needs to deal with a multidimensional oscillatory integral. This problem was solved by using Gaussian quadrature to integrate a five dimensional integral and generate a one dimensional function. The function is dependent on the momentum transfer q and the energy transfer ω. This function is then interpolated with the use of a six term Fourier series using the powerful fitting and interpolation function tool, **cftool**, from MATLAB. This allowed us to either calculate the integral from an analytical function, the integral of the Fourier series, or use MATLAB to use the interpolant and perform the integrations. The calculational burden is then distributed across the cluster nodes allowing an automated procedure to successfully calculate the unpolarized double differential cross section. Furthermore we were able to calculate spin observables using this procedure.

4. *Calculate, for the first time, the unpolarized double differential cross and a complete set of spin observables namely A_y, $D_{\ell',\ell}$, $D_{s's}$, D_{nn}, $D_{s'\ell}$ and $D_{\ell's}$ using relativistic distorted waves.*

   We compared the results of the distorted wave double differential cross sections with that of the plane wave calculations and found that the cross section was reduced in magnitude due to the distortions. Additionally, one sees that the spin observables are complicated to interpret. Traditionally they are displayed between the limits of -1 and 1, and therefore appeared rather flat and structureless. However, these observables have dramatic structures that make it even

more problematic to interpret. However, we are in a position to say that distortions on the projectile and ejectile does in fact have very little influence on spin observables if one was to only consider central potential scattering. This is because the spin components are contained in the Dirac spinors that can be factored out of the integral that contains the eikonal distortions.

We have shown in this work that the eikonal approximation provides an excellent and very powerful means of including distortions in relativistic formalisms that describe nuclear scattering reactions. For this case where we successfully calculated the unpolarized double differential cross section using distorted waves and spin observables the eikonal approximation allowed us to complete this computation in a reasonable amount of time without a loss of accuracy. Furthermore we saw that the cross sections are influenced by the distortion, but that spin observables seem insensitive to the distortions. More quantitative predictions and ultimately comparison with experiment would entail including all the different Lorentz combinations. This is numerically very taxing and is therefore the subject of future study. What we have proved however, is that our formalism is internally consistent and our numerical methods are robust enough in order to obtain a fair balance between accuracy and speed of execution.

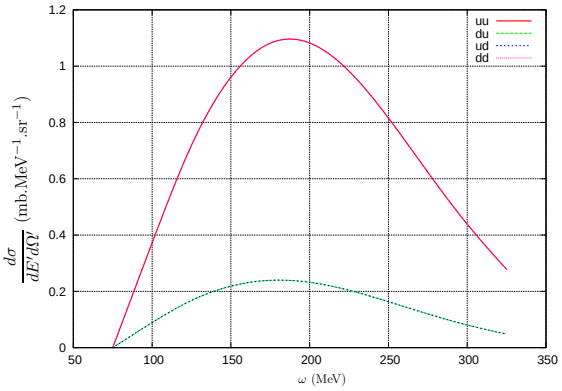

(a) Differential cross section for incoming l axis and outgoing l' axis for the SS interaction.

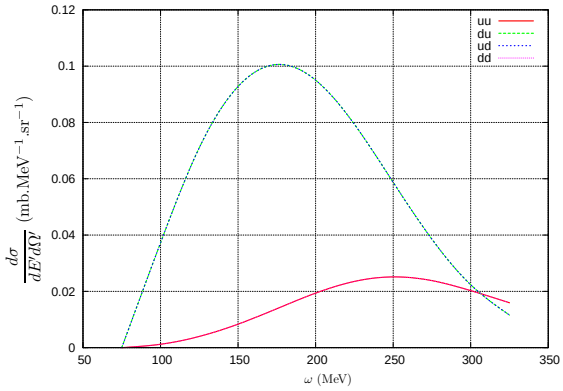

(b) Differential cross section for incoming l axis and outgoing l' axis for the PP interaction.

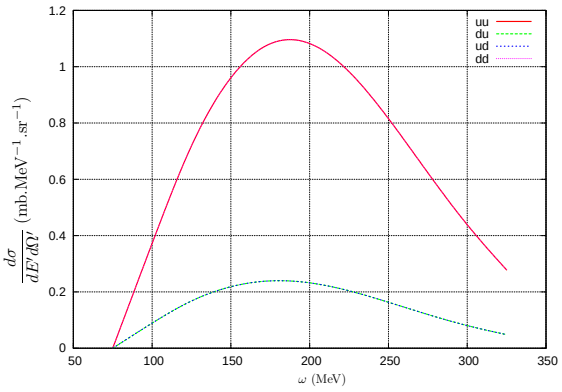

(c) Differential cross section for incoming s axis and outgoing s' axis for the SS interaction.

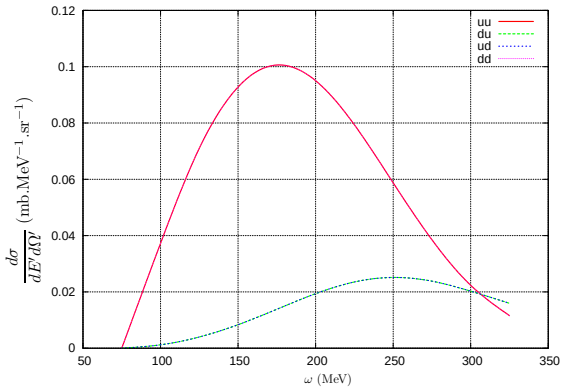

(d) Differential cross section for incoming s axis and outgoing s' axis for the PP interaction.

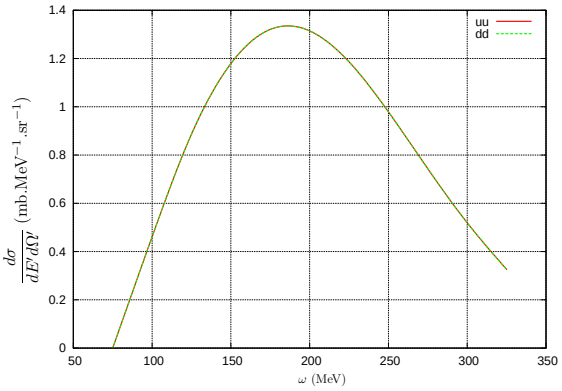

(e) Differential cross section for incoming n axis and outgoing n axis for the SS interaction.

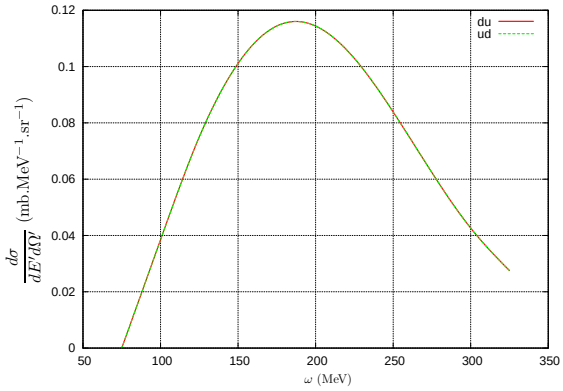

(f) Differential cross section for incoming n axis and outgoing n axis for the PP interaction.

FIG. 4.2: *Polarized double differential cross sections for the plane wave case for the 'l', 's' and 'n' quantization directions at $T_{lab} = 400$ MeV on ^{40}Ca, $\theta_{cm} = 40°$. In the $(\hat{n}, \hat{n})$ cross sections, the uu and dd states are equal and the $du = ud = 0$, hence the single curve. The same applies to the $(\hat{n}, \hat{n})$ cross section in the PP case with the du and ud states equal and $uu = dd = 0$. For the other cross section the uu and dd states are equal and the du and ud states are equal hence only two lines are visible.*

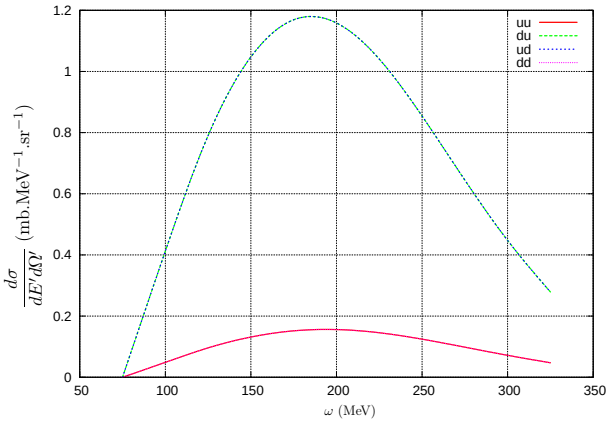

(a) Differential cross section for incoming l axis and outgoing s' axis for the SS interaction.

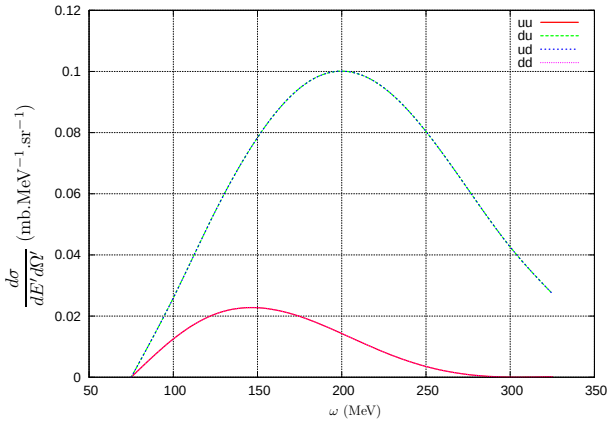

(b) Differential cross section for incoming l axis and outgoing s' axis for the PP interaction.

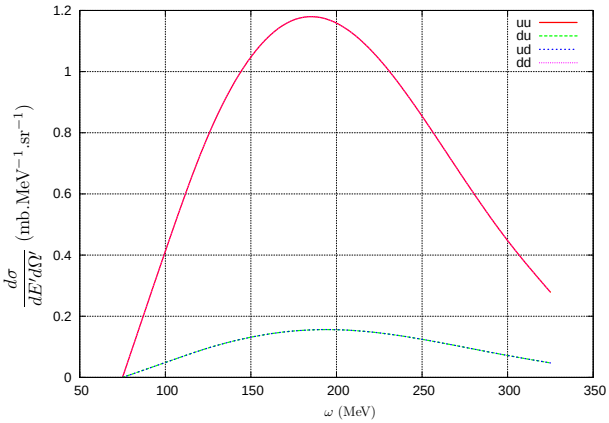

(c) Differential cross section for incoming s axis and outgoing l' axis for the SS interaction.

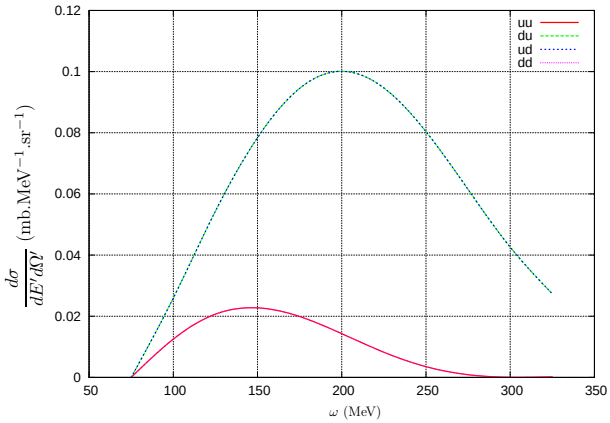

(d) Differential cross section for incoming s axis and outgoing l' axis for the PP interaction.

FIG. 4.3: *Polarized double differential cross sections for the plane wave case for $s'l$ and $l's$ quantization directions at $T_{lab} = 400$ MeV on ^{40}Ca, $\theta_{cm} = 40°$. In the cross sections above the uu and dd states are equal and the du and ud states are equal hence only two lines are visible in each plot.*

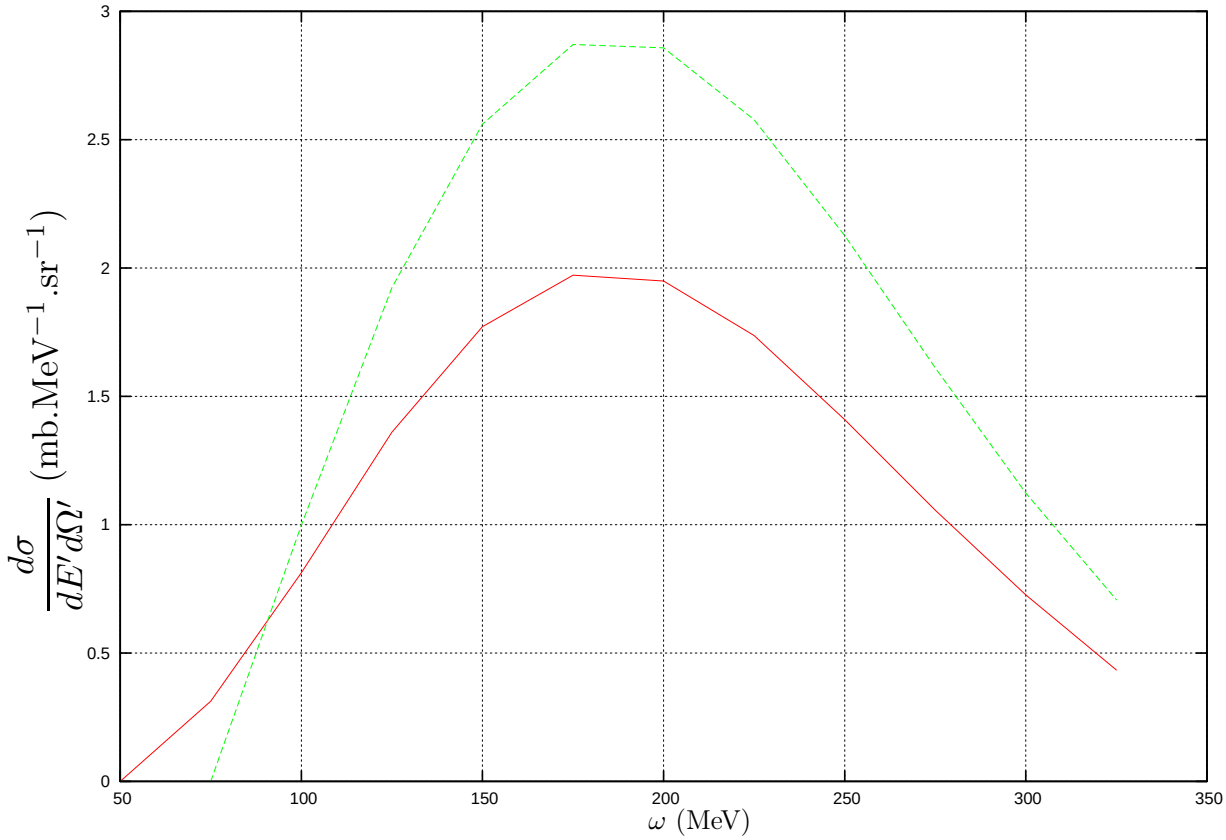

(a) Rank-0 unpolarized differential cross section

FIG. 4.4: *Comparison of the unpolarized double differential cross sections for rank-0 polarizations in the plane wave case compared to that for the distorted wave case for $T_{lab} = 400$ MeV protons on a ^{40}Ca target at $\theta_{cm} = 40°$. The red curve is that of the eikonal distorted wave double differential cross section and the green dashed line is that for the plane wave calculation. The abrupt end of the plane wave calculation at 75 MeV is due to the approximation of the $\delta(0)$ factor.*

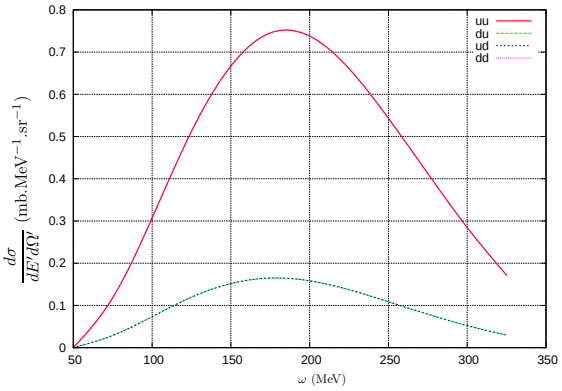

(a) Differential cross section for incoming l axis and outgoing l' axis for the SS interaction.

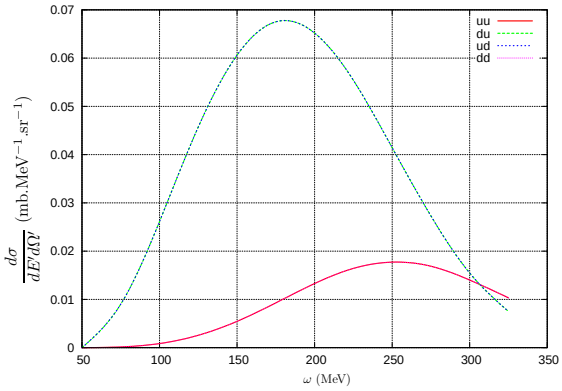

(b) Differential cross section for incoming l axis and outgoing l' axis for the PP interaction.

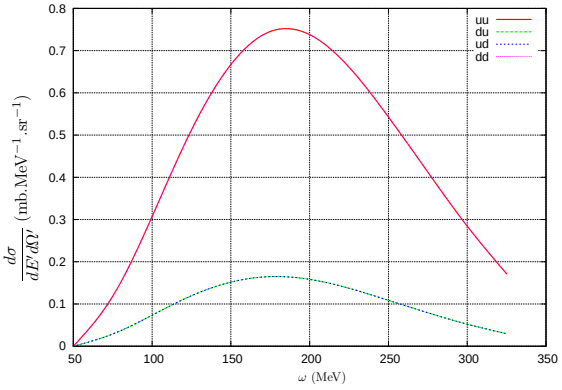

(c) Differential cross section for incoming s axis and outgoing s' axis for the SS interaction.

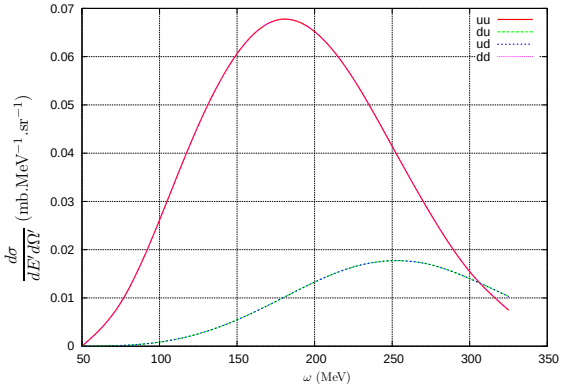

(d) Differential cross section for incoming s axis and outgoing s' axis for the PP interaction.

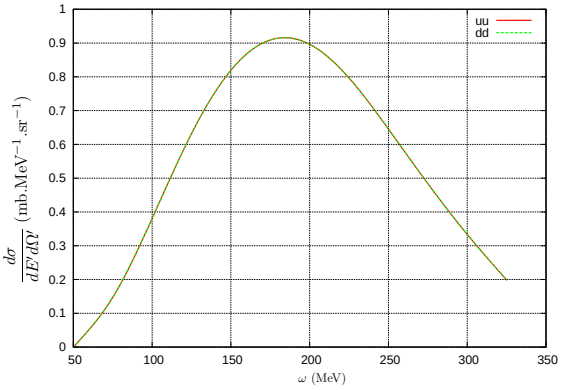

(e) Differential cross section for incoming n axis and outgoing n axis for the SS interaction.

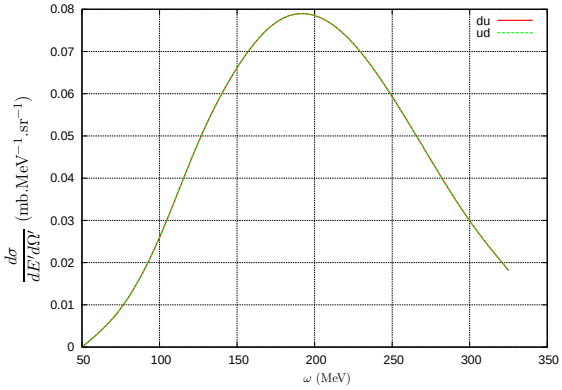

(f) Differential cross section for incoming n axis and outgoing n axis for the PP interaction.

FIG. 4.5: *Polarized double differential cross sections for the distorted wave case for 'l', 's' and 'n' quantization directions at $T_{lab} = 400$ MeV on ^{40}Ca, $\theta_{cm} = 40°$. In the $(\hat{n}, \hat{n})$ cross sections, the uu and dd states are equal and the $du = ud = 0$, hence the single curve. The same applies to the $(\hat{n}, \hat{n})$ cross section in the PP case with the du and ud states equal and $uu = dd = 0$. For the other cross sections the uu and dd states are equal and the du and ud states are equal hence only two lines visible.*

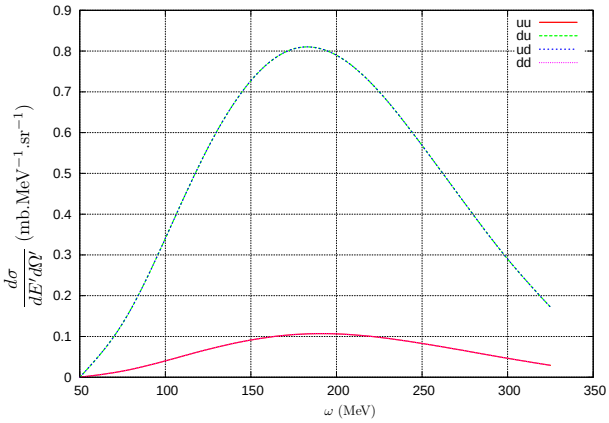

(a) Differential cross section for incoming l axis and outgoing s' axis for the SS interaction.

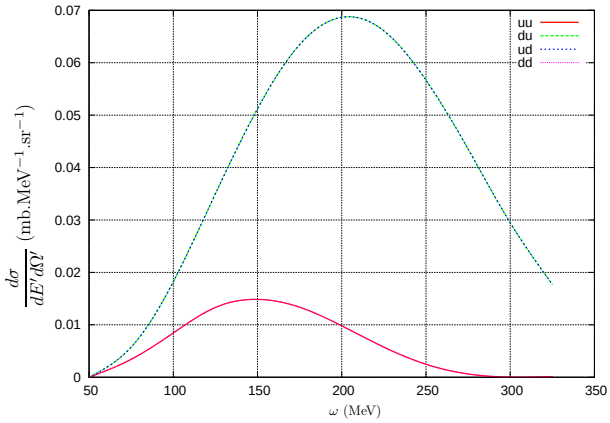

(b) Differential cross section for incoming l axis and outgoing s' axis for the PP interaction.

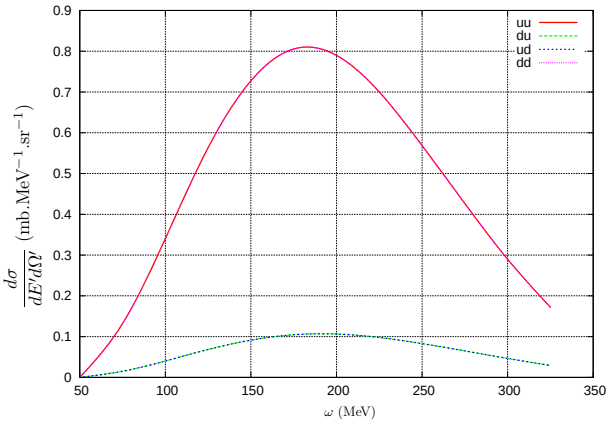

(c) Differential cross section for incoming s axis and outgoing l' axis for the SS interaction.

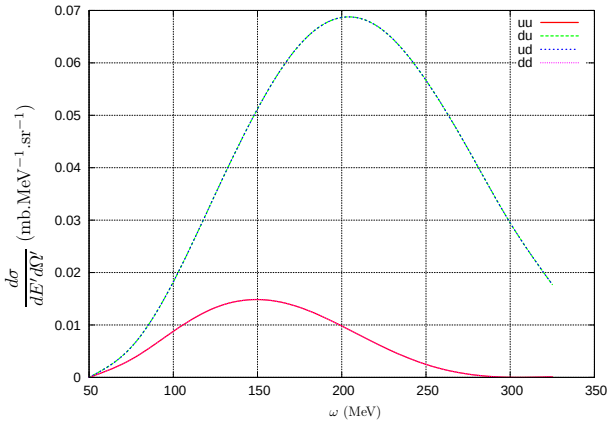

(d) Differential cross section for incoming s axis and outgoing l' axis for the PP interaction.

FIG. 4.6: *Polarized double differential cross sections for the plane wave case for $s'l$ and $l's$ quantization directions at $T_{lab} = 400$ MeV on ^{40}Ca, $\theta_{cm} = 40°$. In the cross sections above the uu and dd states are equal and the du and ud states are equal hence only two lines are visible in each plot.*

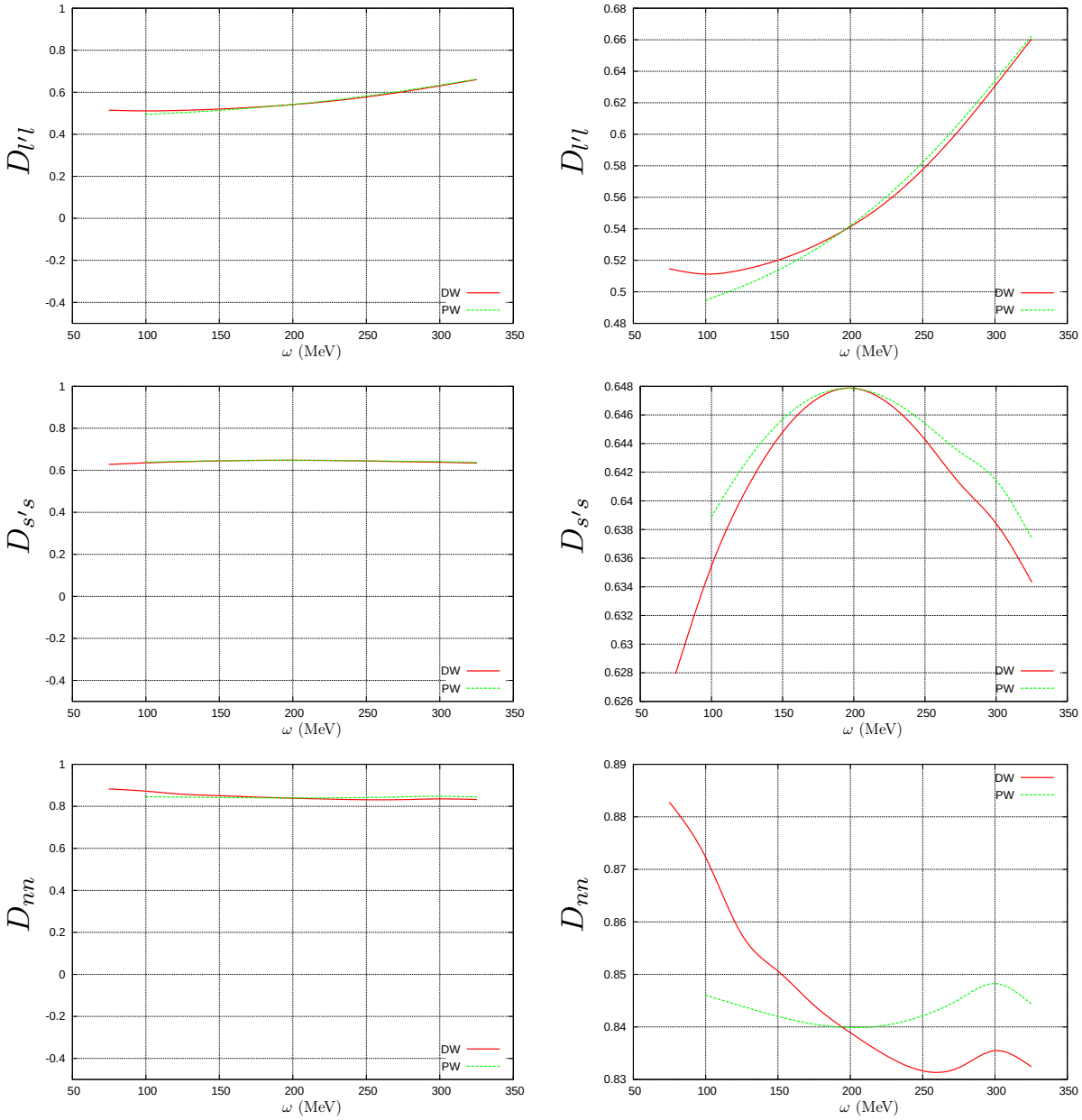

FIG. 4.7: *Plane wave and distorted wave spin observables values for $D_{l'l}, D_{s's}$ and D_{nn} for protons with laboratory incident of $T_{lab} = 400$ MeV on ^{40}Ca for quasielastic scattering at a center-of-mass scattering angle of $\theta_{cm} = 40^{\,0}$. The distorted wave observables are the solid red lines and that of the plane wave calculations are the dashed green lines. The figures on the right are "zoomed-in" presentations of the figure to their immediate left.*

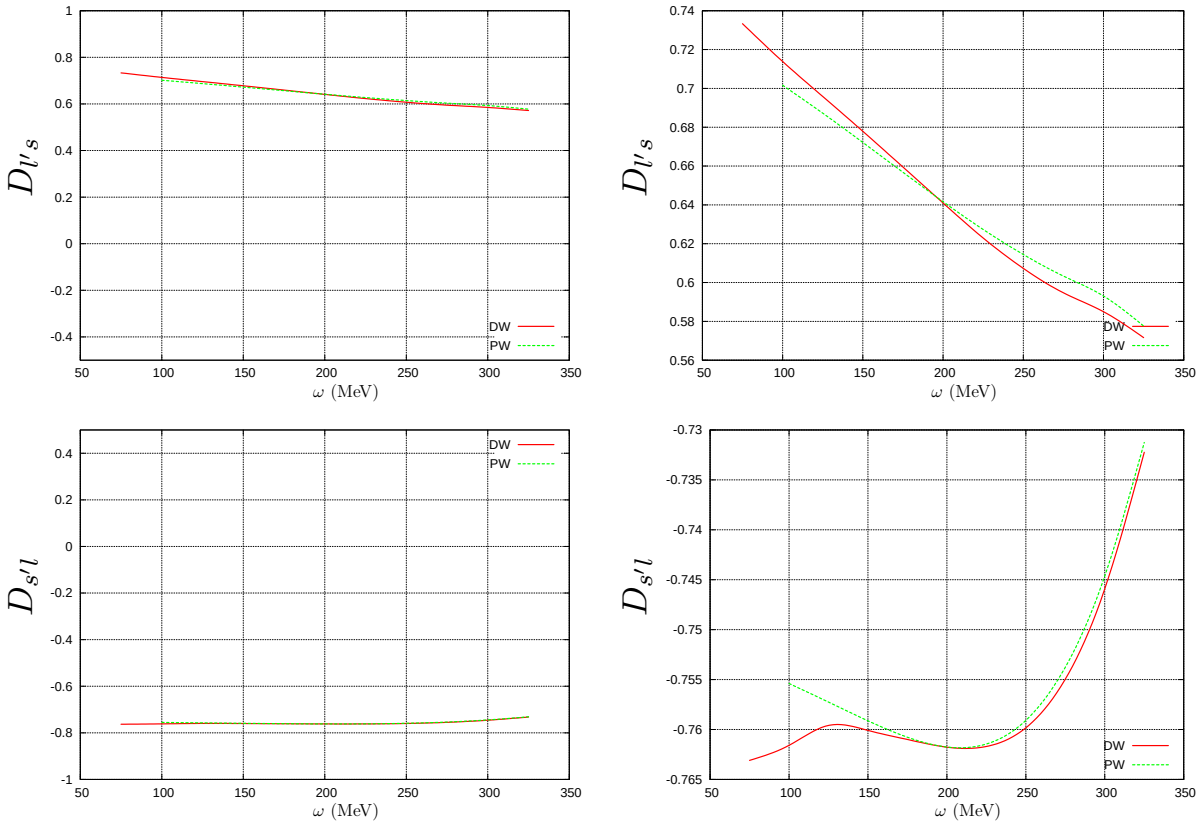

FIG. 4.8: *Plane wave and distorted wave spin observables values for $D_{l's}$ and $D_{s'l}$ for protons with laboratory incident of $T_{lab} = 400$ MeV on ^{40}Ca for quasielastic scattering at a center-of-mass scattering angle of $\theta_{cm} = 40^0$. The distorted wave observables are the solid red lines and that of the plane wave calculations are the dashed green lines. The figures on the right are "zoomed-in" presentations of the figure to their immediate left.*

Bibliography

[1] G. C. Hillhouse, Ph.D. thesis, University of Stellenbosch, 1999.

[2] H. Otsu, Ph.D. thesis, University of Tokyo, 1997.

[3] C. J. Horowitz and M. J. Iqbal, Phys. Rev. C **33**, 2059 (1986).

[4] C. J. Horowitz, Phys. Rev. C **31**, 1340 (1985).

[5] C. J. Horowitz and D. P. Murdock, Phys. Rev. C **37**, 2032 (1988).

[6] T. Wakasa *et al.*, Phys. Rev. C **59**, 3177 (1999).

[7] G. C. Hillhouse and P. R. De Kock, Phys. Rev. C **49**, 391 (1994).

[8] G. C. Hillhouse and P. R. De Kock, Phys. Rev. C **52**, 2796 (1995).

[9] B. I. S. Van der Ventel, G. C. Hillhouse, and P. R. De Kock, in *Proceedings of RCNP International Symposium on Nuclear Responses and Medium Effects*, edited by T. Noro, H. Sakaguchi, H. Sakai, and T. Wakasa (Universal Academy Press Inc., Osaka, Japan, November 1998), p. 183.

[10] G. C. Hillhouse, B. I. S. van der Ventel, S. M. Wyngaardt, and P. R. De Kock, Phys. Rev. C **57**, 448 (1998).

[11] B. I. S. Van der Ventel, G. C. Hillhouse, P. R. De Kock, and S. J. Wallace, Phys. Rev. C **60**, 064618 (1999).

[12] B. I. S. Van der Ventel, G. C. Hillhouse, and P. R. De Kock, Phys. Rev. C **62**, 024609 (2000).

[13] J. A. Tjon and S. J. Wallace, Phys. Rev. C **35**, 280 (1987).

[14] C. J. Horowitz and J. Piekarewicz, Phys. Rev. C **50**, 2540 (1994).

[15] J. R. Shepard, E. Rost, and J. Piekarewicz, Phys. Rev. C **30**, 1604 (1984).

[16] J. Piekarewicz, Phys. Rev. C **32**, 1693 (1985).

[17] B. Van Overmeire, W. Cosyn, P. Lava, and J. Ryckebusch, Phys. Rev. C **73**, 064603 (2006).

[18] D. Debruyne, J. Ryckebusch, W. Van Nespen, and S. Janssen, Phys. Rev. C **62**, 024611 (2000).

[19] J. D. Bjorken and S. D. Drell, *Relativistic Quantum Mechanics* (McGraw-Hill College, New York, 1965).

[20] W. Greiner, *Quantum Chromodynamics* (Springer-Verlag, Berlin, 1994).

[21] D. P. Murdock and C. J. Horowitz, Phys. Rev. C **35**, 1442 (1987).

[22] D. P. Murdock, Ph.D. thesis, Massachusetts Institute of Technology, 1987.

[23] D. L. Adams and M. Bleszynski, Physics Letters B **136**, 10 (1984).

[24] T. Matsui and B. D. Serot, Annals of Physics **144**, 107 (1982).

[25] J. R. Shepard, J. A. McNeil, and S. J. Wallace, Phys. Rev. Lett. **50**, 1443 (1983).

[26] J. A. McNeil, J. R. Shepard, and S. J. Wallace, Phys. Rev. Lett. **50**, 1439 (1983).

[27] J. Piekarewicz, R. D. Amado, and D. A. Sparrow, Phys. Rev. C **32**, 949 (1985).

[28] R. A. Arndt and D. Roper, *VPI and SU Scattering Analysis Interactive Dial In Program and Data Base*.

[29] K. Wehrberger, Physics Reports **225**, 273 (1993).

[30] J. J. Sakurai, *Modern Quantum Mechanics (Revised Edition)*, 2nd ed. (Addison Wesley, New York, 1993).

[31] B. I. S. Van der Ventel, Ph.D. thesis, University of Stellenbosch, 1999.

[32] E. Rost, J. R. Shepard, E. R. Siciliano, and J. A. McNeil, Phys. Rev. C **29**, 209 (1984).

[33] E. Rost and J. R. Shepard, Phys. Rev. C **35**, 681 (1987).

[34] R. J. Glauber, in *Lectures in Theoretical Physics* (Wiley, New York, 1959), Vol. 1, p. 315.

[35] S. J. Wallace, Annals of Physics **78**, 190 (1973).

[36] S. J. Wallace, Phys. Rev. D **8**, 1934 (1973).

[37] A. Baker, Phys. Rev. D **8**, 1937 (1973).

[38] R. D. Amado, J. P. Dedonder, and F. Lenz, Phys. Rev. C **21**, 647 (1980).

[39] R. D. Amado, J. Piekarewicz, D. A. Sparrow, and J. A. McNeil, Phys. Rev. C **29**, 936 (1984).

[40] D. Waxman, C. Wilkin, J.-F. Germond, and R. J. Lombard, Phys. Rev. C **24**, 578 (1981).

[41] T. W. Chen, Phys. Rev. C **30**, 585 (1984).

[42] S. J. Wallace and J. L. Friar, Phys. Rev. C **29**, 956 (1984).

[43] R. D. Amado, J. Piekarewicz, D. A. Sparrow, and J. A. McNeil, Phys. Rev. C **28**, 1663 (1983).

[44] S. Hama *et al.*, Phys. Rev. C **41**, 2737 (1990).

[45] S. Jeschonnek and J. W. Van Orden, Phys. Rev. C **78**, 014007 (2008).

[46] G. A. Evans and J. R. Webster, Journal of Computational and Applied Mathematics **112**, 55 (1999).

[47] J. Piekarewicz, R. D. Amado, D. A. Sparrow, and J. A. McNeil, Phys. Rev. C **28**, 2392 (1983).

[48] A. L. Fetter and J. D. Walecka, *Quantum theory of many-particle systems* (McGraw-Hill, New York, 1971).

[49] G. B. Arfken and H. J. Weber, *Mathematical Methods for Physicists*, 4th ed. (Academic Press, London, 1995).

[50] A. Garcia, *Numerical Methods for Physics*, 2nd ed. (Cambridge University Press, Englewood Cliffs NJ, 2000).

[51] J. M. Thijssen, *Computational Physics* (Cambridge University Press, Cambridge, 2000).

[52] W. H. Press and N. R. S. Firm, *Numerical recipes in FORTRAN 77 and FORTRAN 90 the art of scientific and parallel computing* (Cambridge University Press, Cambridge [England] ; New York, N.Y., 1996).

[53] P. Bratley and B. L. Fox, ACM Trans. Math. Softw. **14**, 88 (1988).

[54] H. Niederreiter, *Random number generation and quasi-Monte Carlo methods* (Society for Industrial and Applied Mathematics, Philadelphia, PA, USA, 1992).

[55] W. J. Morokoff and R. E. Caflisch, SIAM J. Sci. Comput. **15**, 1251 (1994).

[56] S. Joe and F. Y. Kuo, SIAM Journal on Scientific Computing **30**, 2635 (2008).

[57] G. A. Evans, J. Comput. Appl. Math. **163**, 1 (2004).

[58] S. Olver, Ph.D. thesis, University of Cambridge, 2008.

[59] J. Li, X. Wang, T. Wang, and C. Shen, Applied Mathematics and Computation **209**, 327 (2009).

[60] L. N. G. Filon, Proceedings of the Royal Society of Edinburgh **49**, 38 (1928).

[61] D. Levin, Mathematics of Computation **38**, 531 (1982).